Driver Models to Emulate Human Anomalous Behaviors Leading to Vehicle Lateral and Longitudinal Accidents

by

Hsin-Hsiang Yang

A dissertation submitted in partial fulfillment
of the requirements for the degree of
Doctor of Philosophy
(Mechanical Engineering)
in The University of Michigan
2010

Doctoral Committee:

Professor Huei Peng, Chair
Professor Timothy Gordon
Professor A. Galip Ulsoy
Assistant Professor Ryan Eustice

TABLE OF CONTENTS

LIST OF FIGURES

LIST OF TABLES

LIST OF APPENDICES

CHAPTER 1
INTRODUCTION

1.1 Motivation

Driver behavior and man/machine interactions are important topics for transportation and ground vehicle research. The way drivers respond to the surrounding traffic influences roadway design, traffic rules and the human-vehicle interface. For example, driver's inattention or distraction is responsible for 25%-30% of police-reported crashes [1]. Inattentive drivers were found to have three to six times higher near-crash/crash risk than drivers who are attentive [2]. Over the past decade, Active Safety Technology (AST) was developed to assist human drivers in avoiding or mitigating accidents. They are helpful when the driver is either making a wrong move or is not able to handle the situation. To evaluate the effectiveness of AST, driver models that achieve driving tasks normally are not very useful. A new kind of driver model is needed to emulate anomalous driving behaviors. This type of driver model will be developed based on the concept that a driver model that normally achieves driving tasks could be perturbed to emulate anomalous behaviors like human drivers by considering human's inherent limitations or by incorporating error mechanisms. If driver limitations or error mechanisms are properly designed, the driver model can generate accident or near-accident behaviors that are of interest to engineers who are developing AST.

Driver limitations can be physical and/or mental. Physically, drivers have crossover frequencies less than 1.5 rad/sec [3], due to neuromuscular delay and perceptual limitation. These physical constraints limit driver's performance in some maneuvers, e.g. lane changing, disturbance rejection, etc. Physical limitations are usually included in conventional driver models. However, physical limitations alone are not enough to explain driving accidents that may be due to mental limitations. For example, a driver may panic during certain circumstances or fail to understand and handle the

vehicle characteristic at extreme maneuvers. Those limitations may cause driving accidents and need to be considered in the model. Another major contributor of driving accidents is driving error. Driving errors may arise from driver's distraction, delay in response, or in the recognition of information needed for the driving task. Modeling driving error is different from modeling driver limitations because error is generally a stochastic event. For example, driver distraction is sometimes caused by the use of cellular phones [4] or other in-vehicle devices [5], the presence of other passengers or simply being "lost in thought" [6]. Unlike driver limitations, driving errors usually happened in a routine and long driving task without any hard constraints, e.g. speed regulating or car-following. Most existing models focus on describing driver behavior under those tasks, and few of them include driving errors. The main contribution of this study is to partially fulfill the missing link between modeling normal driving tasks and modeling driving accidents. The development of architecture and modeling process for driver models that emulate anomalous behaviors will be provided. Despite our best effort, no research on such driver models was found in the literature.

The model architecture and modeling process will be demonstrated by two examples. Lateral disturbance rejection for a lane-keeping task will be used to illustrate driver behavior under lateral disturbance. Another example studies the effect of driving errors during longitudinal car-following. Lateral disturbances may come from road superelevation or un-aligned suspensions for a mild disturbance, and impact with other vehicle or strong crosswinds for a larger disturbance. The phenomenon and modeling process related to impact with other vehicles can be found in [7]. In this study, driving accidents under strong crosswind will be discussed. In the US, highways in certain areas have seasonal and year-round crosswinds strong enough to cause traffic accidents. In addition, vehicles driving on long span bridges and bridges with high piers could experience structure induced winds that pose severe threats. Vehicles with large side cross-section area such as buses and semi-trucks are especially vulnerable. Active safety systems such as differential braking and/or active steering can be used to address this problem. However, the effectiveness of those active safety systems interacting with human driver's intervention needs to be studied. A lateral driver model that can reproduce human behaviors, both normally and anomalously, will be helpful. The goal of

this example is to analyze crosswind induced vehicle stability problems and the driving accident induced by human driver limitations. Both numerical simulations and driving simulator experiments will be conducted to collect lateral driving behaviors. Lateral normal driving behaviors and accident inducing behaviors will be studied. The lateral driver model with accidents will be developed and used to evaluate vehicle crosswind stability and active safety system design.

In the second example, we will focus on longitudinal car-following behavior, which is important because rear-end collisions account for about 30% of all crashes [8]. Rear-end collision warning/collision avoidance (CW/CA) systems were developed to avoid or mitigate these type of accident. The effectiveness of CW/CA system working with a human driver or other human controlled vehicle needs to be evaluated exhaustively to ensure safety. A very large percentage of longitudinal driving accidents are caused by driving errors. An errable driver model constructed and used properly, can capture human/control interaction and thus accelerate the CW/CA system development process. To make a model errable, mechanisms of driving errors and their effects on driving must be understood. Driver errors can be viewed as a recurring event which, when combined with events from surrounding vehicles, could result in an accident. For example, a driver may be distracted or engaged in alter-control tasks and thus fail to adjust vehicle speed properly. If the leading vehicle happens to decelerate at the wrong moment, a rear-end collision could happen. Human behavior (e.g. distraction) and lead vehicle deceleration can both be described by stochastic processes. If proper human cognition/error mechanisms are included and proper probability distribution functions are used to introduce human errors, it is possible to reproduce accident/incident behavior that is statistically similar to field testing results.

1.2 Literature Review

1.2.1 Lateral Driver Model Review

Different philosophy and structure are proposed in the literature to develop lateral driver models. The simplest way to model lateral driving behaviors is by a feedback control

model (Fig. 2.1). A feedback control model assumes that the driver has a desired trajectory (y_d). A feedback controller is used to drive output y to track y_d.

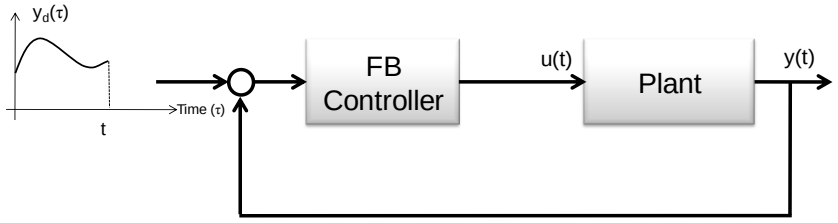

Fig. 2.1 Feedback driver model structure

One of the earliest feedback driver models was proposed by McRuer [9]. A transfer function with lead, lag time constants and time delay was used to characterize a driver's behaviors. And those constants can be determined by satisfying the "crossover frequency" assumption and by fitting test data. A more complex transfer function model was presented by Hess [10]. Different transfer functions were used to describe driver's behavior at low and high frequencies. Transfer function type feedback models generally deal with single-input systems. A multi-input example was suggested by Horiuchi [11]. In his model, an outer-loop with lead compensator was used for predicting yaw angle and an inner-loop of lead/lag compensator for regulating yaw motions. Another multi-input example was provided by Wallentowitz [12]. In this model, vehicle states are lateral position, yaw angle, yaw angle rate, and steering torque. The desired output is zero and steering dynamics and time delays are included.

When the desired output y_d is not zero, a feed-forward preview control can be added to model a driver's look-ahead behavior (Fig. 2.2). In a feed-forward preview architecture, a previewed desired trajectory ($y_d(t+\tau), \tau \in [0, t_{la}]$) are needed. One of the earliest concepts was introduced by Sheridan [13]. Sheridan described this concept as an "extended convolution" model which has a feedback controller and feed-forward preview controller.

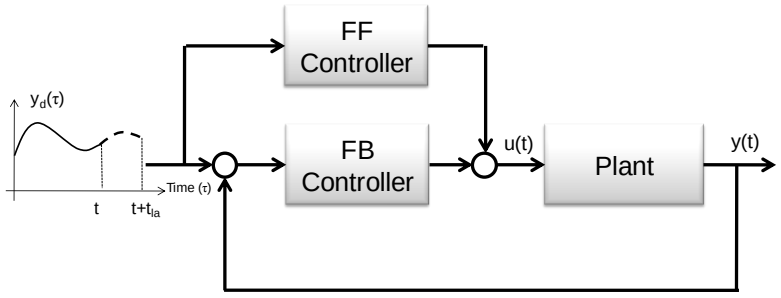

Fig. 2.2 Feedback and feed-forward preview driver model

A simpler one point preview feedback/feed-forward control model was proposed in [14]. In this model, the yaw angle at a near point is used for feedback correction and the previewed yaw angle at a far future point is used for the feed-forward control. Only one future point ($y_d(t+t_{la})$) is needed rather than a future trajectory ($y_d(t+\tau), \tau \in [0, t_{la}]$). Other than feed-forward control, the future desired trajectory can be used to compare with the estimated future vehicle states for feedback control (Fig. 2.3). A prediction estimator was used to predict vehicle future states ($y'(t+\tau), \tau \in [0, t_{la}]$) based on current states. Then, the predicted error can be used as input to the feedback controller.

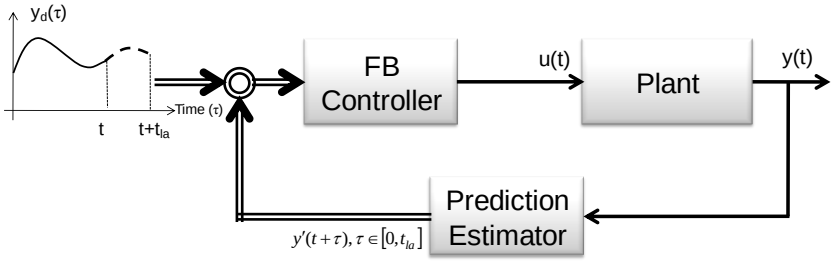

Fig. 2.3 Feedback and prediction estimator driver model

An example of a prediction estimator can be found in Yip and Crolla [15]. The vehicle future lateral displacement was calculated from linear extrapolation of the current yaw angle. More accurate prediction estimation can be done by utilizing current input. The resulting model can be depicted by the diagram shown in Fig. 2.4.

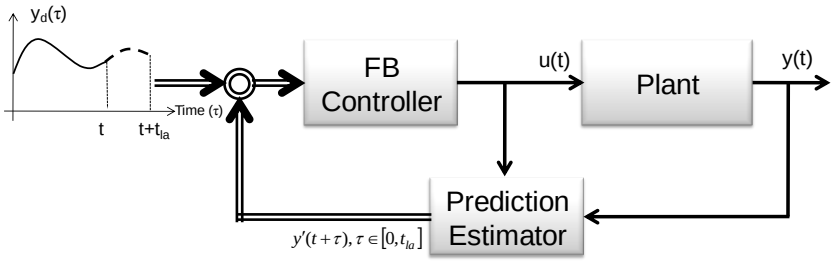

Fig. 2.4 Feedback and prediction estimator with current input

The approach in Fig. 2.4 can be found in Maruyama [16] as a single-point preview with a kinematic prediction estimator. A kinematic relationship was used to estimate vehicle future states and a feedback control was used to correct the prediction error. Furthermore, a dynamic prediction estimator can be used for better accuracy. In Sharp [17], vehicle states were predicted by a vehicle dynamic model and full state feedback was used to achieve the desired yaw angle and lateral displacement. A remaining design question is on the selection of full state feedback gains.

The well-known MacAdam's model was first presented in [18]. Starting with the preview control concept, the MacAdam's model provides an optimal solution for selecting state feedback gains in Fig. 2.4. The original MacAdam's model performs very well for normal lateral driving behaviors. For near/at limit vehicle handling problems, MacAdam proposed a more comprehensive driver model in [18]. This model included more vehicle states such as steering angle, side slip, and roll angle in the cost function. The optimal control input was calculated through an optimization scheme. Finally, a more complicated concept for driver modeling was shown in Fig. 2.5. Instead of assuming input as a constant over the preview horizon, a variable input sequence was introduced. Possible iterations would be needed for obtaining the optimal solution. No current driver model has the structure in Fig. 2.5. However, a simpler form of which was proposed in Ungoren's work [20]. Assuming the driver can update steering input over the preview horizon, this model replaced the constant input in MacAdam's model by a input sequence.

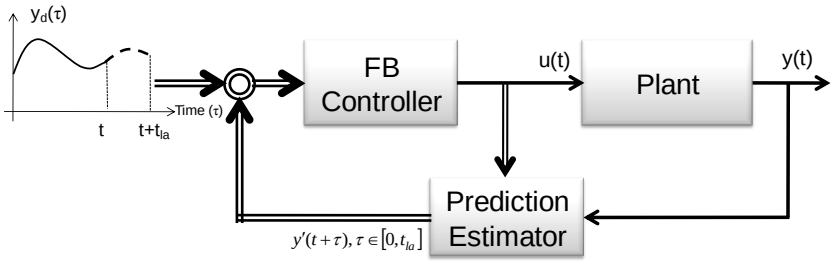

Fig. 2.5 Prediction estimator with current and iterated future input

To model driving accidents under strong crosswind, we need a driver model that can work under normal situations and can generate accidents when the driving task goes beyond the driver's capability. A feedback driver model is good for modeling different drivers' behavior but it is not clear how a feedback mechanism might change when a driver's capability is exceeded. Parameters of the feedback driver model were found to vary with driver states and time [21]. However, why and how those parameters changed is unclear. A new lateral driver model that account for both normal and accident behaviors will be developed. This model will be used to demonstrate the effect of driver inability on the lateral driving and will be used to evaluate vehicle crosswind stability.

1.2.2 **Crosswind Driver/Vehicle Stability Evaluation Method**

A new lateral driver model will be used to evaluate vehicle crosswind stability. However, the concept of crosswind stability is not clearly defined or accepted in the literature. Most research defined crosswind stability based on driver's subjective assessments. To do that, a new vehicle design was test-driven by a human driver and subjective ratings were collected. Comparing with other design candidates, the most preferred design was considered as having the best crosswind stability. This procedure is time-consuming and costly. An alternative is to obtain the vehicle crosswind sensitivities by experiments or by simulations. Crosswind sensitivity is often used to refer vehicle "open-loop" responses under crosswind. The correlations between "crosswind sensitivity" and "subjective rating" can be drawn. If particular crosswind sensitivity has high correlation with subjecting assessment, this crosswind sensitivity would be used to infer crosswind stability (Fig. 2.6). However, the results are usually unsatisfactory except for yaw-rate ([23], [24]). Nevertheless, the crosswind sensitivity analysis is still the most popular method for assessing crosswind stability. In this section, several prior works regarding

the crosswind sensitivity will be reviewed and some other alternative methods for directly assessing crosswind stability will be discussed.

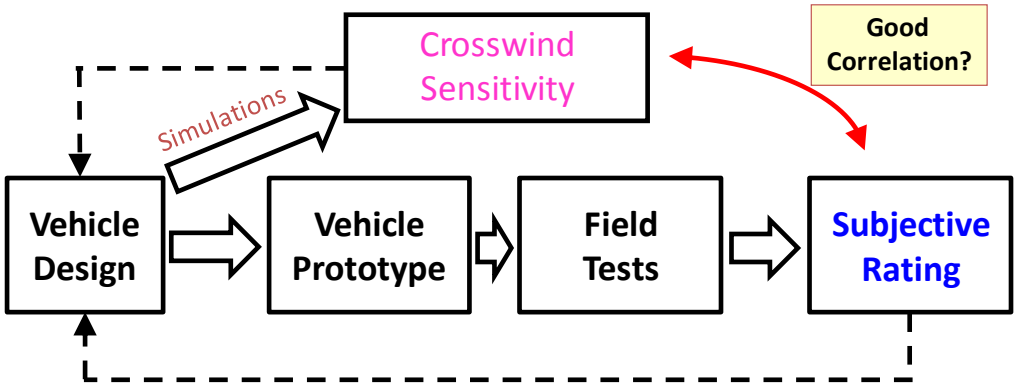

Fig. 2.6 Concept for correlating crosswind sensitivity and subjective rating

One of the earliest crosswind sensitivity analyses was done by Uffelmann [22]. The vehicle design parameters were divided into two categories: body (aerodynamic, dimensions) and chassis (suspension and roll stiffness). Vehicle response under crosswind was described by wind-sensitivity which is a combined formula of those two parameter categories. In his research, peak yaw response time was found to have the highest correlation with driver subjective rating. Another crosswind sensitivity analysis was done by Willumeit [23]. Six blowers were installed on a proving ground and a fixed open-loop steering vehicle was driving by. Closed-loop tests with drivers under the same crosswind were also conducted and driver subjective assessments were collected. The analysis shows yaw-rate, lateral acceleration, steering wheel angle, and yaw angle have good correlations with the driver subjective rating. A similar experiment was done in [24]. Yaw-rate, again, has the highest correlation with the driver subjective rating. An equation for calculating crosswind sensitivity was also provided for evaluating preliminary designs. Aerodynamic effects on the vehicle are another research focus for evaluating the vehicle crosswind behavior. In [25], an aerodynamic attachment was used to change vehicle characteristics. The result shows that roll rate is the most related measurement to the subjective feeling assessment under high vehicle speed and mild crosswind.

All of the above research tries to find the correlation between open-loop crosswind sensitivity and closed-loop driver subjective rating. A direct approach for

quantifying the closed-loop crosswind behavior was proposed by Wallentowitz [12]. An equipped vehicle was driven on the road to measure the crosswind and the driver vehicle behavior. Measured steering angle was used to calculate the yaw-rate due to steering through a bicycle model. The calculated yaw-rate was subtracted from measured yaw-rate. Therefore, the driver's steering influence could be removed and the open-loop vehicle yaw-rate due to only crosswind was obtained. Frequency response of the crosswind force to the yaw-rate and frequency response of both the crosswind force and the steering to yaw-rate were calculated. In [26], the intensification factor was introduced to quantify the driver's interaction with vehicle under crosswind. The intensification factor was defined as the peak magnitude of the closed-loop frequency response over the peak of the open-loop frequency response. Intensification factor larger than unity means that the driver amplifies vehicle responses under the crosswind. A higher intensification factor may suggest a higher "crosswind sensitivity" by the driver's subjective evaluation. This analysis method is easy to calculate, by experimental results on a track or from driving simulator; but may not have high correlation to the driver subjective assessment. Furthermore, real drivers will be involved for the evaluation of different vehicle designs, which will increase time and cost. Another closed-loop evaluation of crosswind driver-vehicle behavior was done by [27]. A driver model was used to derive the driver vehicle transfer function. A closed-loop performance index is defined to evaluate the vehicle behavior under crosswind. Compared with crosswind sensitivity, closed-loop performance index shows a better correlation with the driver subjective rating.

To obtain open-loop crosswind sensitivity, an experiment or simulation is needed. Experiments can be conducted either on test facilities or on the open road. In a test facility, like a wind tunnel or a proving ground, a series of wind blowers are usually used to generate a step crosswind input ([12], [22], [24], [28]). Test vehicle drives through the step crosswind at different vehicle speeds and wind speeds. Vehicle responses are measured and their sensitivities to the crosswind input can be calculated. This step crosswind input can also be found in simulations. Another commonly used input type is random or natural crosswind input [22]. This input type is usually used in simulations.

Power spectral density of natural wind is measured and modeled in simulations. Frequency response is usually used for analyzing crosswind sensitivity.

Closed-loop tests are also used for obtaining the driver subjective rating. The simplest way to conduct a closed-loop test is to use the same crosswind input as in the open-loop experiment. There is also a kind of crosswind inputs designed specifically for closed-loop [24]. This so-called "gauntlet" input provides a stronger vehicle driver response for the driver subject rating. The gauntlet input uses eight fan units located in an alternating manner on the opposite side of the road. Similar scenarios for closed-loop simulations can also be found in [24]. Other than conducting the closed-loop test at a test facility, open road tests were also conducted in [12] and [26]. An equipped vehicle with real drivers was used. The driving behavior and crosswind data were both measured and used for evaluating the vehicle crosswind stability. Several crosswind experiment/simulation conditions were summarized in Table 2.1. The test vehicles are generally running at high speed between 100 to 200 km/h. The crosswind speed is about 40 to 100 km/h and constant crosswind is the most common type of input because it is easy to produce in a test facility.

Table 2.1 Crosswind experiment/simulation setup summary

	Test Facility	Driver	Vehicle Speed	Wind duration	Crosswind	Crosswind Speed	Crosswind Angle
MacAdam [24]	wind tunnel	yes	160 km/h (100 mph)	0.68s (100 ft)	constant	40 km/h (25 mph)	90
	wind tunnel	yes	160 km/h (100 mph)	2.39s (350 ft)	gauntlet	40 km/h (25 mph)	90
Uffelmann [22]	simulation	no	100 km/h	-	constant	70 km/h	35
	simulation	model	100 km/h	-	random	natural	
Willumeit [23]	wind tunnel	no	130 km/h	0.46s (16.6 m)	constant	75.6 km/h (21m/s)	60
	wind tunnel	yes	130 km/h	0.46s (16.6 m)	constant	75.6 km/h (21m/s)	60
	motorway	yes	140 km/h	-	natural	(max 45km/h)	
Wallentowitz [12]	wind tunnel	no	100 km/h (27.7 m/s)	-	constant	72 km/h (20m/s)	90
Yip [15]	simulation	no	162 km/h (45 m/s)	-	constant	36 km/h (10m/s)	125

	simulation	model	162 km/h (45 m/s)	-	random		
Maeda [25]	Test track	yes	200 km/h	-	natural		
Orady [29]	simulation	model	100 km/h	-	random	(mean 5m/s)	
Maruyama [30]	simulation	no	40 - 100 km/h	1s	constant	90 km/h (25m/s)	90
	simulator	yes	90 km/h	0.6s (15 m)	constant	81 km/h (22.5m/s)	90
	simulator	yes	80,100,120 km/h	2s	constant	81 km/h (22.5m/s)	90
Hanke [28]	simulation	no	100 - 180 km/h	0.72s - 0.4s (20m)	constant	100km/h	90

Designing a vehicle with good crosswind stability is non-trivial, mainly because the definition of crosswind stability is not clear. Perhaps the most trustworthy assessment is the driver subjective rating. However, conducting a driving test to obtain the driver subjective rating for every new vehicle design is not practical. A faster and easier method is needed. Measuring crosswind sensitivity is easy by experiments or simulations. If there is a good correlation with subjective rating, crosswind sensitivity can be used to infer crosswind stability. In this research, we propose a new method to assess crosswind stability. A vehicle and driver model is developed for crosswind maneuvers. And, the closed-loop vehicle response is obtained through simulations. Finally, the simulated closed-loop response is used to predict the driver subjective rating (Fig. 2.7). Once the vehicle and driver model are developed, this method can evaluate vehicle crosswind stability almost as easy as using the crosswind sensitivity approach.

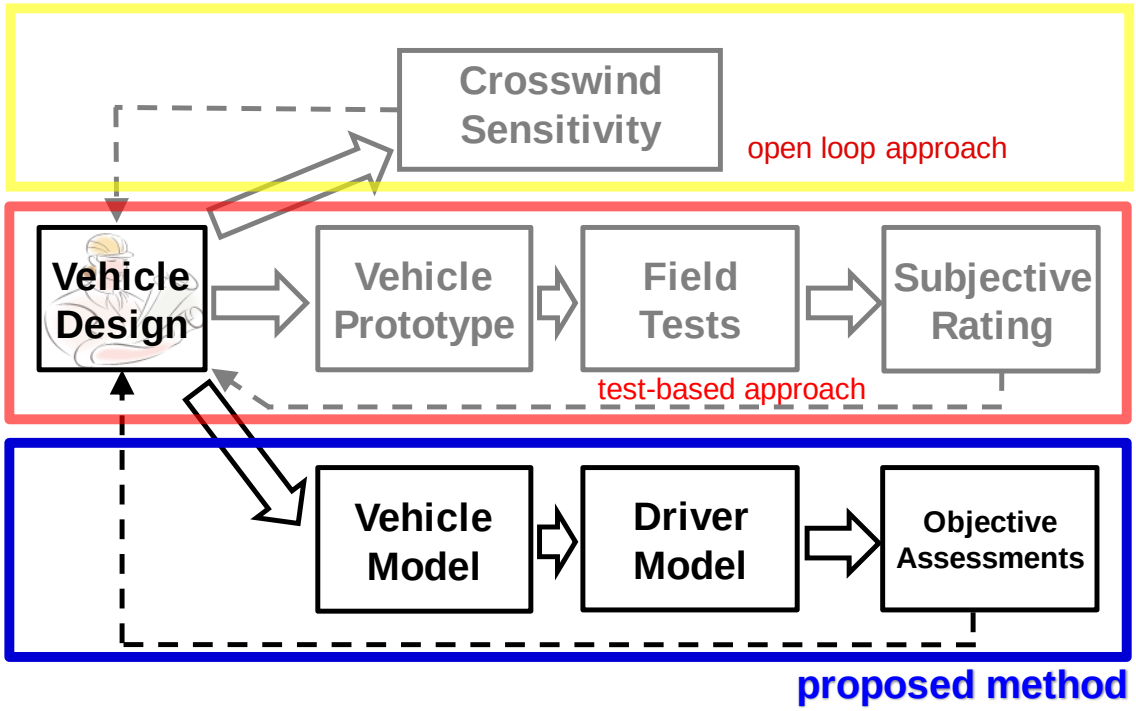

Fig. 2.7 Proposed method diagram for assessing crosswind stability

1.2.3 **Longitudinal Driver Model Review**

Car-following driver models have been developed to evaluate traffic capacity and congestion. A linear follow-the-leader model was first suggested by Pipes [31]. Car-following was modeled as a process where the driver follows the lead vehicle speed by controlling the acceleration with a linear proportional gain. Gazis [32] modified the linear follow-the-leader model with a nonlinear gain. The proportional gain of acceleration in Pipes' model was replaced by a function of m^{th} power of range and l^{th} power of the following vehicle speed. The parameters m and l were estimated by several researchers [33]-[35]. Newell [36] proposed another nonlinear model where the desired speed is a function of range error and is achieved in an exponential fashion. All the models above describe driver behavior as regulating either zero range error or zero range-rate. Intuitively, drivers are likely to do both. This hypothesis was first discussed by Helly [37]. In Helly's model, the acceleration is a function of both range error and range-rate. Furthermore, the desired range was represented by following vehicle speed and acceleration. Tyler [38] used the linear optimal control approach and derived a similar conclusion. A quadratic function of range error and range-rate was optimized and the

resulting model has the same form as Helly's except that the desired range is only a function of the following vehicle speed. Other than following the leader, a safe distance strategy was proposed by Gipps [39]. By estimating a kinematic relationship between the lead vehicles, the following vehicles, and road conditions, a safety distance was maintained in congested traffic flow. A second mode was added in the Gipps' model to describe free flow condition by fitting the vehicle dynamics. By switching between the two modes, this model can capture driver behavior under different driving situations. Bando [40] adopted a hyperbolic tangent function to mimic the switch mechanism. By doing so, a single equation model can be used to describe both free and congested traffic flow.

Other than measuring dynamic variables and modeling driver decisions as a continuous dynamic process, psychophysical studies provided an alternative for modeling car-following behaviors. Michaels [41] argued that drivers would perceive the change of range through the change of lead vehicle size. Once the change exceeded a threshold, the driver would adjust vehicle acceleration until a proper perceptual size was regained. Driver behavior was modeled as a sequential control. The driver responds to an event (exceeding threshold) and resets the action when a new event is triggered. Some basic concepts and criteria were provided in Michaels work but no specific model was presented. Lee [42] claimed that drivers use time-to-collision as a threshold for braking and used τ (angular separation over separation rate) to estimate time-to-collision. In Lee's hypothesis, the driver initiates brake action based on a τ threshold and controls the brake force based on the time rate of change of τ. The hypothesis was verified by Yilmaz [43]. Reiter [44] used range as the perceptual threshold and provided experimental results to obtain model parameters. Brackstone [45] conducted experiments based on a similar approach, but he used range-rate instead of τ. All driver models above try to model or explain normal driving behavior. Good fitting results and "crash-free" are generally considered as good model performance. In our study, the goal is to develop a driver model that fits both normal and anomalous driving behaviors. In other words, "crash-free" is no longer a requirement. Instead, a model that generates crash or near-crash behavior, which has not been previously studied in the literature, is our main interest.

1.2.4 **CW/CA Algorithms**

Collision Warning Device/Algorithms were developed for aviation applications as early as 1957 [46], [47]. Simple devices were developed to provide warning for conflicting air traffic. Vehicle safety and related issues were first discussed by Gibson [48]. In his paper, Gibson described the concept of collision and safe travel. But the concept of CW/CA has not been studied until the late 80's. The Ministry of Construction in Japan organized a committee to focus on the study of several advanced vehicle technologies, including obstacle detecting and collision avoidance [49]; an early collision warning algorithm was introduced in [50], [51]. In the early 90s, the NHTSA's Intelligent Vehicle Highway System (IVHS) program initiated a study on collision warning/avoidance [52]-[54].

In the 1990's, Burgett et al. [55] proposed a rear-end collision warning algorithm. The collision situations were divided into three zones based on initial conditions. The boundary conditions and warning criteria were defined accordingly. Kiefer et al. [56] reported minimum elements required for the development of forward collision warning system. Crash alert timing requirements were studied by conducting human factor analysis. Doi et al. [57] developed an algorithm based on kinematic relationships between two vehicles and addressed the collision problem in both straight and curved roads. Brunson et al. [58] refined the algorithm developed by Burgett and others at NHTSA. Their algorithm used current vehicle states and assumed driver reaction time to calculate a predicted range; they called it "miss-distance". When the miss-distance is smaller than a threshold, an alert would be issued. Zhang et al. [59] gave another interpretation of Brunson and NHTSA's algorithm. Instead of calculating the miss-distance, they used the vehicle range to calculate a reaction time and called it the "Time to last second braking". They claimed this new approach has better agreement with human judgment and directly quantifies the threat level of the driving situation. All the algorithms above are based on assumed kinematic equations. By measuring engineering variables such as range, speed, and acceleration, the severity of collision threats can be assessed.

An alternative approach was to use time to collision as the warning criteria. As discussed by Gibson [60] and Lee [42], time to collision seems to be used by human for

collision judgment rather than range or time headway. Lee et al. [61] provided a systematic method for evaluating collision warning algorithms and they claimed that using time to collision (TTC) as a metric for collision threat is better compared with other kinematic algorithms. Using TTC and lead vehicle acceleration would further improve the performance in terms of warning precision and true positive rate. Hirst et al. [62] suggested a TTC algorithm with speed penalty. Miller et al. [63] added an extra term for TTC algorithm. This extra term includes human reaction time, reduced speed, and estimated road coefficient. The reaction time modeled a human's ability of reaction and the reduced speed and the estimated road coefficient can be adjusted depending on the severity of the situation.

1.2.5 **CW/CA Algorithm Design and Evaluation Methods**

CW/CA algorithms have been studied for more than fifty years. Corresponding parameter design and evaluation methods were also developed. Most of them are scenario-based methods. In this approach, test scenarios or test matrices were first defined. Then, CW/CA algorithms can be simulated under the test matrix with Monte Carlo method and their performance can be evaluated. Engineering tuning processes were often required and field operation tests would be conducted afterwards. The whole procedure can be illustrated by the diagram shown in Fig. 2.8.

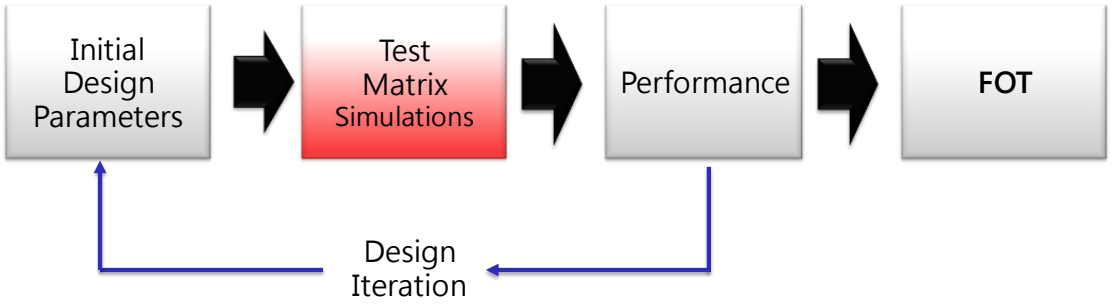

Fig. 2.8 Scenario-test approach diagram for CW/CA algorithm design

A series of experimental studies supported by NHTSA is a representative work of this evaluation approach. The ACAS FOT report [64] summarized the final results and the definition of the test matrix can be found in [65], [66]. However, this approach required numerous design iterations, and the performance of the algorithm was not guaranteed. Therefore, an alternative scenario-test approach was proposed by Yang [67].

They proposed a performance-base approach for designing and evaluating CW/CA algorithm (Fig. 2.9). A so-called performance boundary was first defined, and then the test matrix was used to search for the parameters of CW/CA algorithm that can satisfy the performance boundary. A stochastic driver model and a test matrix were adopted from the ACAS FOT. Yang claimed that the resulting CW/CA algorithm guarantees the performance without hand tuning iterations.

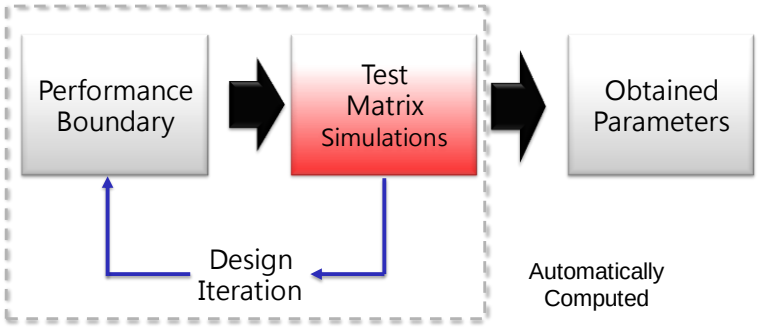

Fig. 2.9 Performance-base scenario-test approach for CW/CA algorithm design

However, this approach still needs prescribed test scenarios which might not represent real human behaviors leading to crashes. A human centered approach was developed to compensate for this disadvantage [61]. A significant amount of naturalistic human driving data were analyzed and the threatening situations were defined and identified. Then, the threatening scenarios were used to evaluate CW/CA algorithms. This human centered approach benchmarks CW/CA algorithm performance by realistic human driving behaviors and provides an optimization method for obtaining algorithm parameters. Nevertheless, the evaluating data was collected from a human driving database without any real crash. In other words, the defined threatening situations may not be as severe as real crashes. An errable driver model could further improve this deficiency. By introducing proper human cognition/error mechanisms, it is possible to reproduce accident/incident behavior. Therefore, a more rigorous human-centered evaluation can be achieved.

1.3 Contributions

A new closed-loop crosswind stability evaluation method will be proposed to demonstrate the effect of driver limitations. This method can evaluate vehicle crosswind stability almost as easy as using the crosswind sensitivity approach. Unlike the traditional method of obtaining open-loop sensitivity, this closed-loop method can provide more detailed information for vehicle design. Meanwhile, a new way to analyze driving data and categorize driving style will be demonstrated throughout the development process. Finally, a lateral driver model that emulates anomaly behaviors for crosswind maneuver will be proposed. This driver model is a combination of MacAdam's driver model and an instantaneous feedback correction for strong crosswind disturbances. This model can capture the driving behavior better than MacAdam's driver model alone. The ability of reproducing yaw-rate responses will make this model suitable for evaluating the vehicle crosswind stability.

A longitudinal errable driver model is developed for understanding anomalous behaviors due to driving errors. This model will normally achieve car-following task and will be made to make mistakes due to driving errors. Those mistakes will be induced based on the same mechanisms that could cause accidents in actual driving. The accident or error behaviors will emulate real human behaviors, and the error rate, ideally, will match the real driving error rates statistically. This model will be used for the evaluation and development of a humanized CW/CA algorithm. Because of the difference among human drivers, and the difference within a single driver temporally, it is difficult for a conventional CW/CA algorithm to decide on the timing for issuing warnings. To achieve high precision, it is necessary to issue warnings for all potential threatening events; however, this may cause a high false alarm rate as well. Well studied and modeled human near-crash behaviors will be the key to lower false alarm rates while maintaining high accuracy. A major contribution of this dissertation is to answer this challenge. The developed errable driver model could become an important tool for active safety research, useful for driving simulators, evaluation of CW/CA systems, etc.

CHAPTER 2
LATERAL DRIVING BEHAVIOR STUDY

2.1 Motivation

The goal of this study is to analyze vehicle stability problems under crosswind and driving accidents induced by human driver limitations. The potential of using widely available active safety technology (AST) such as active front steering to improve crosswind stability is also investigated. The most challenging issues are to simulate a wide array of wind excitations and to accurately capture human behaviors. Both numerical simulations and driving simulator experiments were conducted to collect lateral driving behaviors. A 5-DOF wind-steer model developed at the University of Michigan Transportation Research Institute ([68], [69]) was used for the purpose of driver dynamic analysis and control design. A target vehicle is also modeled in CarSim software for the driving simulator test. Lateral normal driving behaviors and accident inducing behaviors is studied. A lateral driver model with accidents is developed and used to evaluate vehicle crosswind stability and active safety system design.

2.2 Vehicle Model Development and Simulator Test

An analytical model was developed for the purpose of driver dynamic analysis and control design. The wind induced vehicle motion is the focus of the model development. A CarSim model is also built for a fixed base driving simulator test. Twenty-four test participants were recruited and successfully completed the simulator test. Test results are presented in section 2.3 and are used to develop a lateral crosswind driver model in Chapter 3.

2.2.1 **UMTRI Wind-Steer Model**

The UMTRI 5-DOF wind-steer vehicle model was developed ([68], [69]) to calculate vehicle steering response under crosswind disturbances. It is meant to be accurate up to 0.3g of lateral acceleration and frequencies below 2Hz. The Wind-Steer vehicle model is an extension of Segal's 3DOF (lateral/yaw/roll) model [70] and has five DOF (lateral, vertical, pitch, yaw, roll) plus suspension kinematics, where the longitudinal speed is assumed to be constant. The suspension is purely kinematic (use quasi-static force balance, i.e., force is calculated from sprung mass motion only). The MacAdam's driver model is included as an option of the wind-steer model, so that driver's response under crosswind disturbance can be analyzed.

The block diagram of this wind-steer model is shown in Fig. 2.1. If the driver model is used, the input will be a desired path (f_{path}) that the driver tries to follow. If there is no driver model, the input will be steering wheel angle (δ_H). An additional input is crosswind disturbance (V_{wind}) which needs to be defined by wind speed and wind direction.

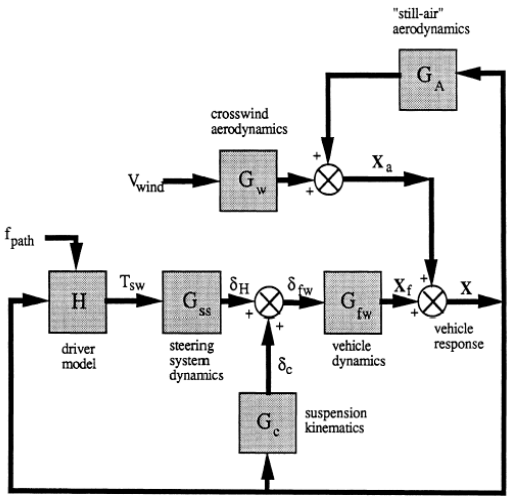

Fig. 2.1 Block diagram of UMTRI wind-steer model [68]

The UMTRI wind-steer vehicle model was calibrated by using a set of road test data. The open-loop test set up to obtain the test data is shown in Fig. 2.2. The vehicle speed is 100 km/h and the vehicle parameters are for a mid-size Sports Utility Vehicle.

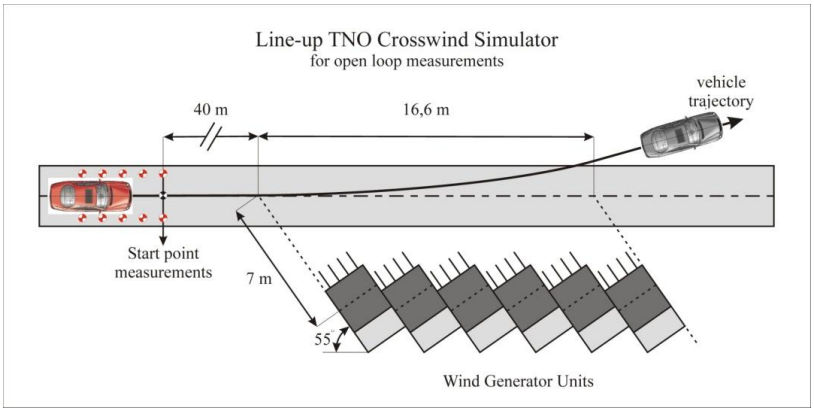

Fig. 2.2 Open-loop test setup for obtaining road test data

The crosswind disturbance was approximated as Fig. 2.3. The crosswind angle is assumed to be 90° fixed perpendicular to the vehicle x-axis. The simulation generated by this crosswind speed profile is the closest one to the road test result.

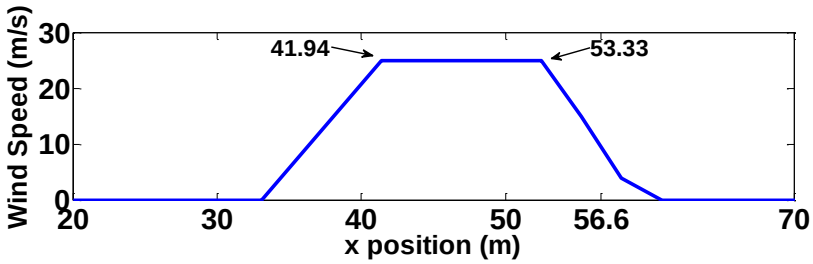

Fig. 2.3 Estimated crosswind disturbance of open-loop test setup in Fig. 2.2

It can be seen in Fig. 2.4 that the vehicle model response under approximated crosswind is similar to the road test result.

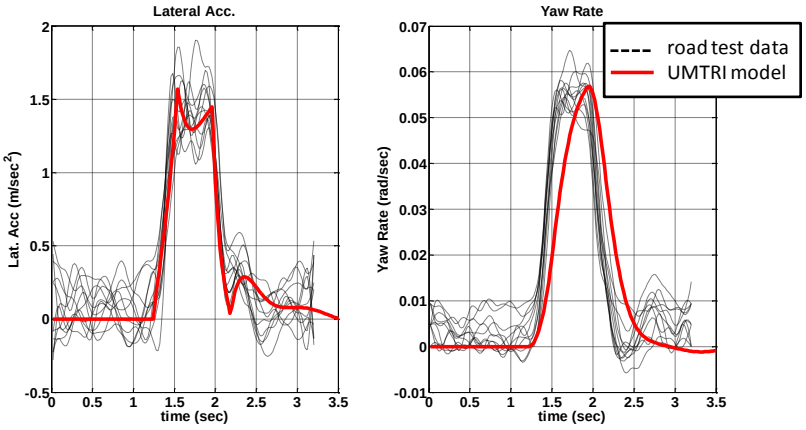

Fig. 2.4 UMTRI wind-steer model simulation compared with road test result

The goal of this study is to analyze driver-vehicle crosswind stability. First, the term "crosswind stability" needs to be explicitly defined, as it seems from literatures that this term was only vaguely referred and not rigorously defined. Frequently, performance evaluation for crosswind stability was based on driver subjective assessments. Subjective assessment is used to categorize driver preference of vehicle response under crosswind. Meanwhile, many papers in the literature reported that vehicles developing smaller yaw-rate and/or lateral acceleration under crosswind in an open-loop fashion (i.e., no driver feedback compensation) generally received higher ranking. In other words, it seems crosswind stability can be quantitatively defined by vehicle open-loop "crosswind sensitivity" of yaw-rate and/or lateral acceleration. Crosswind sensitivity obviously is affected by vehicle parameters. Our goal here is to analyze crosswind sensitivity of different vehicle configurations or parameters. The vehicle configurations that are found to be most sensitive (to the crosswind input) will be evaluated in the driving simulator test and their crosswind stability will be analyzed.

A sensitivity analysis was done by using the UMTRI wind-steer model. Fifteen vehicle design parameters were selected (see Table 2.2) and the vehicle open-loop response under impulse crosswind was used to represent the vehicle performance. The impulse crosswind input is similar to the road test condition (Fig. 2.3). Maximum and RMS values of yaw-rate and lateral acceleration were used to evaluate crosswind sensitivity. The vehicle response (both peak value and RMS of yaw-rate and lateral acceleration) under the three most sensitive design parameters are shown in Fig. 2.5-Fig. 2.7. The x-axis shows the normalized parameter value and "1" indicates the nominal (unperturbed) condition. Similarly, the vehicle response shown in the y-axis is also normalized and a value "1" indicates the nominal vehicle response. It can be seen that these three vehicle parameters are perturbed by ±30% and the vehicle response changes by as large as 80%.

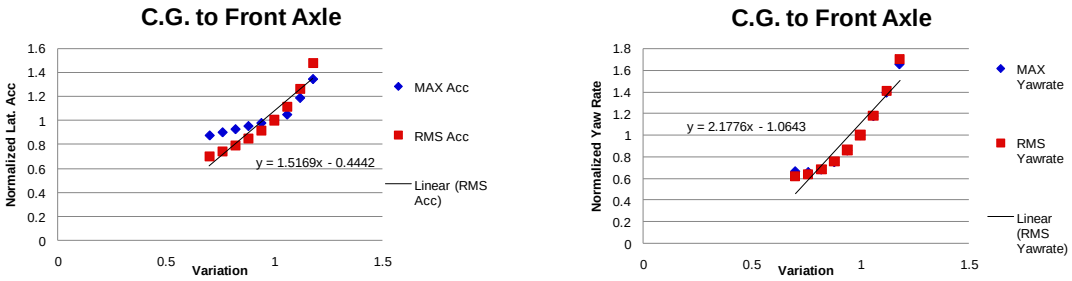

(a) Lateral acceleration (b) Yaw-rate

Fig. 2.5 C.G. position sensitivity to crosswind disturbance

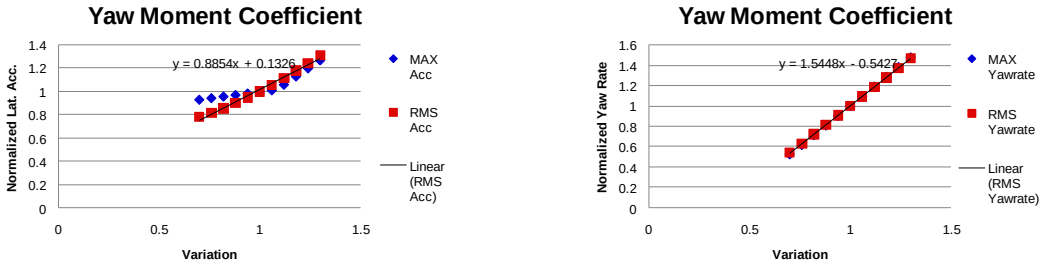

(a) Lateral acceleration (b) Yaw-rate

Fig. 2.6 Yaw moment coefficient sensitivity to crosswind disturbance

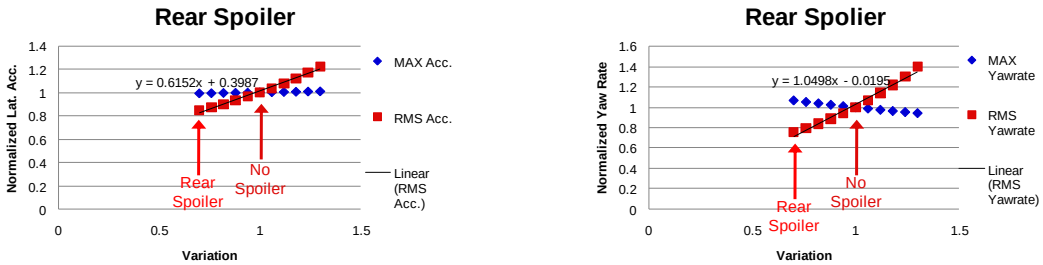

(a) Lateral acceleration (b) Yaw-rate

Fig. 2.7 Spoiler sensitivity to crosswind disturbance

C.G Position was found to be the most effective variable for influencing the lateral acc. and yaw-rate responses (see Table 2.1). Therefore, adding cargo weight, which changes the C.G position fore/aft, is an important perturbation that needs to be evaluated in the driving simulator test. Aerodynamic yaw moment coefficient is the second most effective and the presence of spoiler also has a significant effect of reducing vehicle motions under crosswind and comes in third in importance. Other vehicle

parameters such as the front wheel tire cornering stiffness, also has non-negligible effect on vehicle responses. The rest of the parameters are much less effective.

Table 2.1 Crosswind sensitivities of vehicle design parameters

	Lateral. acc	Yaw-Rate
C.G to Front Axle	**1.5169**	**2.1776**
Aerodynamic Yaw Moment	0.8854	1.5448
Rear Spoiler	0.6152	1.0498
Cornering Stiffness (Front)	-0.5751	-0.9868
Aerodynamic Roll Moment	0.3260	0.6384
Aerodynamic Lift Force	0.3715	0.5361
Aerodynamic Pitch Moment	0.2363	0.5007
Cornering Stiffness (Rear)	0.2445	0.4148
Aligning Torque Compliance	0.1946	0.3492
Lateral Force Compliance	-0.1261	-0.2201
Aerodynamic Side Force	-0.2314	0.1607
Suspension Stiffness (Rear)	-0.0319	-0.0189
Suspension Stiffness (Front)	0.0151	0.0103
Suspension Compliance Steer	-0.0035	0.0008
Aerodynamic Drag Force	0	0

2.2.2 **CarSim Model**

CarSim is a commercial software widely used for automotive dynamic simulations. It uses a nonlinear lookup table for suspension and tire models and is quite suitable for simulating vehicle response with significant roll motions (+- 10 degrees of roll angle). A CarSim model was constructed and used in the CarSim simulator for the crosswind experiment. The CarSim model is also calibrated by road test data. The crosswind input is the same as Fig. 2.3. The calibration result is shown in Fig. 2.8.

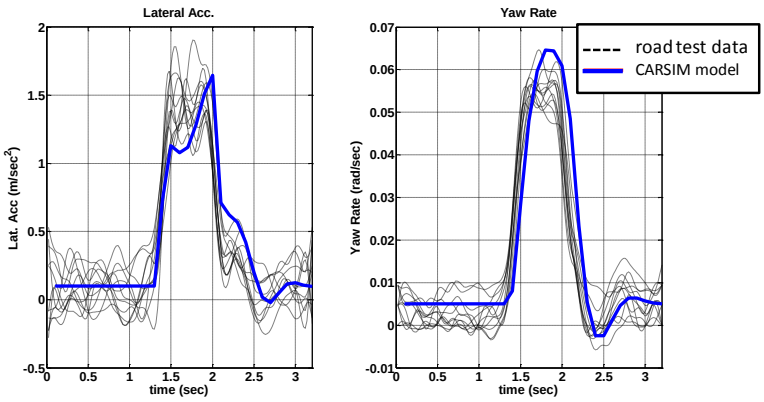

Fig. 2.8 CarSim vehicle model simulation compared with road test result

In the next section, a fixed-base driving simulator test is presented. The CarSim vehicle model is implemented in this driving simulator with crosswind inputs. Five vehicle configurations are test-driven and evaluated. The collected data is used for the development of a lateral driver model under crosswind.

2.2.3 **Driving Simulator Test**

A driving simulator test is conducted to collect data for analyzing driver-vehicle behaviors under crosswind. The goals of this driving simulator test are (i) to develop a lateral driver model under crosswind; and (ii) to assess the vehicle crosswind stability. The target vehicle for the driving simulator test is a mid-size sports utility vehicle and five different vehicle configurations are implemented. Two types of crosswind disturbance input are used to excite the driver-vehicle system to generate results for the driver model identification as well as the vehicle stability analysis.

The driving simulator test is built in CarSim DS with five different vehicle configurations and two different crosswind input scenarios. The driving simulator test is set up in the standard CarSim environment, under the following conditions:

- Clear weather.
- Standard two lanes highway with pave mark.
- Straight road with no surrounding traffic.
- Two test speeds (100 km/h 160 km/h).
- Cruise control is used to help the participants to maintain constant vehicle speed.

Based on the sensitivity analysis results, five vehicle configurations are selected:

- Baseline vehicle
  - Mid-size SUV
- Baseline vehicle with added cargo weight
  - 150 kg at 50 cm behind rear axle: C.G. position to front axle +15%, total mass +8%, yaw moment of inertia +12%, pitch moment of inertia +13%
- Baseline vehicle with rear spoiler
  - Aerodynamic lift and pitch moment coefficients -50%
- Baseline vehicle with increased aerodynamic yaw moment
  - Aerodynamic yaw moment coefficients +30%
- Baseline vehicle with reduced aerodynamic yaw moment
  - Aerodynamic yaw moment coefficients -30%

Two different crosswind inputs are used to excite the vehicle dynamics. The first type is impulse input motivated by sweeping sinusoidal and the second type is natural crosswind input adapted from measured data. In system identification, a sweeping sinusoidal signal (Fig. 2.9) is commonly used. Since the frequency of this signal sweeps through a range, it provides rich and wide-spectrum excitation that is suitable for identification of dynamic model of the vehicle.

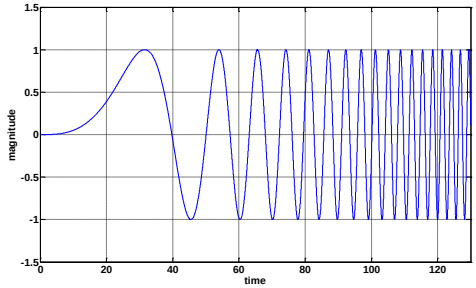

Fig. 2.9 Sweeping sinusoidal signal

In the simulator test, the sweeping sinusoidal input is not used in its original form, because the continuous wind input is not representative of wind disturbances commonly experienced in the real world. Instead, a modified series of impulse signals are used (Fig. 2.10). The series of impulse with an increasing rate of occurrence is used. The first few impulses are separated enough that the driver-vehicle response would have settled before

the next impulse. Therefore, they provide some repetition to be used for developing driver model with a higher statistical confidence.

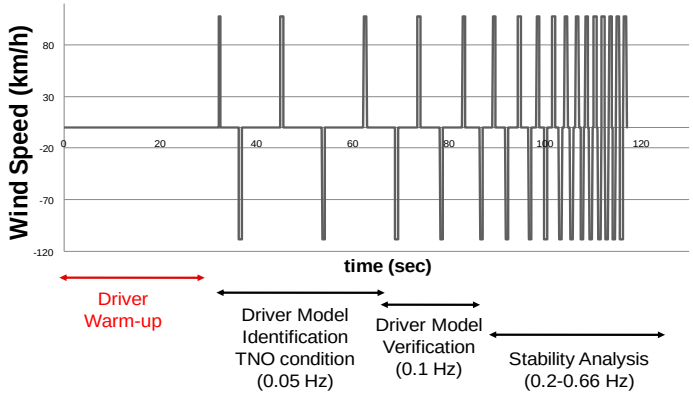

Fig. 2.10 Impulse crosswind disturbance input for simulator test

In this crosswind input, each impulse (except the first one) has identical strength to the impulse disturbance used in the road test (Fig. 2.3). The vehicle and driver response from the impulses 2-5 will be used for driver model identification. The next four impulses will be used for driver model verification. Furthermore, because all impulses are identical to the road test condition, we can compare the driving simulator test results with the road test result for the benchmarking. In addition, the crosswind input is designed to maintain the open-loop vehicle stability and similar magnitude in yaw-rate and lateral acc (Fig. 2.11). This is because that yaw-rate and lateral acceleration are the two most relevant variables for the driver subjective ranking. By setting the yaw-rate and lateral acceleration as controlled variables, we can analyze the effect of driver vehicle stability under high crosswind input frequency.

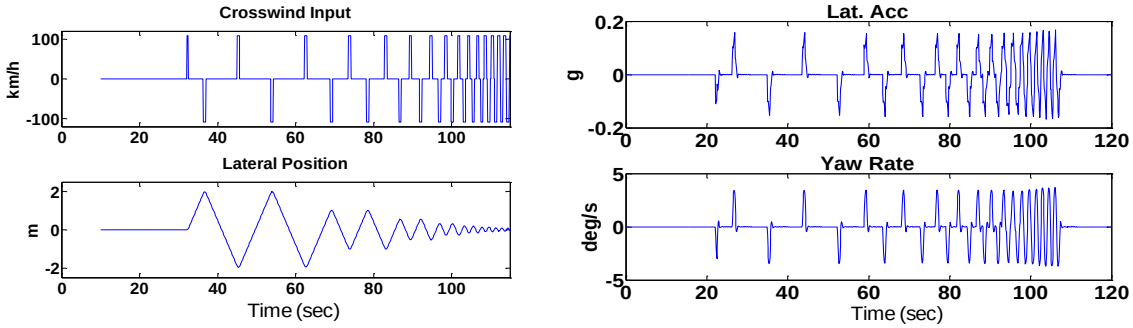

(a) Vehicle lateral position (b) Vehicle motion

Fig. 2.11 Vehicle open-loop simulation under the impulse input

Besides impulse crosswind disturbance, random or natural crosswind disturbance is also implemented. Natural crosswind input, with a wider spectrum of input frequency content, can be used to study the driver behavior in a more natural setting. Furthermore, it can also be used to verify the driver model and for the frequency analysis of driver behavior. The natural wind profile is measured from a road test and adapted for the driving simulator test. The crosswind speed and orientation are shown in Fig. 2.12. The simulator wind speed input is started from zero because the test vehicle speed starts from zero. After the vehicle reaches a constant speed (~20 sec), the wind speed converged to road test profile with a hyperbolic tangent scaling function.

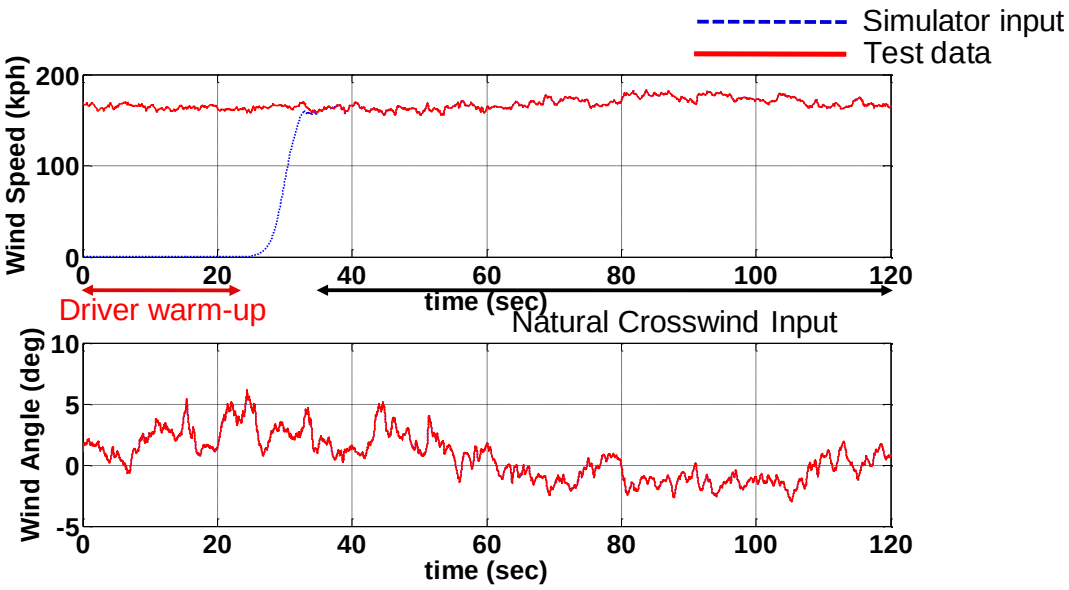

Fig. 2.12 Natural crosswind disturbance input for simulator test

Before the driving simulator test, open-loop simulations were done in the CarSim to understand the dynamic response of different vehicle configurations. The baseline vehicle response has already been shown in Fig. 2.11. Responses under the other four configurations are shown in the plots below (Fig. 2.13-Fig. 2.16). The responses of the first impulse is highlighted and compared with the baseline vehicle.

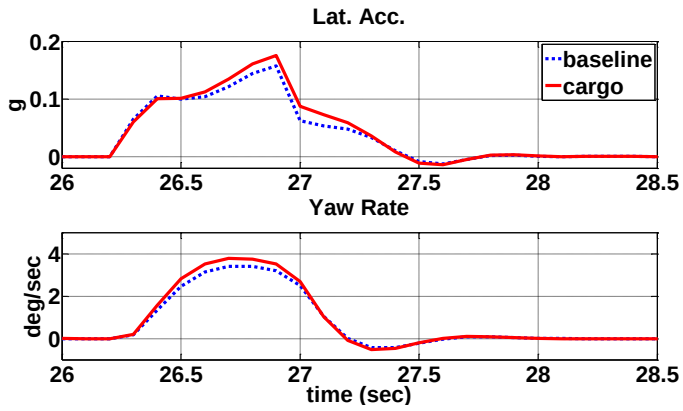

Fig. 2.13 Vehicle response with added Cargo weight

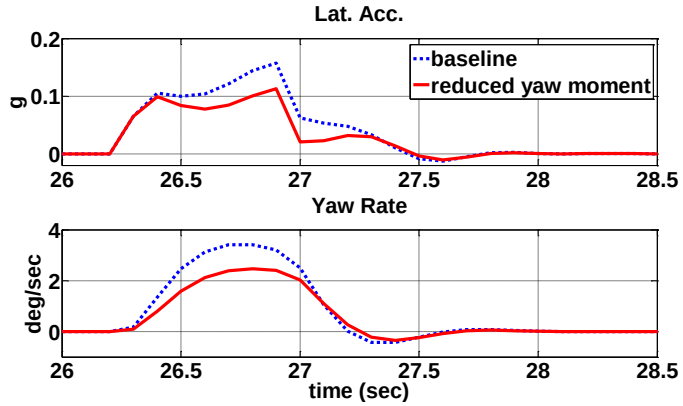

Fig. 2.14 Vehicle response with reduced yaw moment coefficient

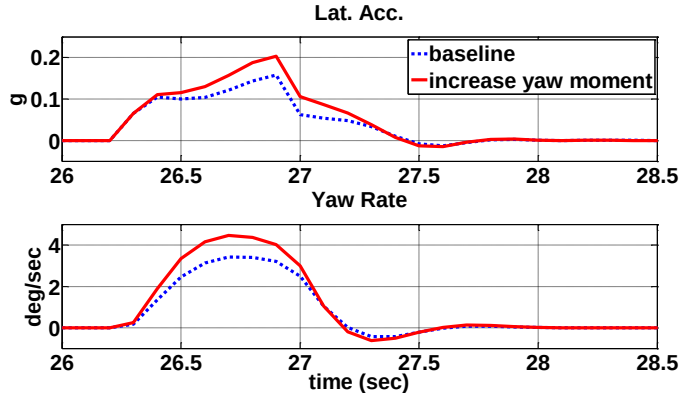

Fig. 2.15 Vehicle response with increased yaw moment coefficient

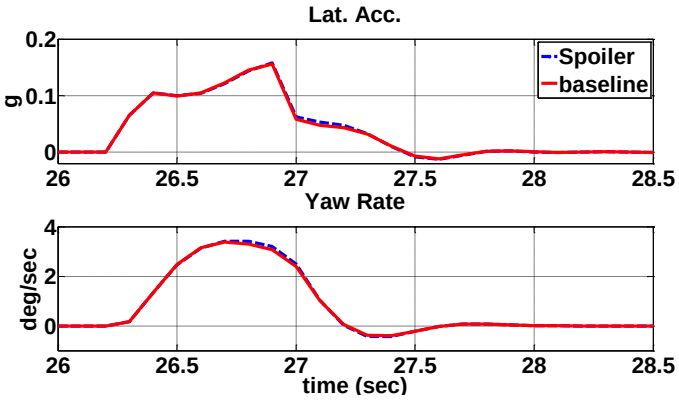

Fig. 2.16 Vehicle response with added spoiler

From the simulation results, it can be seen that the vehicle with increased yaw moment coefficient developed the highest vehicle dynamic response (yaw-rate and lateral acceleration) under the impulse crosswind input and the vehicle with decreased yaw moment coefficient has the smallest response. Since yaw-rate and lateral acceleration are the most dominant vehicle responses for the driver subjective rating, the vehicle with increased yaw moment coefficient can be expected to have the worst crosswind stability assessment.

Twenty-four test subjects were recruited to participate in the driving simulator test. They were asked to perform lane keeping task at their best. Before the test starts, each driver was given ten minutes of introduction and twenty minutes of practice to become familiar with the driving simulator. Each of them then received twelve test runs (five vehicle configurations with impulse crosswind input at two different vehicle speeds, plus baseline and cargo configurations with natural crosswind input). Each run was conducted for two minutes and a three minutes break/setup time was given. Therefore, the total active test time was roughly ninety minutes for each driver, which amounts to thirty-six hours for the whole test. On average, four participants participated in the test each day for a total of six days. Including orientation, CarSim software setup, shipping, setting up and tear-down, the actual test period was about twelve days. A subjective assessment was conducted during the test to obtain subjective evaluation of vehicle stability under different configurations. The questionnaire is shown in Appendix A. The basic information is summarized below:

- Participant information sheet
    - Participants background information.
- Crosswind stability assessment sheet
    - Driving simulator performance assessment
    - Subject vehicle stability assessment

2.2.4 **Summary**

Both an analytical vehicle model (UMTRI wind-steer model) and a complex commercial software (CarSim) model are used. Both models are calibrated against the road test data. The analytical model is implemented in MATLAB/Simulink and is suitable for driver vehicle dynamic response analysis. The CarSim model is used for simulator test and potential AST design. The analytical model (UMTRI wind-steer model) is used to analyze the vehicle crosswind sensitivity. Based on the sensitivity analysis, variation in C.G. position is found to have the highest sensitivity to the crosswind input. Along with four other highest design parameters, five vehicle configurations are implemented for fixed base driving simulator test. Twenty four test participants are recruited and successfully complete the simulator test.

2.3 Simulator Test Analysis

Twenty-four test participants completed the driving simulator test. Each of them finished all designed test runs except participant twenty-one. Due to the temporary steering wheel malfunction, participant twenty-one did not finish the natural crosswind input of the extra -cargo configuration. The steering wheel malfunction was resolved immediately and the remaining participants finished all tests without further difficulty. The participant driving experience information is shown in Appendix B.

2.3.1 **Simulator Test Result**

The test results of twenty-four participants are shown in Fig. 2.17 - Fig. 2.19. Vehicle CG positions are plotted with pave-mark to illustrate the lane-keeping task performance.

At 100 km/h (Fig. 2.17), most participants can control their vehicle such that the C.G. positions stay in the right lane throughout the test.

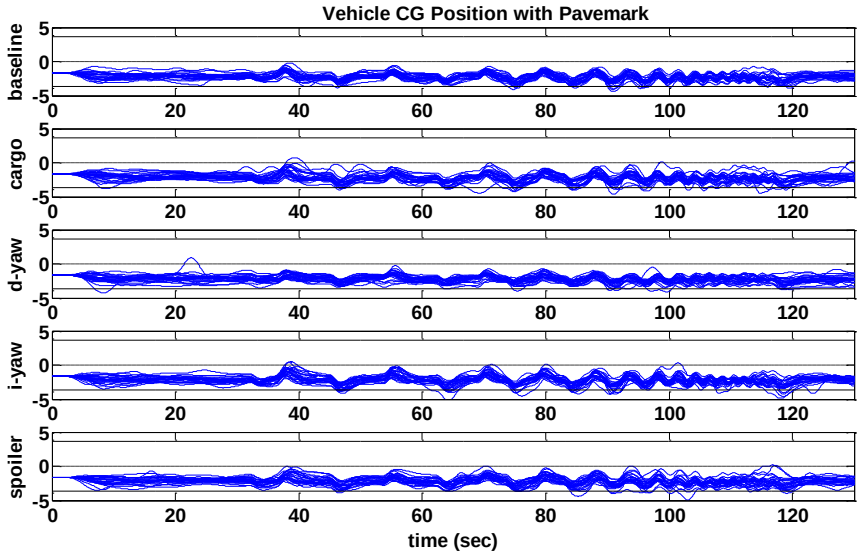

Fig. 2.17 Simulator test data under impulse input (100 km/h)

At higher speed (160 km/h), participants have difficulty maintaining the course and some participants even spin out (Fig. 2.18). The spin-out cases are summarized in Appendix C.

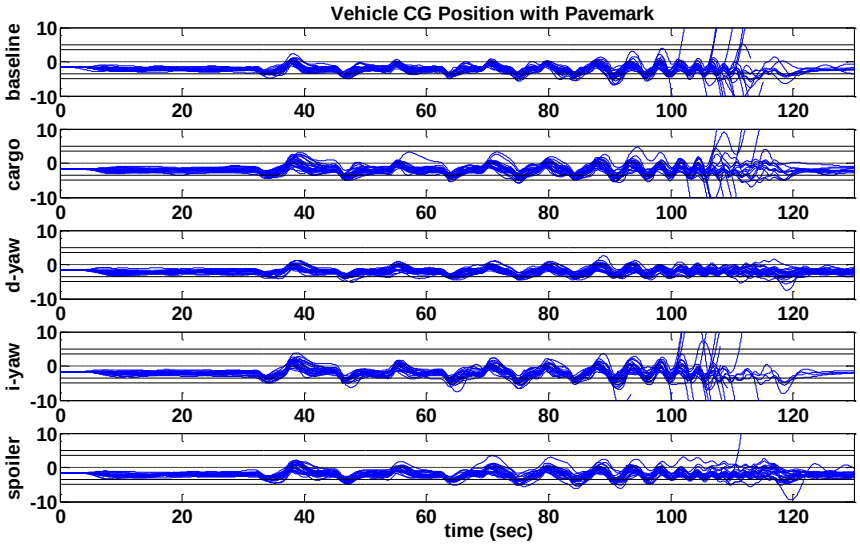

Fig. 2.18 Simulator test data under impulse input (160 km/h)

The natural cross-wind input test results are shown in Fig. 2.19. Only two vehicle configurations are employed in the simulator test. Because the natural crosswind input

magnitude is smaller than the impulse input, participants show better lane-keeping performance. Test results from the baseline vehicle driving at 160 km/h under impulse input will be used to develop a lateral driver model in the next chapter. Test results from other speed and configurations will be used for the verification.

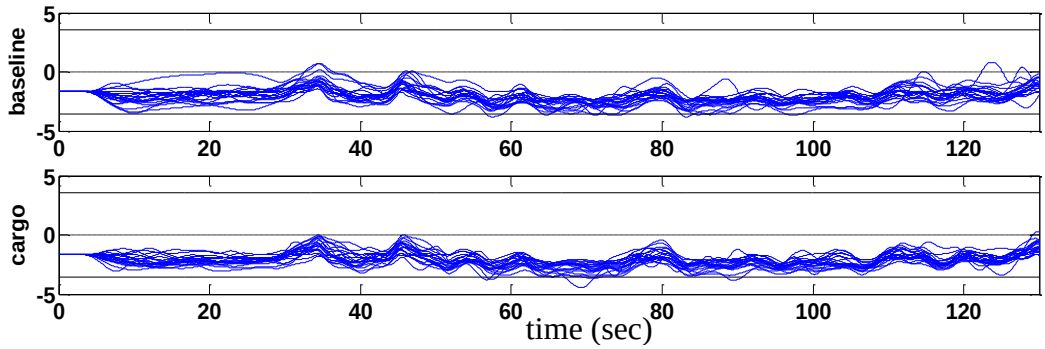

Fig. 2.19 Lateral position of simulation results from natural crosswind input (160 km/h)

2.3.2 **Driving Style Identification**

The driving simulator test results will be used for driver model identification. A driver model structure will be developed and the impulse input crosswind test result will be used to fit the parameters. The impulse crosswind test is selected because identical impulses provide enough excitation and repetition. The impulses 2-5 are used for identification because they are separated enough that the driver-vehicle response would have settled before the next impulse. Fig. 2.20 shows twenty-four participants' yaw-rate responses of impulses 2-5. The four impulses are shifted and plotted on top of each other. It is shown that different driving styles exiting between drivers and even for the same drivers. If driving styles can be categorized, the basis of lateral driving may be able to be identified. And a lateral driving model structure can be developed based on that basis.

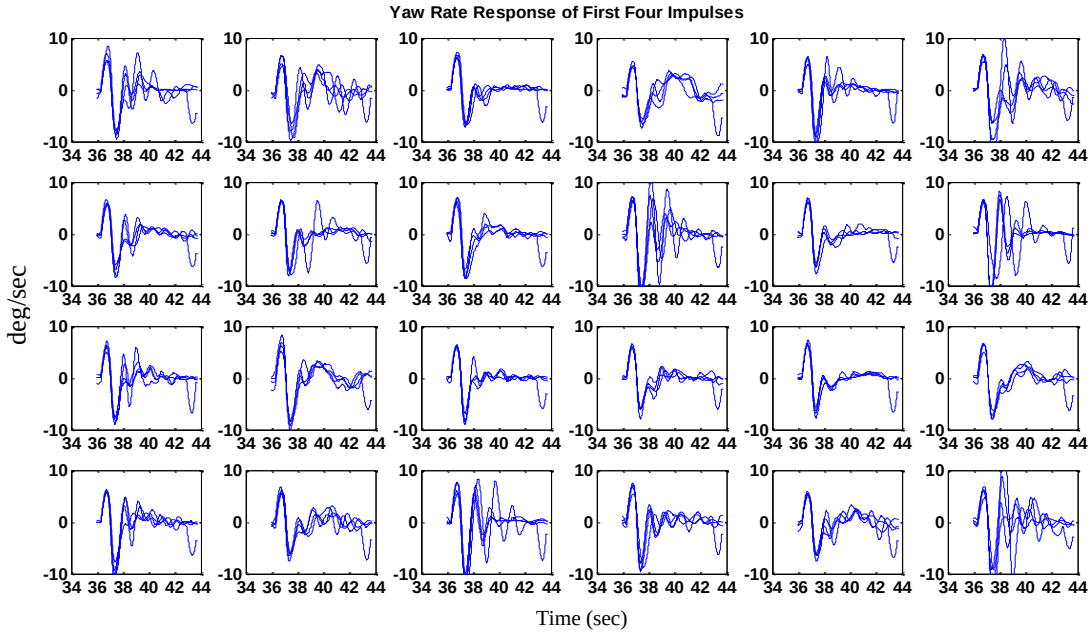

Fig. 2.20 Yaw-rate responses of the first four impulses from all test participants

To help indentifying driving styles and reducing uncertainties, averages of impulses 2-5 response are taken. An example from driver 1 is shown in Fig. 2.21. The four impulse responses are from 35 sec to 70 sec in the original data. They are divided into 8 sec segment and sign conventions of the second and the fourth are modified based on the crosswind direction.

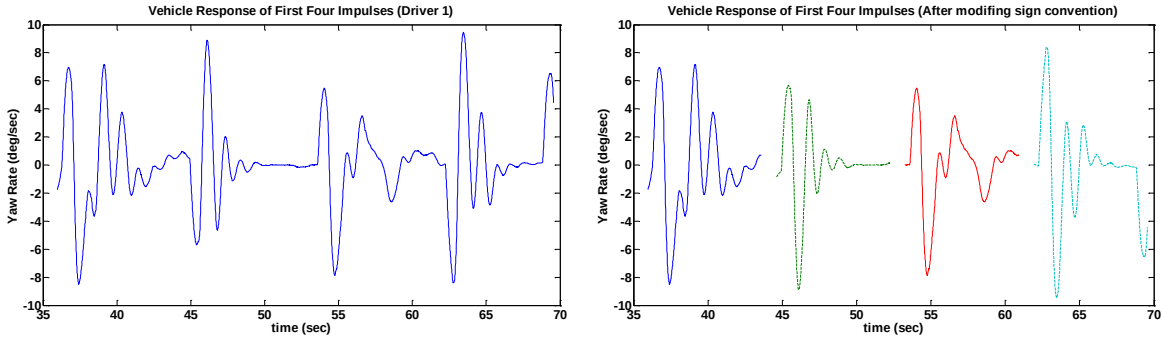

Fig. 2.21 The yaw-rate responses of driver 1 under the first four impulses

The average of driver 1 is calculated and the steering wheel angle and yaw-rate plot is shown in Fig. 2.22.

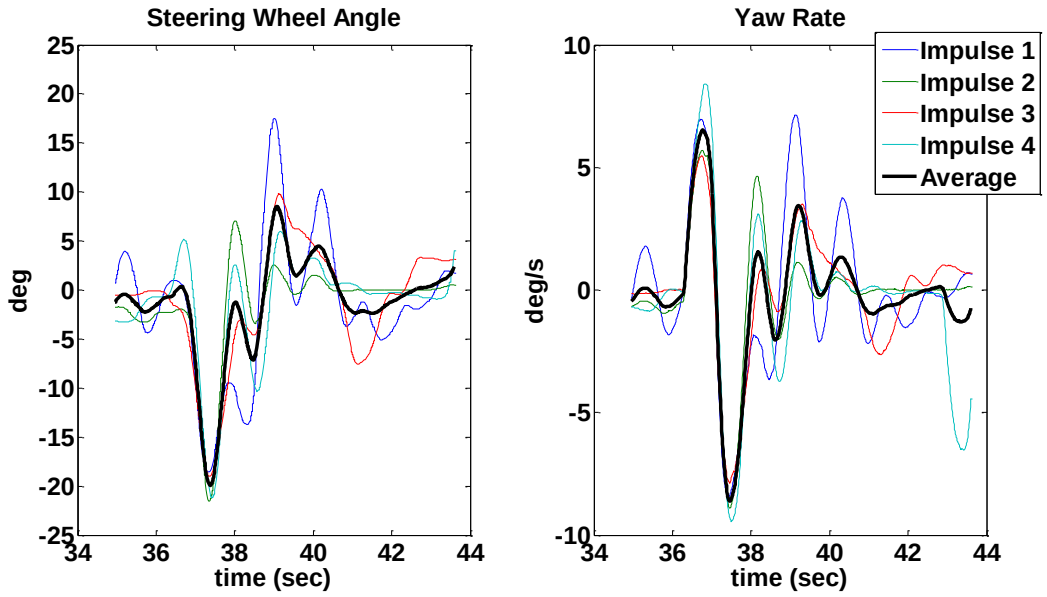

Fig. 2.22 Example plot of steering wheel angle and yaw-rate after averaged

Averages of the twenty-four drivers are calculated and the results are shown in Fig. 2.23. The difference within drivers is reduced and their driving styles can be easier to categorize.

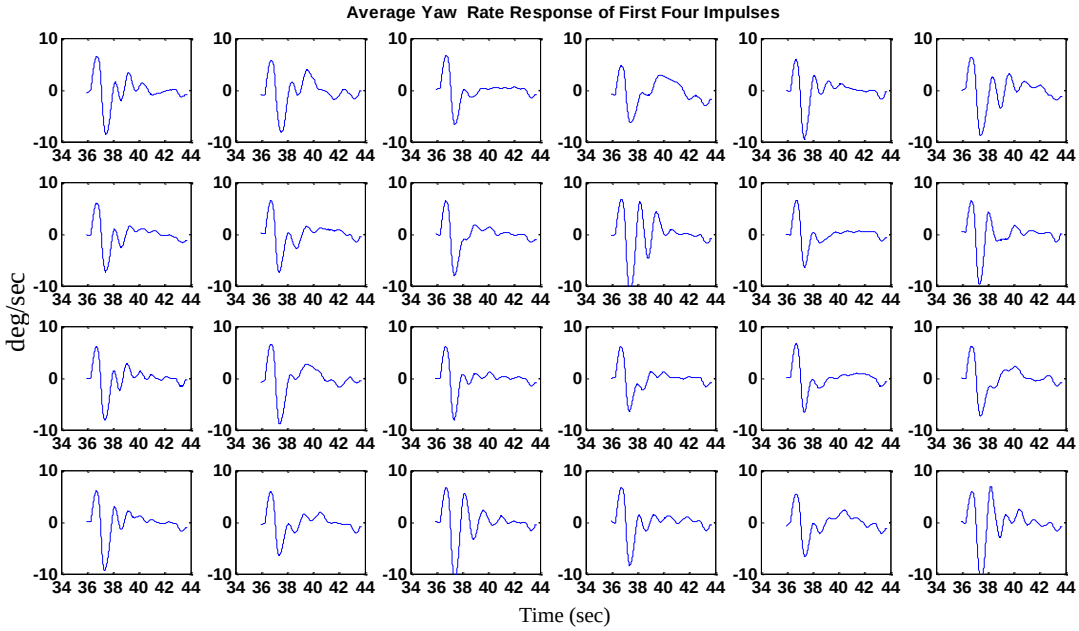

Fig. 2.23 Averaged yaw-rate responses of the first four impulses from test participants

To validate this procedure, the average of the next four impulses are also calculated and compared with the first four (Fig. 2.24). Behaviors in the first four and the

second four impulses responses are very similar, which confirm that the average can better highlight the individual driving style.

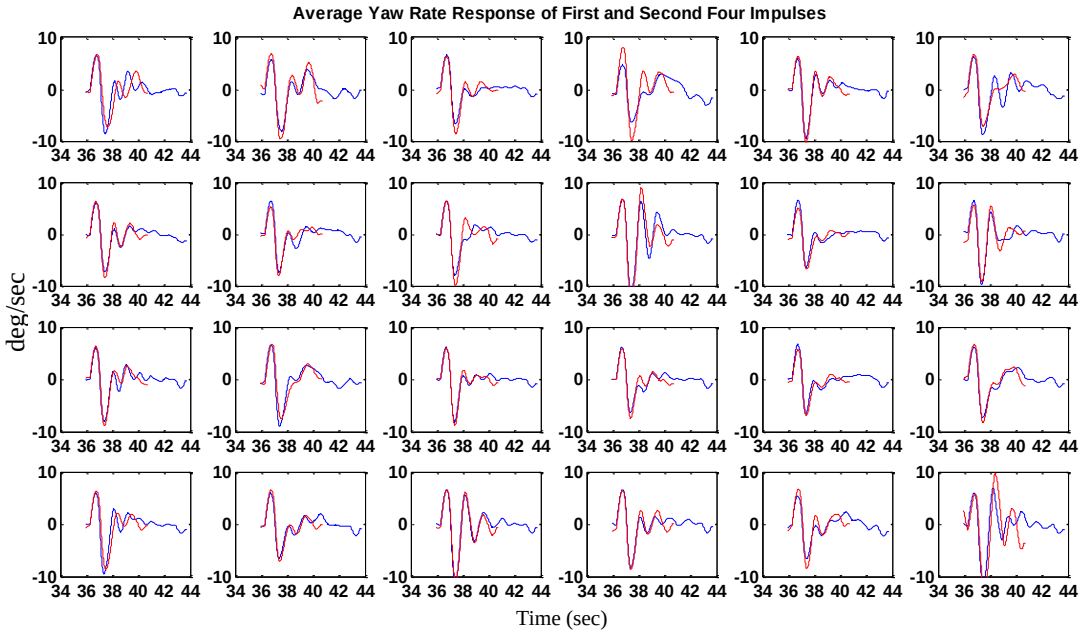

Fig. 2.24 Averaged yaw-rate responses of the first four and the second four impulses

The individual driving styles are categorized into four groups, smooth, rough, precise and over-reacting (Fig. 2.25). Smooth drivers have less oscillations and slower responses; rough drivers have more oscillations but faster responses. The precise drivers have the fewest oscillations and the fastest response. Finally, the over-reacting drivers have the largest overshot. In the next chapter, a lateral driver model will be developed based on the analysis of these four driving styles. A lateral driver model structure will be developed and the model performance will be evaluated using the fitting results of four driving styles.

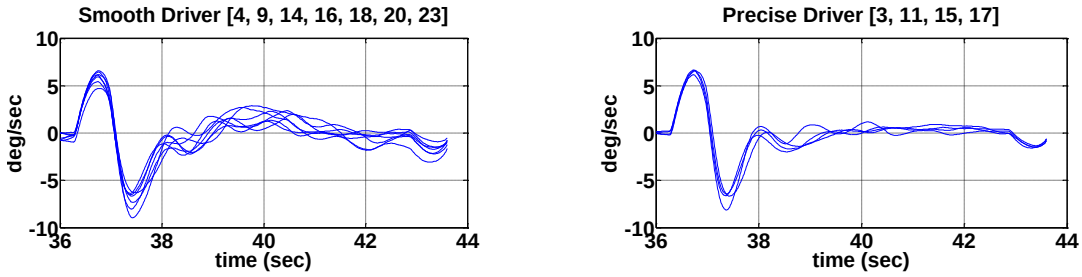

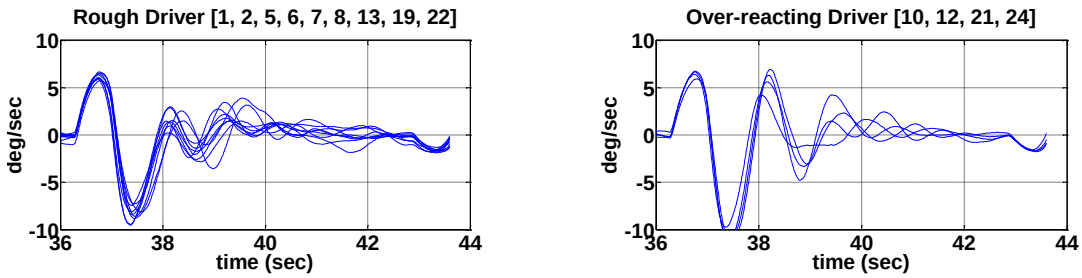

Fig. 2.25 Driving style categorized from averaged impulse responses

2.4 Summary

An analytical vehicle model (UMTRI wind-steer model) is developed for driver vehicle dynamic response analysis and CarSim model is used for the driving simulator test and potential AST design. Both models are calibrated against the road test data. The analytical model is used to analyze vehicle crosswind sensitivity. Based on the sensitivity analysis, variation in C.G. position is found to have the highest sensitivity to the crosswind input. Along with the next four highest design parameters, total five vehicle configurations are selected for the fixed-base driving simulator test. Twenty four test participants are recruited and successfully complete the simulator test. The simulator test results are presented and four driving styles are identified in the impulse crosswind input test. The four driving styles will be used for developing a lateral driver model under crosswind.

CHAPTER 3
LATERAL DRIVER MODEL DEVELOPMENT

3.1 Motivation

The simulator test results are used to develop a lateral driver model under crosswind in this chapter. This driver model can capture driver's behavior under the strong crosswind, including during spin-outs that are observed in the test data. Lateral driver model performance is assessed in both time and frequency domain. A linear analysis is also provided for understanding the stability problem due to driver limitations. Finally, two excises are presented to demonstrate the benefit of this lateral driver model.

3.2 Lateral Driver Model for Strong Crosswind

The goal is to develop a lateral driver model that can capture both normal and anomalous driving behaviors. This driver model needs to be flexible enough for fitting different driving styles and, at the same time, includes driver limitations so that this model will spin out like test participants do. Four driving styles categorized in the previous chapter are used to help understand the fundamental of lateral driving under crosswind. MacAdam's driver model [18] will be a bench-marking model to start with because of its proven performance of modeling the lateral driving. Then, a modification to the MacAdam's model is introduced and its performance is assessed. In time domain, yaw-rate is considered to be the most important index for predicting crosswind stability. So yaw-rate fitting result is our primary performance index. In frequency domain, the model's ability to capture the characteristics of test participants is shown.

3.2.1 **MacAdam's Driver Model**

MacAdam's driver model considers the lateral driving as both prediction and optimization process. The optimal steering input that minimizes the error between desired vehicle states and predicted vehicle states in a preview horizon is calculated. The simplest MacAdam's driver model assumes the steering input remains constant in the preview horizon and considers the lateral displacement as the only desired trajectory to follow. Under a strong crosswind, yaw-rate response is very important for the driver subjective feeling. Therefore, both lateral displacement and yaw-rate are choosing as the desired vehicle states in this study. The resulting cost function in MacAdam's driver model is shown in equation (3.1) and w_r is the weighting for the yaw-rate.

$$J = \frac{1}{T}\int_0^T \left\{ \left[y(t) - y_d(t) \right]^2 + w_r \cdot \left[r(t) - r_d(t) \right]^2 \right\} dt \tag{3.1}$$

The preliminary fitting results (Fig. 3.1) show that the MacAdam's driver model can model general behavior of the crosswind maneuver. However, the MacAdam's driver model is obviously too smooth. It captures the average driving behavior but misses some high frequency contents.

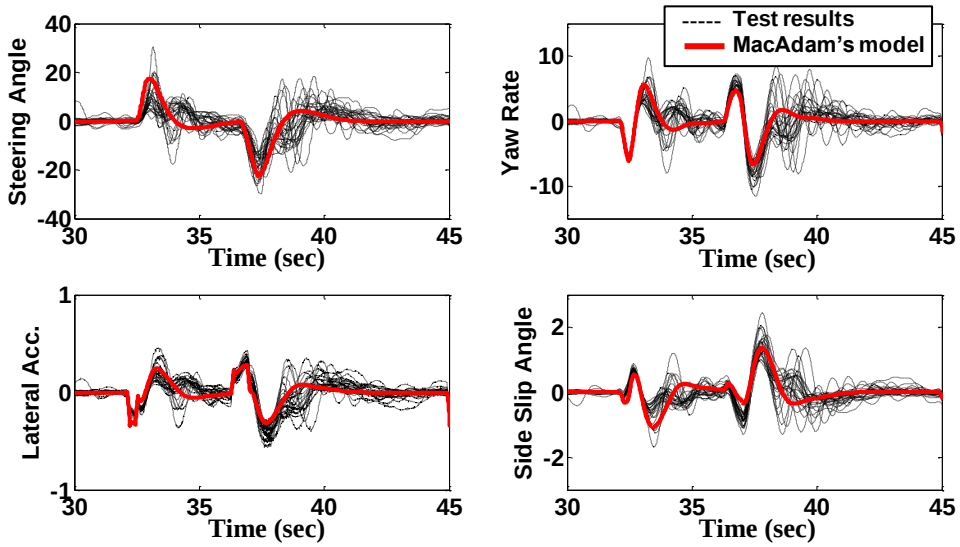

Fig. 3.1 MacAdam's driver model fitting results compared with four driving styles

Fitting residues from the MacAdam's model are significant but interesting (Fig. 3.2). The residues seem to have the shape of an impulse response of second order

systems for all driving styles. This impulse response of second order systems may be a result of an instantaneous feedback reaction to crosswind disturbances. MacAdam's model assumes drivers control the vehicle with preview and prediction mechanisms. Drivers can anticipate future vehicle states and perform optimal driving controls. However, when a unexpected disturbance happened, drivers may not be able to anticipate and some instantaneous feedback reactions may occur. This unanticipated or, perhaps, "panic" behavior can be modeled by an impulse response of second order systems. When drivers encounter a sudden disturbance, an impulse response is induced. The characteristics of this impulse response should be independent to the vehicle because it may be a result of panic, not a result of preview and prediction controls. The impulse will die out depending on the characteristic of the second order system and the MacAdam's model part will regain the control and continue the path following task. The overall crosswind driving behavior can be described by the MacAdam's driver model which dominates the normal lateral driving; and a second order system impulse response which models an instantaneous feedback reaction of crosswind disturbances.

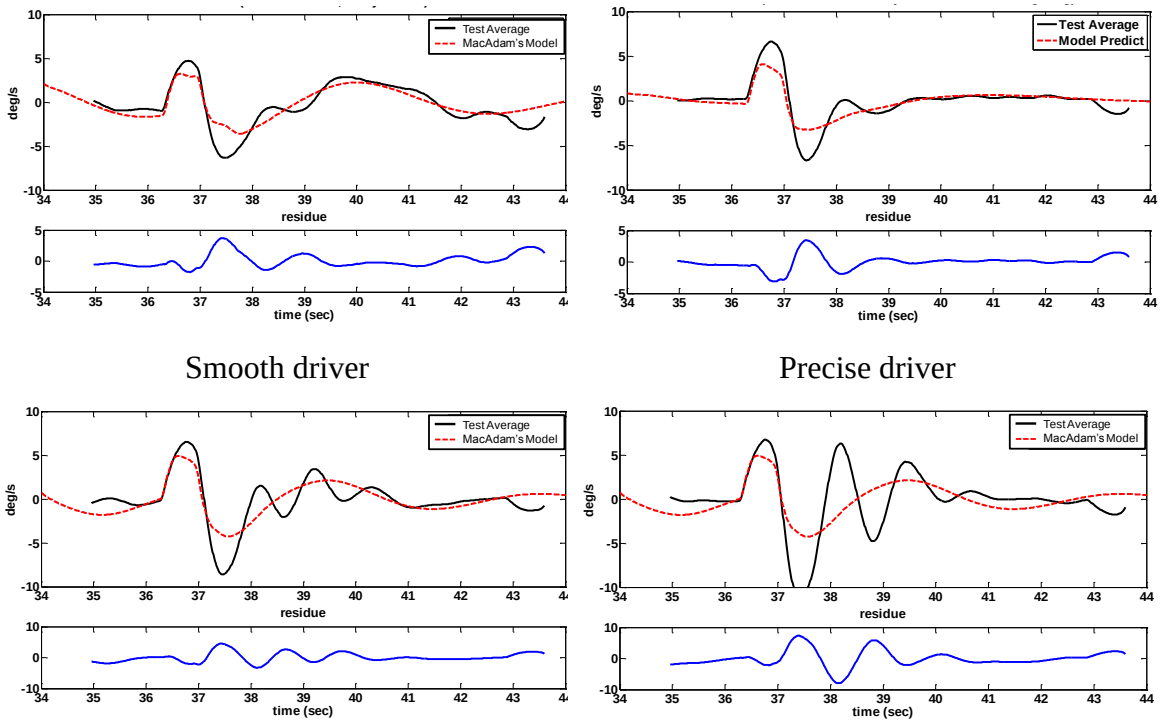

Smooth driver Precise driver

Rough driver Over-reacting driver

Fig. 3.2 Fitting residues of MacAdam's driver model

3.2.2 **Feedback MacAdam's Driver Model**

A new driver model that combines the MacAdam's driver model and an instantaneous feedback reaction for lane-keeping under crosswind disturbances is shown in Fig. 3.3. The desired lateral displacement (y_d) and the desired yaw-rate (r_d) are inputs of the MacAdam's driver model along with the current lateral displacement (y), lateral velocity (Vy), yaw angle (Ψ) and yaw-rate (r) for predicting vehicle future states. Time delay (T_d) is included to model the neuromuscular delay. The instantaneous feedback reaction is modeled as a second order system which has an input: lateral acceleration.

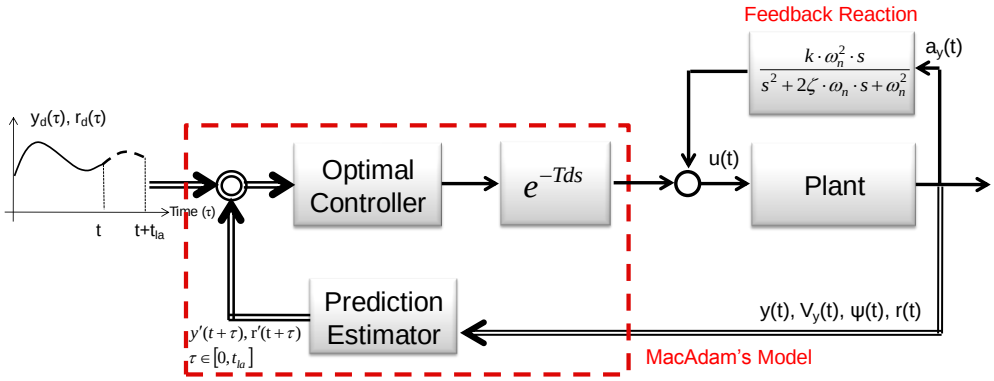

Fig. 3.3 MacAdam's driver model with feedback reaction

This feedback MacAdam's driver model is fitted against four driving styles. One fitting result is shown in Fig. 3.4. The feedback MacAdam's driver model fits steering wheel angle and yaw-rate much better than the original MacAdam's model.

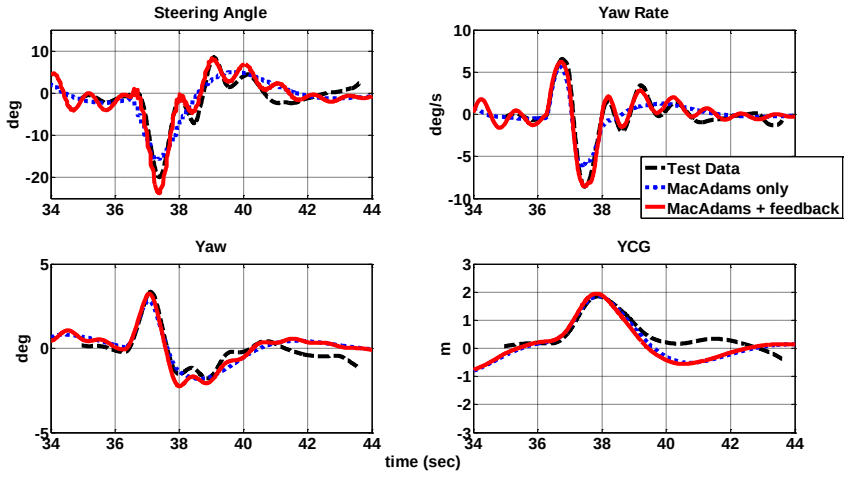

Fig. 3.4 One fitting example of feedback MacAdam's driver model

The feedback MacAdam's driver model is fitted to all four driving styles. The results are shown in Fig. 3.5. The feedback MacAdam's model shows sufficient flexibility to model different driving styles. It can model the slow responses of smoother drivers as well as the excessive over-shoot of over-reacting drivers.

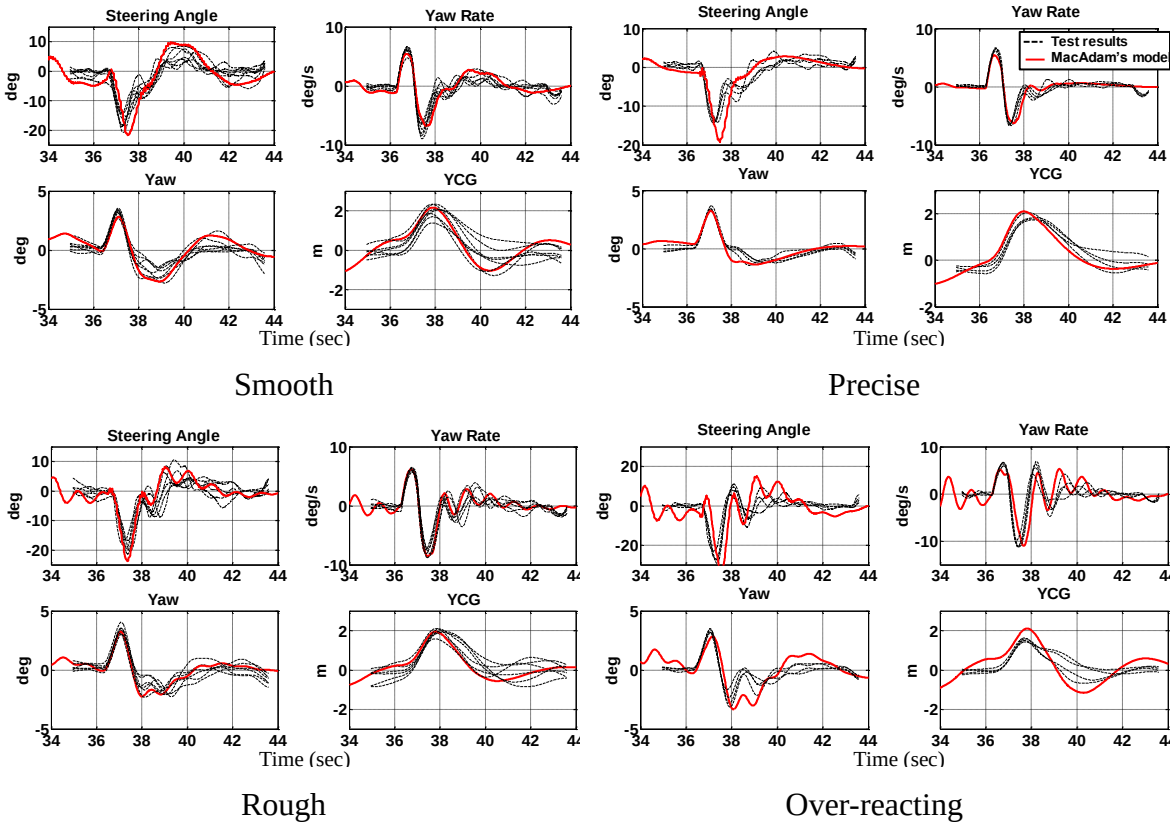

Fig. 3.5 Fitting result of feedback MacAdam's driver model with four driving styles

The RMS error between the yaw-rate of test data and the model prediction yaw-rate is used as a performance index. The smaller RMS error represents a better model fitting performance. The results are shown in Table 3.1. The feedback MacAdam's driver model shows about 20% smaller RMS error than the MacAdam's model. The "precise" driver type has less improvement perhaps because it has the least effect from the feedback reaction, which can be shown in their parameters values (Table 3.2).

Table 3.1 RMS error of yaw-rate prediction comparison

		Rough	Smooth	Over-reacting	Precise
MacAdam's driver model	**deg/s (STD)**	1.116 (0.186)	0.962 (0.228)	2.028 (0.157)	0.789 (0.031)
Feedback MacAdam's driver model	**deg/s (STD)**	0.898 (0.171)	0.770 (0.185)	1.307 (0.252)	0.732 (0.121)
		-19.5%	-20%	-35.6%	-7%

The parameter values of driver models are listed in Table 3.2. Smooth drivers have the largest time delay, hence, slower response. Over-reacting drivers have the largest feedback gain thus excessive over-shoot. Precise drivers have the longest preview time, the smallest feedback gain, and the highest weighting on yaw-rate, all contributing to a better control effort and less panic reaction. The flexibility of the feedback MacAdam's model is demonstrated by fitting different driving styles. The less yaw-rate prediction error verifies the time domain performance of this model. The frequency analysis will be provided in the next section and its ability to model both normal and difficult driving will be demonstrated.

Table 3.2 Parameters of feedback MacAdam's driver model for the four driver types

		Rough	Smooth	Over-reacting	Precise
Parameters for MacAdams Model	**Tp (sec)**	1.7	1.7	1.4	**1.9**
	Td (sec)	0.5	**0.7**	0.4	0.4
	Yaw-Rate Weighting (w_r)	50	150	50	**200**
Parameters for Feedback Reaction	**gain (x10^{-4})**	2.5	1.5	**3.4**	**0.375**
	damping (ζ)	0.63	0.2	0.53	0.2
	stiffness (w_n) (rad/s)	6.32	6.32	7.07	6.32

3.3 Frequency Responses of the Feedback MacAdam's Driver Model

The objective here is to analyze driver behavior under frequency domain and to validate the feedback MacAdam's model. Wallentowiz's method [12] is used to analyze the frequency response. The test data is divided into two sets based on crosswind input frequency (Fig. 3.6). The slow crosswind input includes impulse 2-9. It represents an easier driving task because impulses are separated enough that the driver-vehicle

response would have settled before the next impulse. The fast crosswind input includes all the rest impulses. It is considered as a difficult driving task because most of the test drivers spin out within this region.

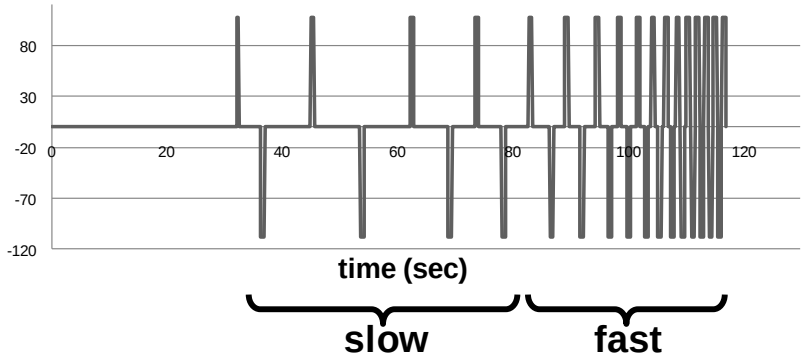

Fig. 3.6 Definition of fast and slow crosswind input for frequency analysis

3.3.1 **Frequency Analysis**

The frequency analysis method proposed by Wallentowiz emphases the relative magnitude of the open-loop vehicle frequency response and the closed-loop driver vehicle frequency response. It is suitable for this research because the driver's effect on vehicle behavior is one of our major focuses. Wallentowiz's method [12] uses measured closed-loop vehicle responses on the real road to the obtain open-loop vehicle response, because direct measurement of the vehicle open-loop response on the real road is difficult. In his method, measured steering angle is used to calculate the yaw-rate due to the steering through a bicycle model. The calculated yaw-rate is then subtracted from the measured yaw-rate. Thus, the driver's steering influence could be removed and the open-loop vehicle yaw-rate due to only crosswind is obtained. However, in a simulator test, direct measurement of the vehicle open-loop response under crosswind is feasible. Therefore, we obtain both vehicle open-loop frequency responses and closed-loop frequency response from simulations directly (Fig. 3.7).

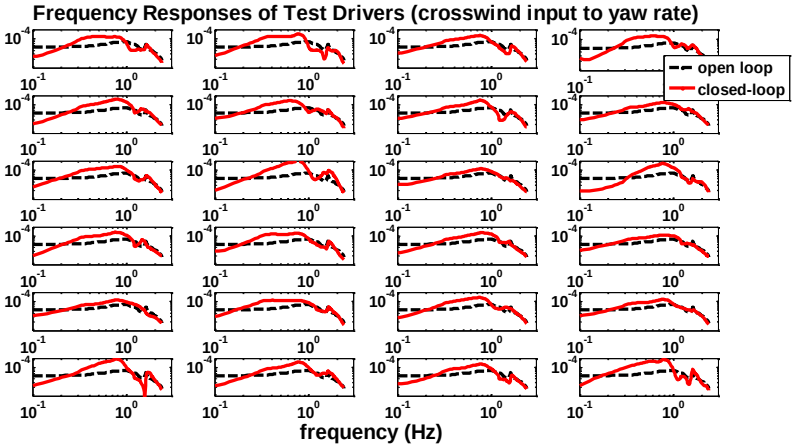

Fig. 3.7 Frequency responses of test participants (160 km/h)

Wallentowiz describes that if the magnitude of the closed-loop frequency response is smaller than the magnitude of the open-loop response, the driver is attenuating the crosswind disturbance (frequently the case in the lower frequency range). If the magnitude of the closed-loop response is larger, the driver is amplifying the crosswind disturbance (in the intermediate frequency range). Finally, if the closed-loop and the open-loop response are close, it means the driver has exceeded his/her bandwidth and no longer controls the vehicle (in the high frequency range). Basically, this analysis is focus on the relative magnitude of the open-loop and the closed-loop response. Therefore, the closed-loop response can be normalized against the open-loop response to simplify this analysis. One example is shown in Fig. 3.8. If the magnitude is lower than one, the driver is attenuating the crosswind disturbance. If the magnitude is larger than one, the driver is amplifying the crosswind disturbance.

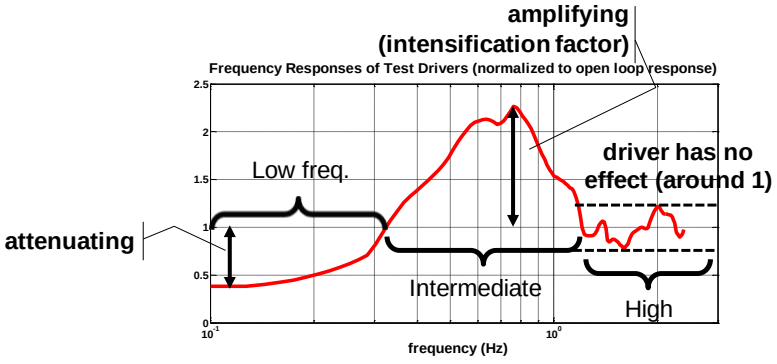

Fig. 3.8 Normalized frequency response

The normalized frequency responses from the slow crosswind input of all twenty-four drivers are shown in Fig. 3.9. In the slow crosswind input, all drivers can attenuate the crosswind effect at lower frequency (< 0.3 Hz). Different drivers have different amplifications at intermediate frequency (0.3-1 Hz). Finally, they all have a bandwidth that they cannot response to crosswind input (> 1 Hz) anymore.

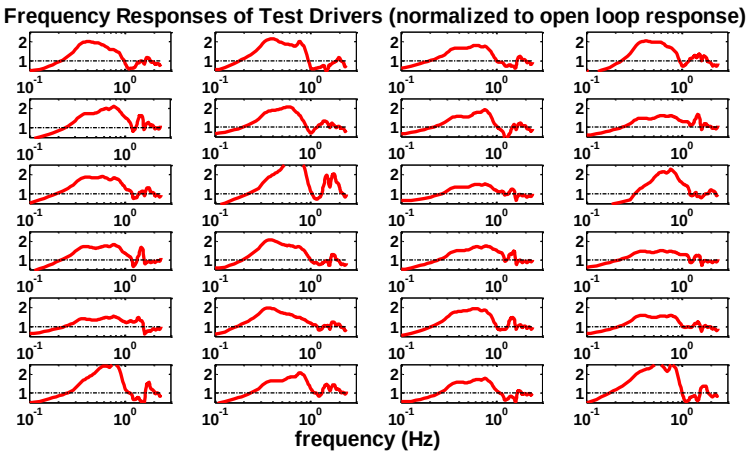

Fig. 3.9 Normalized frequency responses of test participants

In Fig. 2.25, four different driving styles are categorized. The same groups of drivers are plotted in frequency domain (Fig. 3.10). Over-reacting drivers have the highest amplification in 0.3-1 Hz and precise drivers have the lowest amplification. And there is no significant difference between smooth and rough drivers in the frequency analysis. The normalized frequency responses of the MacAdam's model and the feedback MacAdam's model are both calculated and compared with four driving styles.

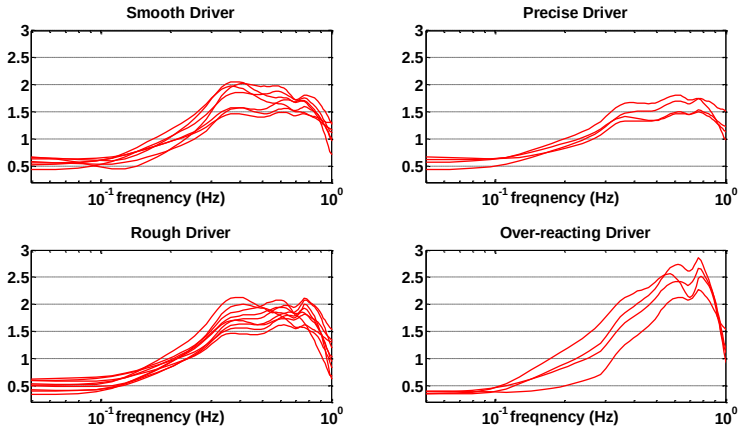

Fig. 3.10 Normalized frequency responses of four driving styles under slow inputs

The normalized frequency responses of the slow and the fast crosswind input are compared in Fig. 3.11. It can be seen that, under fast crosswind input, the attenuation is not as significant as under the slow crosswind input. Most drivers even amplify vehicle responses (normalized frequency responses larger than one) at lower frequencies. This suggests a more difficult driving task in the fast crosswind input than in the slow crosswind input.

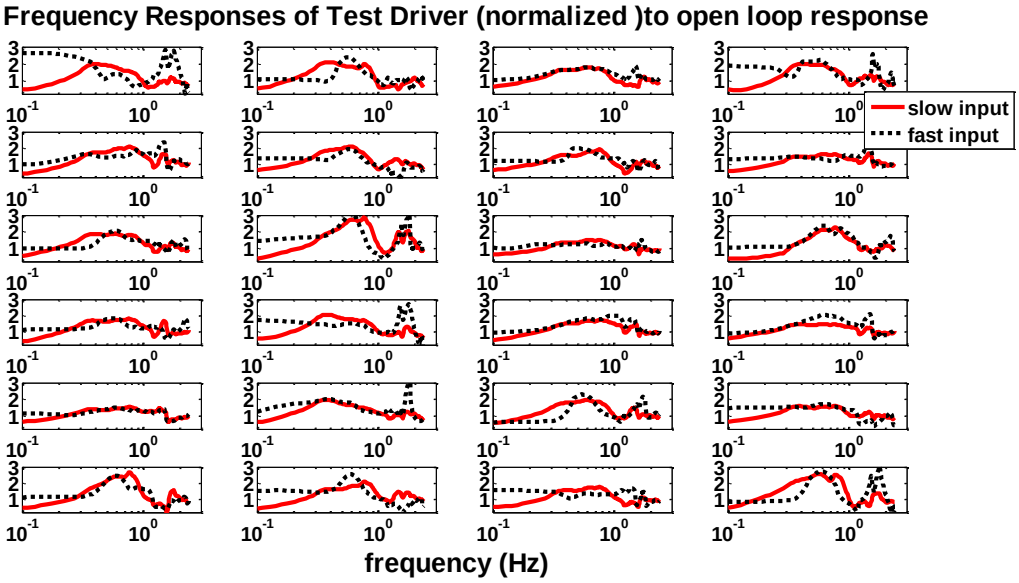

Fig. 3.11 Normalized frequency responses of the twenty-four test participants (fast and slow inputs)

Frequency responses of driver models are shown in Fig. 3.12 and Fig. 3.13 to compare their performance. The MacAdam's model has peak intensification at around 0.2-0.5Hz, which is lower than test drivers (Fig. 3.12). The MacAdam's model also has fewer high frequency components, especially compares with over-reacting drivers. The lack of high frequency components explains the smoother response of the MacAdam's model observed in the time domain. Under the fast crosswind input, the MacAdam's model is also quite different from test drivers. Test drivers have frequency responses around one (which means no attenuation) at frequency below 0.4 Hz and high intensifications above 0.4 Hz. However, the MacAdam's model still shows attenuations at lower frequency and a smoother transaction to higher frequency.

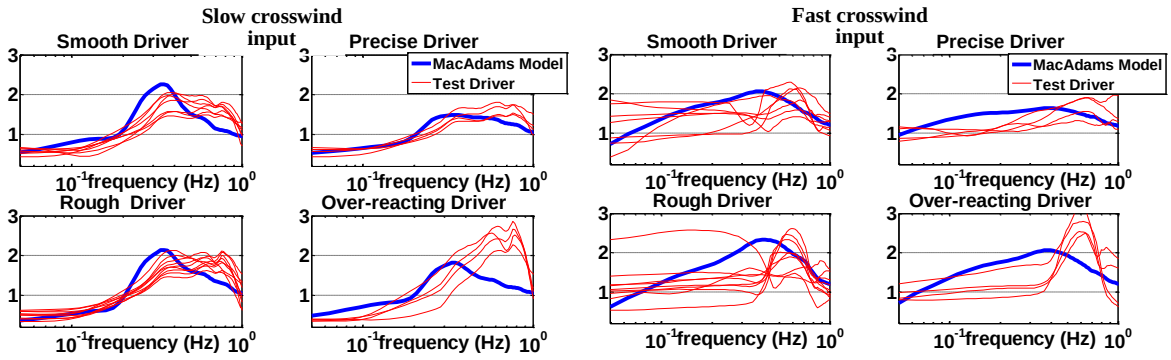

Fig. 3.12 Frequency responses of MacAdam's driver model compared with test participants

The frequency response of the feedback MacAdam's driver model is shown in Fig. 3.13. Under the slow crosswind input, the feedback MacAdam's model has high frequency contents, which is similar to frequency responses of test drivers. Under the fast crosswind input, the feedback MacAdam's model has a low frequency response around one and a high intensification above 0.4 Hz. Both are similar to test drivers.

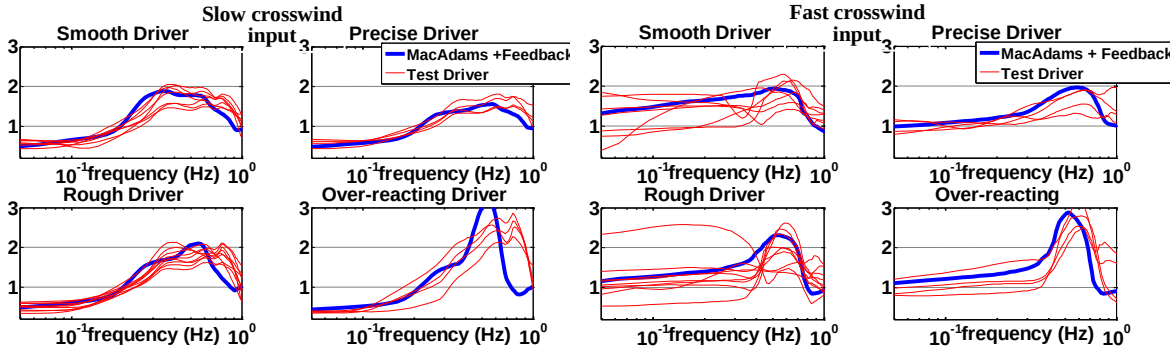

Fig. 3.13 Frequency responses of feedback MacAdam's driver model compared with test participants

3.3.2 **Summary**

A lateral driver model is developed to obtain closed-loop vehicle responses under crosswind. This developed driver model is a combination of the MacAdam's driver model and an instantaneous feedback reaction of crosswind disturbances. Time and frequency responses of this driver model are compared with the MacAdam's driver model. In the time domain, the feedback MacAdam's driver model has smaller RMS yaw-rate error with the test data. In the frequency domain, the feedback MacAdam's driver model also has much similar frequency components in both slow and fast

crosswind input. The feedback MacAdam's model is shown to be able to model the human normal driving behavior under crosswind. In the next section, the analysis of anomalous behaviors under crosswind will presented and the ability to model those behaviors, which lead to driving accident, will also be shown.

3.4 Lateral Human Anomaly Behaviors Leading to Driving Accident

The goal of this example is to analyze crosswind induced vehicle stability problems and driving accident induced by human driver's limitations. One effect of the vehicle instability under crosswind is spin-out, which is observed in Fig. 2.18. In this section, a linear analysis is provided to explain behaviors that lead to spin-out. Simulations is also used to verify the analysis.

3.4.1 Lateral Driving Accidents under Strong Crosswind Wind

One significant driving accident observed in the simulator test is the spin-out. All participants handle the lane-keeping task very well at the 100 km/h impulse input but most of them spin out at the 160 km/h impulse input. During the 160 km/h impulse input, participants can control the vehicle when crosswind input frequency is slower than 0.1Hz (< 80 sec in the test time). Seventeen out of twenty-four participants spin out when crosswind input frequency is faster than 0.1 Hz (80-120 sec in the test time) (Fig. 3.14). In the following section, we will analyze driver behaviors that cause spin-outs in the driver vehicle stability point of view.

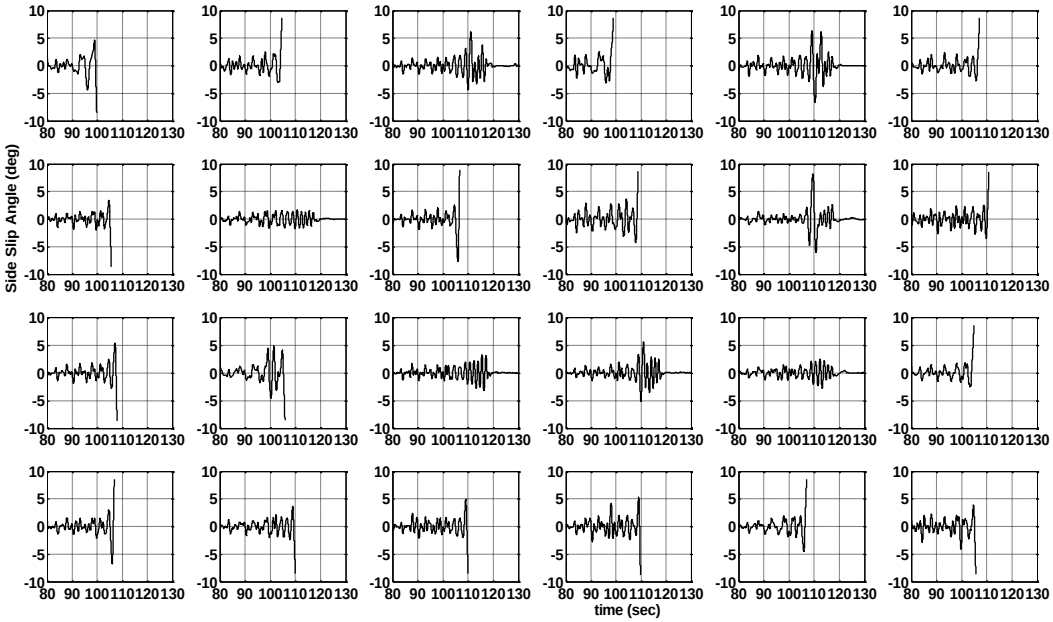

Fig. 3.14 Vehicle side slip angle in spin-out accidents (160 km/h baseline vehicle)

3.4.2 **Linearized Driver Vehicle Model**

The analysis is based on a linearized model. Closed-loop poles of the linearized system are used to indicate the system stability. The proposed model structure includes a block based on the MacAdam's model which provides the preview/predictive functions. The preview/predictive functions are non-linear for the general path following. However, the MacAdam's model can be approximated as a constant feedback controller in lane-keeping maneuvers. As shown in Fig. 3.3, the MacAdam's model has two processes: prediction of future vehicle states in a preview horizon and calculation of the optimal control input that minimizes the error between desired vehicle states and predicted future vehicle states. In this example, we assume the MacAdam's model uses a linear vehicle model for the prediction, so that future vehicle states in a preview horizon only depend on initial vehicle states. Desired vehicle states in the lane-keeping maneuver are assumed to be zero (zero lateral displacement and zero yaw-rate). Therefore, the optimal control input is only depends on predicted vehicle states. Thus, the optimal control input is actually only depends on the initial vehicle states. The MacAdam's model can be approximated as a constant gain state feedback controller with a delay (Fig. 3.15).

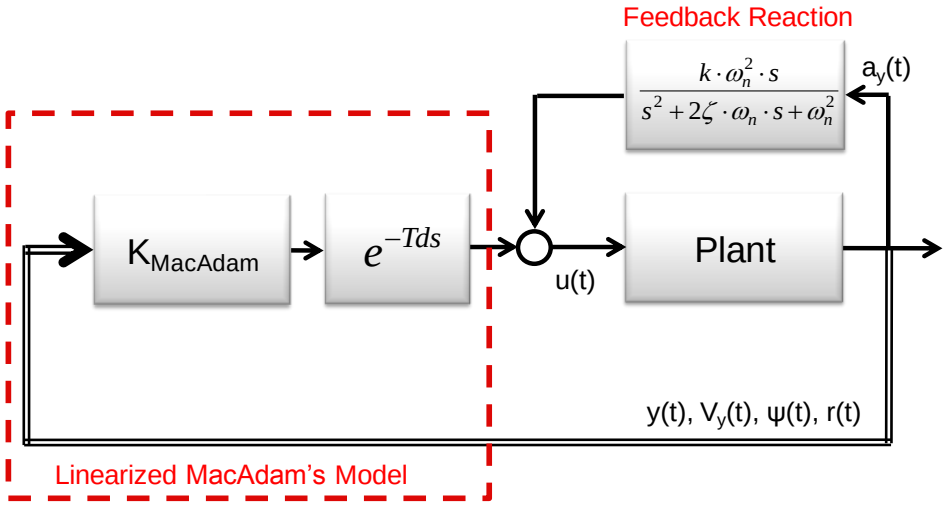

Fig. 3.15 Linearized driver/vehicle system diagram

The constant gain $K_{MacAdam}$ depends on the linear vehicle model, preview time (T_p) and the yaw-rate weighting (w_r). Detailed derivation of $K_{MacAdam}$ can be found in Appendix F. Furthermore, time delay T_d is replaced with a second order pàde approximation. Therefore, poles of the linearized driver/vehicle system can be obtained.

3.4.3 **Driver Limitation Analysis**

There are two questions regarding this analysis: what cause the instability and how severe they can be? In the fixed based simulator test, the open-loop vehicle response is deliberately designed to maintain the stability at both 100 and 160 km/h. However, seventeen out of twenty-four participants spin out during the 160 km/h test. Participants is asked to perform at their best to stay in the lane and there must be some limitations that prevent them doing so. The first possible limitation would be the driver's time delay. Time delay is inherited in all drivers with different length. The linear model is used to analyze the stable limit of time delay at a given preview time and a yaw-rate weighting. A root contour of the dominate poles location is plotted by varying preview time and time delay.

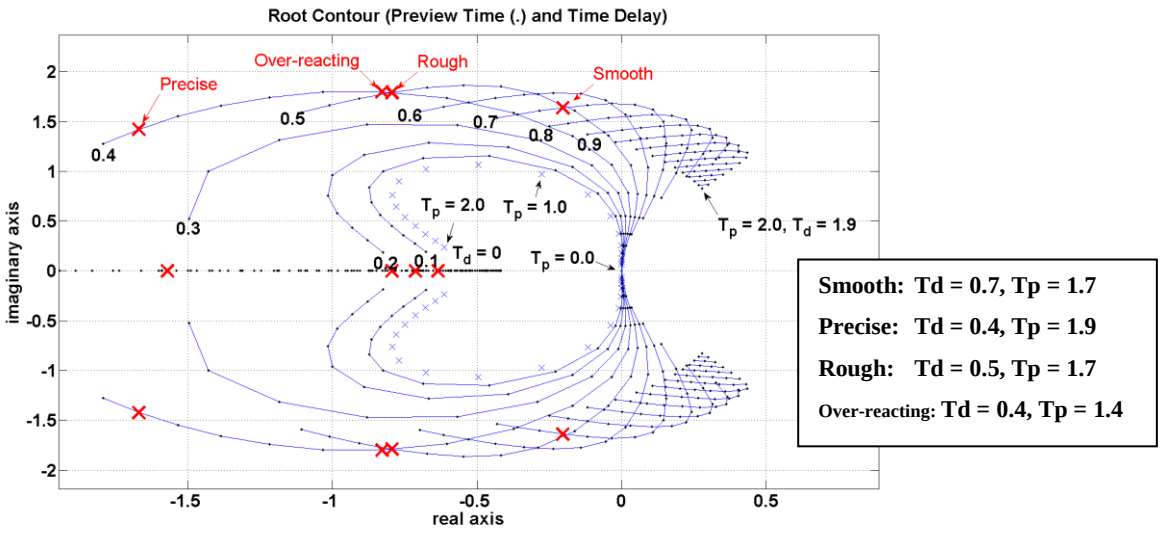

Fig. 3.16 Root contour plot with varying preview time and time delay

The contour starts with a fixed T_d, then increasing T_p from "T_d+0.1" sec to 2.0 sec. For example, if T_d is zero, then T_p is increased from 0.1 sec to 2.0 sec. By doing so, T_p is always larger than T_d. In Fig. 3.16, increasing preview time moves poles to the left and increases the stability. On the contrary, if time delay is larger than 0.4 sec, increasing time delay decreases the stability. The maximum time delay allowable for maintaining the stability can be summarized in Fig. 3.17. For example, if the preview time is 2 sec, time delay cannot be longer than 1 sec. Without the weighting on yaw-rate, time delay needs to be shorter than about half of the preview time. With the weighting on yaw-rate, the model can tolerate longer time delay for the same preview. However, the effect of adding the yaw-rate weighting is small comparing with the effect of time delay. Therefore, we will not focus on yaw-rate weighting in the following analysis.

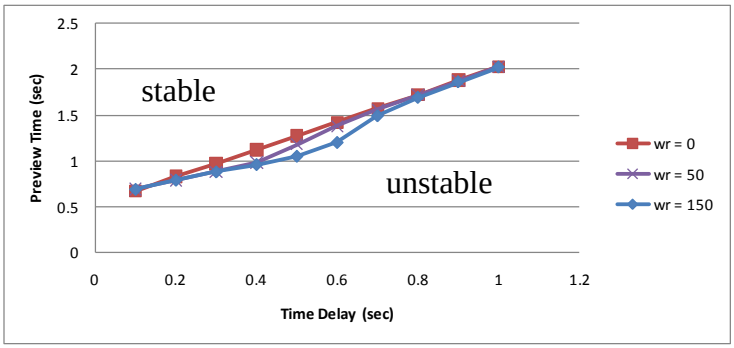

Fig. 3.17 Stability limits of preview time and time delay

Based the analysis, the original MacAdam's model itself can result a spin-out if time delay is large enough or preview time is too short. However, time delay and preview time identified in the test data (in lower crosswind input frequency) are not sufficient for causing instability. Therefore, only time delay is not enough to explain spin-outs in the simulator test. The spin-out happened under high frequency crosswind inputs is either caused by participants' increasing in time delay (which is unlikely) or other mechanisms. The second order system used to model the instantaneous feedback reaction behavior is another possible source of instability. The instantaneous feedback reaction is hypothesized to be a result of panic. Some drivers (precise drivers) assumed to have more experience and confidence that they have small gain in the second order system. Some drivers (over-reacting drivers) have limitations in their control performance and, literately, over-react to the disturbance. The effect of the gain in the second order system is analyzed by a root contour plot with varying the gain and time delay (Fig. 3.18).

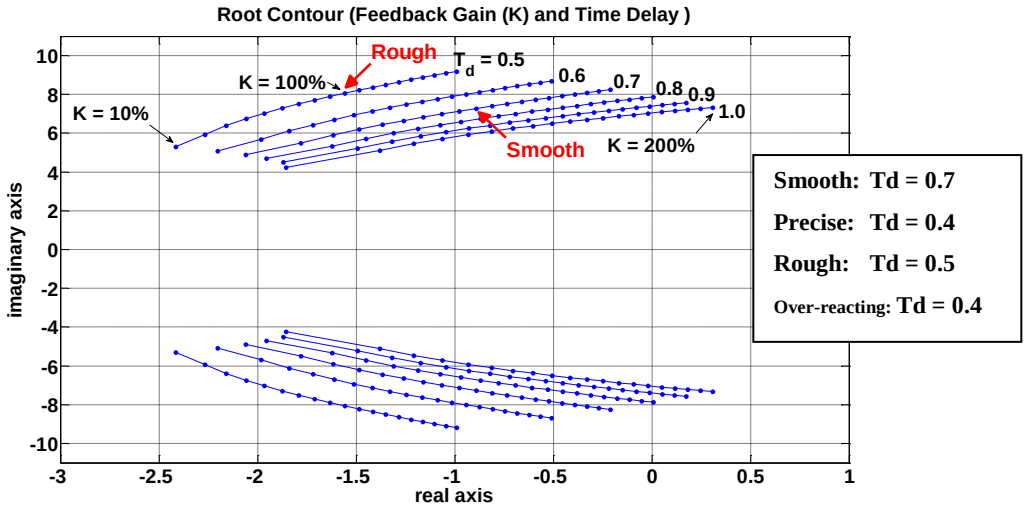

Fig. 3.18 Root contour plot with varying feedback gain and time delay

The second order system gain identified in the test data is varied from 10% to 200%. The analysis shows that increasing the gain moves poles to the right hand side, which decreases stability. However, the second order system gain and time delay identified under the slow crosswind input are still not severe enough to induce instability. This may explain why all participants can maintain stability during the slow crosswind

input. The mechanism that causes spin-outs during fast crosswind input needs further investigation.

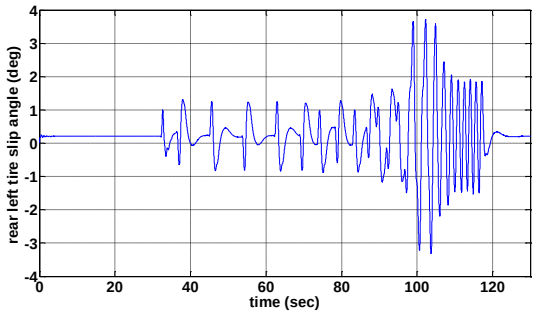

Fig. 3.19 Tire slip angle from CarSim simulator during the impulse input of 160 km/h

Another source of instability is driver's inability to have a perfect internal model. In the MacAdam's model, the driver uses a linear internal model to predict vehicle's future states. The nominal model is linearized assuming the constant forward speed and the zero slip angle. When large vehicle motion is induced (by crosswind), large tire slip angle is generated (Fig. 3.19) and the linear assumption may not be valid anymore. In Fig. 3.20, the actual tire force of front and rear tires from the CarSim is plotted compared with the linear approximated tire model. The right hand plot shows the approximation error in percentage. Despite the large numerical error around the zero slip angle, the approximation error of the linear tire model is small when tire slip angle is small (< 1 deg). However, the approximation error can be very significant when the tire slip angle increases (> 1 deg) and tires become saturated. We assume the driver does not know it and steer the vehicle as if tires can satisfy the lateral force demand. This will introduce additional stability problem.

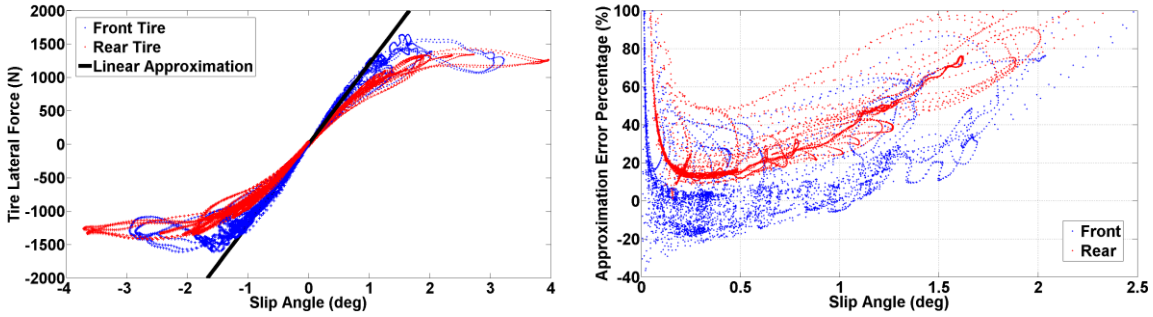

Fig. 3.20 Error between actual tire force and force predicted by a linear tire model

To model the stability problem induced by model uncertainties, the constant state feedback gain ($K_{MacAdam}$) that used to approximate the MacAdam's model is first obtained based on the nominal vehicle model and corning stiffness. Then, the cornering stiffness in the linear vehicle model is varied to study the possible effect of model uncertainties. The root contour with model uncertainties and time delay is plotted in Fig. 3.21. The percentage in model uncertainties represents the variation in the cornering stiffness of both front and rear tires. The increasing of model uncertainties will move system poles to the right. When 30% model uncertainty is introduced, smooth driver becomes unstable. 30% model uncertainty due to the error of linear tire model approximation exists when slip angle is larger than one degree (Fig. 3.20).

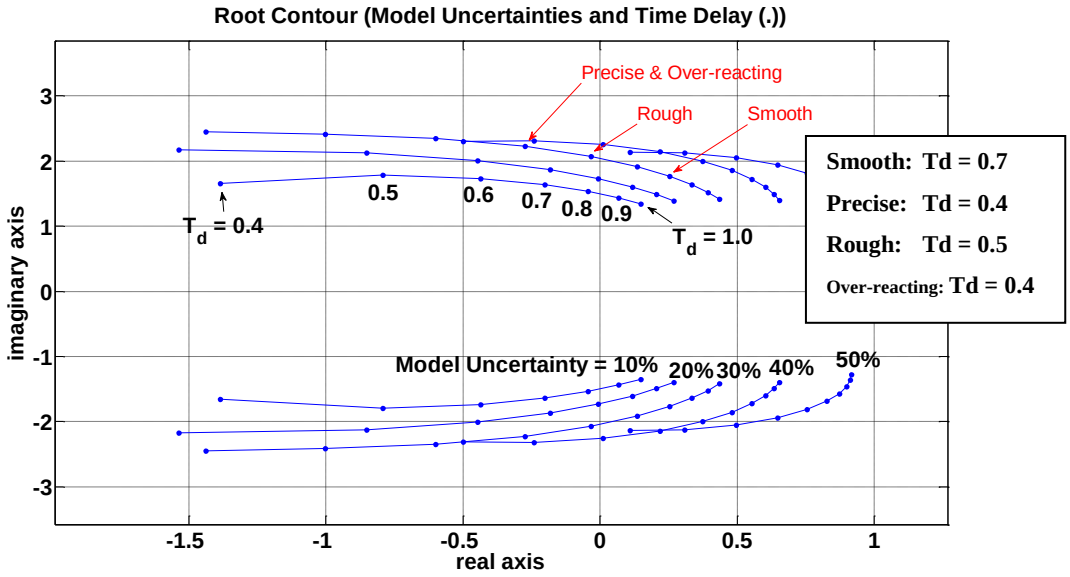

Fig. 3.21 Root contour with varying model uncertainties and time delay

The model uncertainties become significant when tire slip angle is large (> 1 deg). Large tire slip angle is generally observed under high frequency crosswind input in the simulator test. As shown in Fig. 3.19, one degree of tire slip angle is easily exceeded after 80 sec in simulation. This may explain why participants can handle the lower frequency crosswind input but spin out after 80 sec in simulation. Under the lower frequency crosswind input, participants can control the vehicle even with time delay and panic behaviors because tires are not saturated and the linear assumption holds. At higher frequency, tires are saturated due to large tire slip angle induced by both

crosswind and drivers themselves. The model uncertainties increases and driver vehicle/system becomes unstable.

3.4.4 **Simulation Results**

Twenty-four sets of parameters were fitted from the test drivers under impulse input 160 km/h (Appendix E). Those twenty-four sets of parameters are used to simulate the spin-out (Fig. 3.22). The MacAdam's model with time delay as the only instability components was simulated first. In the twenty-four sets of parameters, only eight of them spin-out. The feedback MacAdam's models were, then, simulated and nineteen of them spin-out because the extra unstable component in the feedback part.

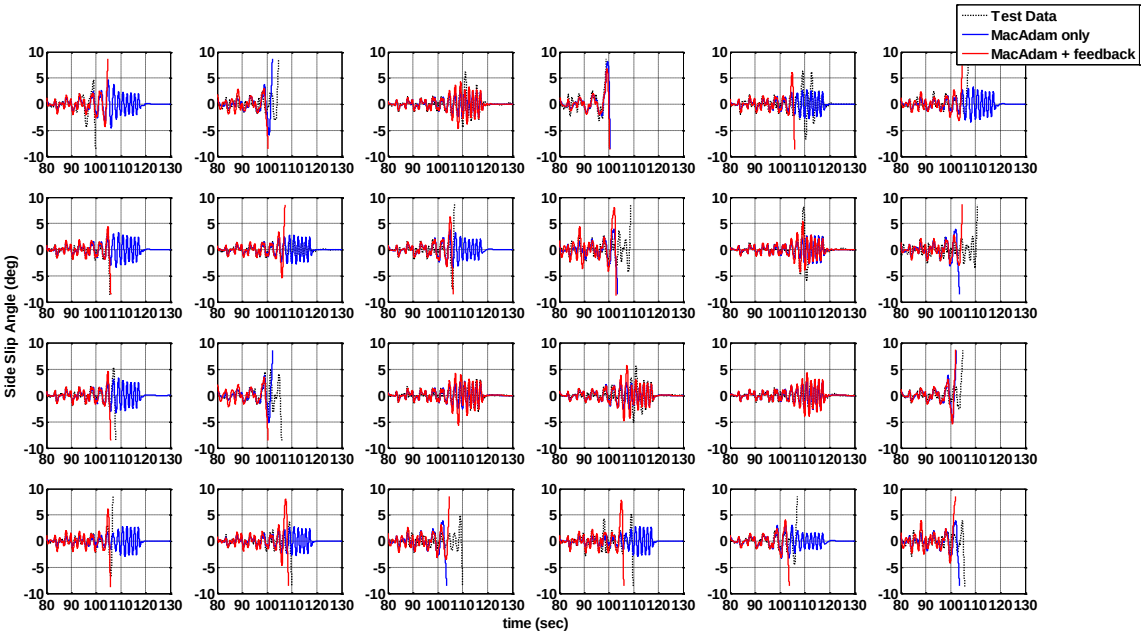

Fig. 3.22 Model predicted spin-out accident compared with test data

The simulation result is summarized in Table 3.3. Among the seventeen participants who spin-out, the MacAdam's model only captures eight of them (2, 4, 10, 12, 14, 18, 21, and 24). The feedback MacAdam's model can model all seventeen spin-outs observed in test participants, but it introduces two more spin-outs that is not observed in tests (5 and 8). Only time delay in the original MacAdam's model is not enough to capture all seventeen spin-out participants' behavior. The MacAdam's model with feedback reaction is needed to capture more spin-out behavior.

Table 3.3 Model predicted spin-out accident compared with test data

sec	1	2	3	4	5	6	7	8	9	10	11	12
Test Data	**Spin-out**	Spin-out	N/A	Spin-out	N/A	**Spin-out**	**Spin-out**	N/A	**Spin-out**	Spin-out	N/A	Spin-out
MacAdam only	**N/A**	Spin-out	N/A	Spin-out	N/A	**N/A**	**N/A**	N/A	**N/A**	Spin-out	N/A	Spin-out
MacAdam + feedback	**Spin-out**	Spin-out	N/A	Spin-out	Spin-out	**Spin-out**	**Spin-out**	Spin-out	**Spin-out**	Spin-out	N/A	Spin-out
	13	14	15	16	17	18	19	20	21	22	23	24
Test Data	**Spin-out**	Spin-out	N/A	N/A	N/A	Spin-out	**Spin-out**	**Spin-out**	Spin-out	**Spin-out**	**Spin-out**	Spin-out
MacAdam only	**N/A**	Spin-out	N/A	N/A	N/A	Spin-out	**N/A**	**N/A**	Spin-out	**N/A**	**N/A**	Spin-out
MacAdam + feedback	**Spin-out**	Spin-out	N/A	N/A	N/A	Spin-out	**Spin-out**	**Spin-out**	Spin-out	**Spin-out**	**Spin-out**	Spin-out

The hypothesis behind two spin-outs that do not happened in the simulator test is: participants changed their driving strategy during the high frequency crosswind input. Some drivers panicked and increased the steering motion, which can be modeled by the feedback reaction module. However, some may released the steering wheel so that they wouldn't spin out. This time-varying behavior was not modeled, therefore, two unexpected spin-out happened in simulations.

3.4.5 **Summary**

A linearized driver/vehicle model is used to analysis the stability under crosswind. The preview/prediction function of the MacAdam's model is simplified as a constant state feedback control and time delay is approximated by a second order pàde transfer function. The closed-loop system poles location is used in determine the system stability. The analysis shows that increasing preview time can increase the system stability. And increasing time delay, the feedback gain, and model uncertainties will decrease the system stability. Simulation results show that the feedback MacAdam's model can capture twenty-two out of twenty-four participants in terms of spin-out occurrences. Two case that are unable to modeled may due to the time-varying natural of human.

3.5 Application of the Crosswind Driver Model

A lateral driver model under crosswind is developed. This model uses the MacAdam's driver model for the path following and augments it with a second order system to

simulate panic behavior under the sudden crosswind input. Two excises will be provided in this section to demonstrate applications of this feedback MacAdam's model. In section 3.5.1, closed-loop vehicle responses under crosswind will be obtained using the feedback MacAdam's model and results will be used to evaluate the vehicle crosswind stability. In section 3.5.2, the feedback MacAdam's model will also be used to evaluate active safety systems for improving crosswind stability. Some preliminary analysis will be done for demonstrating the effectiveness of active safety systems and the benefit of using the feedback MacAdam's driver model in the design process.

3.5.1 **Vehicle Stability Assessment**

One major challenge in the vehicle design process is to evaluate the vehicle crosswind stability. Crosswind stability of different vehicle configurations and forward speeds are often evaluated by the driver subjective rating. High level of uncertainty is unavoidable. Therefore, an objective assessment based on the vehicle response measurement is desired for a more precise vehicle crosswind stability evaluation. This objective assessment needs to have high correlation with the subjective rating so that it can be used to predict driver's preference. Meanwhile, a simulation based assessment is also desired such that time and cost can be minimized. The open-loop vehicle crosswind sensitivity is widely used because of its simplicity and sufficient correlation with the subjective rating. Therefore, the open-loop vehicle crosswind sensitivity is first studied. The correlation between the open-loop crosswind sensitivity and the subjective rating is calculated as the bench-mark. Then, a closed-loop objective assessment is proposed and the improvement over the open-loop sensitivity is shown. Finally, a simulation based objective assessment which utilizes the feedback MacAdam's model is presented.

To calculate the correlation, the subjective rating is first obtained from test participants during the fixed based simulator test (section 2.2.3). A 10-point scale is used to rank each configuration regarding driver's general impression of the vehicle stability. A vehicle configuration described as "uncontrollable" would receive a value of 1. Value of 10 would indicate that there is no perceived effect of crosswind. During tests, learning effect is observed and drivers tend to give later configurations higher score perhaps because they perform better in tests due to learning. Therefore, the configuration test

order is shuffled; Twenty-four participants are divided into four different order groups. Furthermore, starting from participant thirteen, a repeated run of baseline vehicle at 160 km/h is added to quantify the learning effect. The subjective rating (listed in Appendix D) is plotted in Fig. 3.23. Their corresponding test order is listed as the label of the x-axis. The bar height represents the average score and the error bar represents one standard deviation. Started from participant thirteen, a repeated run of baseline vehicle at 160 km/h is added as shown by the black error bar. Participants tend to rate the repeated run of baseline vehicle at 160 km/h higher than the original run. A significant learning effect exists.

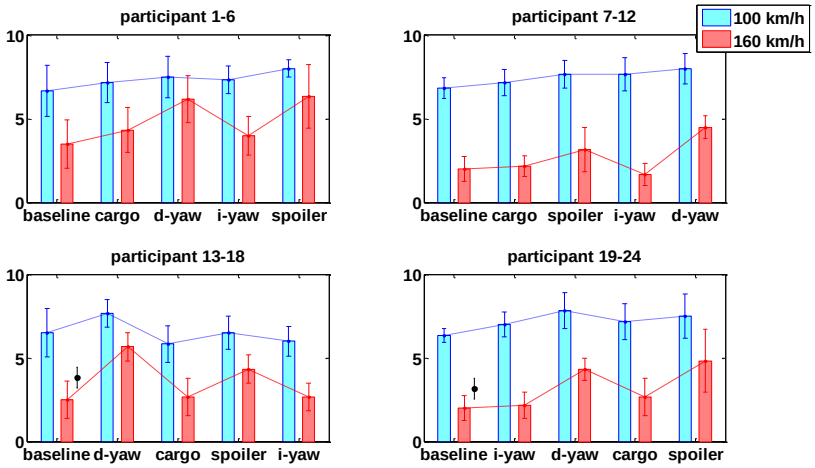

Fig. 3.23 Participants subjective rating with respect to different test order (without adjusting for learning effect)

To compensate for the learning effect, the repeated run of baseline vehicle (black error bar) is used. In Fig. 3.24, subjective rating of participants 13-18 is shown as an example. The learning effect is assumed to increase the subjective rating linearly with respect to time. The linear relation can be drawn between with the original run and the repeated run of baseline 160 km/h (dash arrow in Fig. 3.24). Therefore, increasing in the rating can be calculated and subtracted from the original scores (solid arrow in Fig. 3.24). Individual learning effects are assumed to be the same as the group learning effect regardless of vehicle speed. The same amount of subtraction is applied to all participants in this group and to all speed under the same configuration.

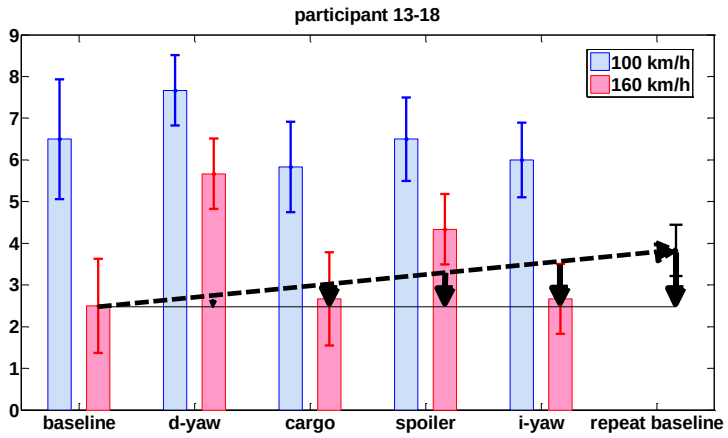

Fig. 3.24 Linear compensation of learning effect

The same procedure is applied to the participants 19-24. Because the lack of the repeated run in participant 1-12, the learning effect is assumed to be the same as the average of group 13-18 and 19-24. Therefore, adjustments are also made in rating results of participants 1-12 accordingly. With this learning effect compensation, the adjusted subjective rating results are obtained (Fig. 3.25). Results show that there is no significant change in participants' preferences regarding to vehicle configurations at 100 km/h. At the higher vehicle speed (160km/h), however, the decreased aerodynamic yaw moment coefficient configuration receives (statistically significant) the highest subjective rating. The spoiler configuration has high average but also high standard deviation, which represents a high level of uncertainty by test participants. The difference of the rest configurations is statistically insignificant.

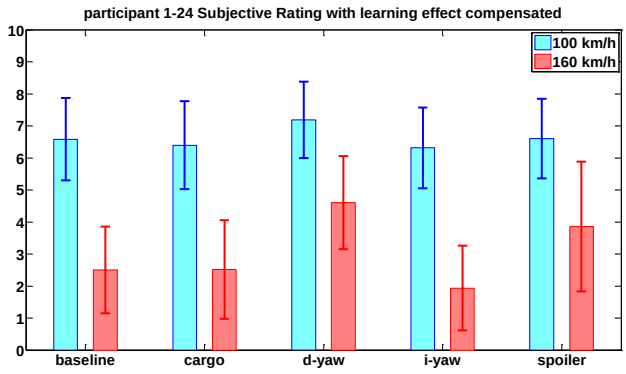

Fig. 3.25 Participants subjective rating (all participants lumped, learning effect compensated)

The driver subjective assessment of some configurations is literally indistinguishable, e.g., for baseline vs. cargo. This is because of fuzzy and imprecise nature of the human subjective rating. We try to define an objective assessment system, which hopefully will provide an evaluation method that is more precise. A major goal of this excise is to find an objective assessment index that can predict the subjective rating without conducting tests. As shown in Fig. 3.26, if a high correlation between the open-loop crosswind sensitivity and the driver subjective rating can be established, this crosswind sensitivity can be used for vehicle design iterations without using test results. The final design will still need to be validated on a real prototype vehicle. But the driver model can be used to reduce time and cost.

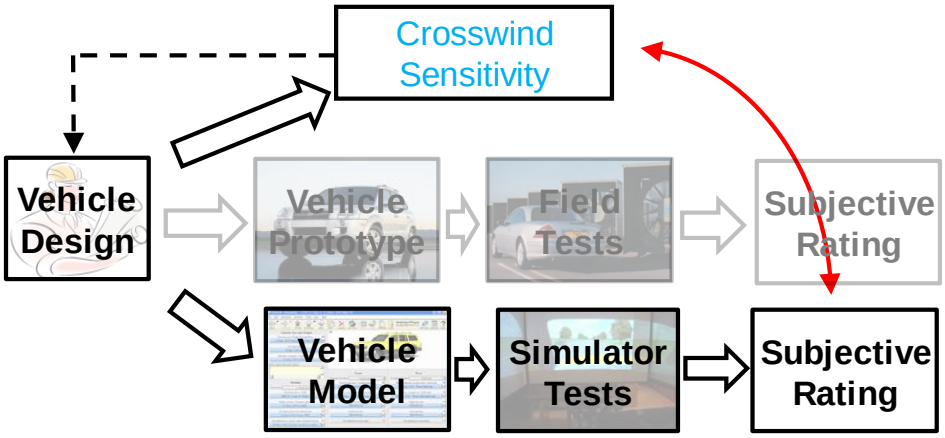

Fig. 3.26 Crosswind sensitivity through simulator test

It is found in the literature that open-loop yaw-rate has good correlation with the driver subjective rating. Therefore, the open-loop yaw-rate is studied first. Different vehicle configurations in the open-loop are simulated with the same impulse crosswind scenarios to obtain open-loop vehicle yaw-rate responses. Open-loop yaw-rate crosswind sensitivities are defined as the RMS yaw-rate response of the crosswind impulse 2-9. A larger RMS of yaw-rate suggests a lower subjective rating that this configuration will get. Therefore, the reciprocal of RMS yaw-rate is used and plotted with the subjective rating in Fig. 3.27.

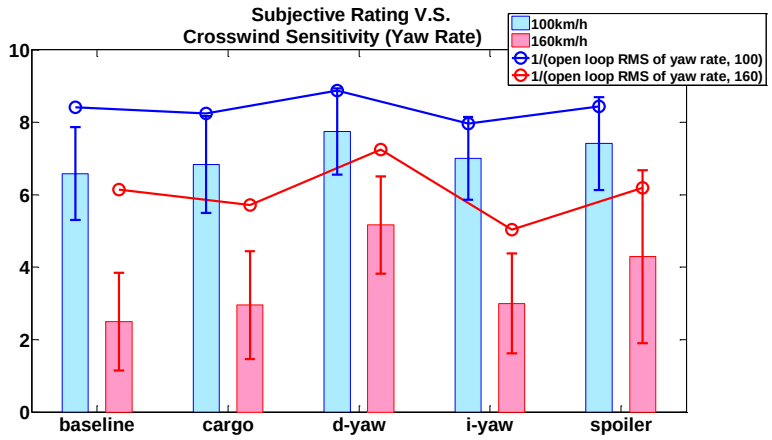

Fig. 3.27 Open-loop yaw-rate vs. lumped driver's subjective rating

Open-loop yaw-rate crosswind sensitivity seems to have reasonable correlation with statistic of the subjective rating. Statistical results of the subjective rating are often used to represent a group of people, but individual responses vary significantly. Disagreement between the open-loop yaw-rate crosswind sensitivity and the individual driver subjective rating can be found. Ten crosswind sensitivities are calculated respect to five vehicle configurations and two speeds each. The correlations between this ten entry vector of crosswind sensitivities and twenty-four individual driver's subjective rating are calculated and shown in Fig. 3.28.

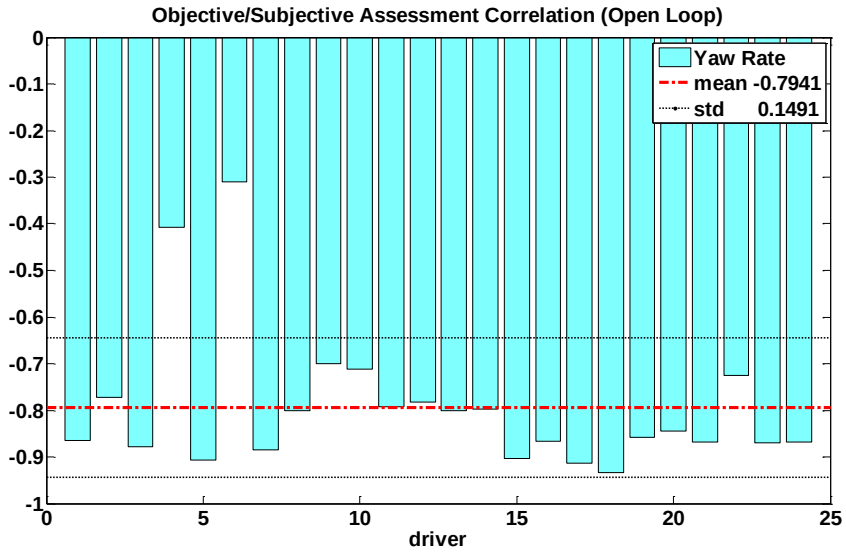

Fig. 3.28 Correlation between open-loop crosswind sensitivity and individual driver's subjective rating

The correlations between the open-loop crosswind sensitivity and the individual driver subjective rating are good (average 0.79). But driver 4 and 6 are significantly low (below 0.4). Open-loop yaw-rate is often considered as a good index in literature, they do not predict individual drivers' preferences well. As shown in Fig. 3.29, we are trying to establish the correlation between the subjective rating and the closed-loop objective assessments. The hypothesis is: Closed-loop responses are a better index for representing individual preferences because they factor in individual driver's behavior.

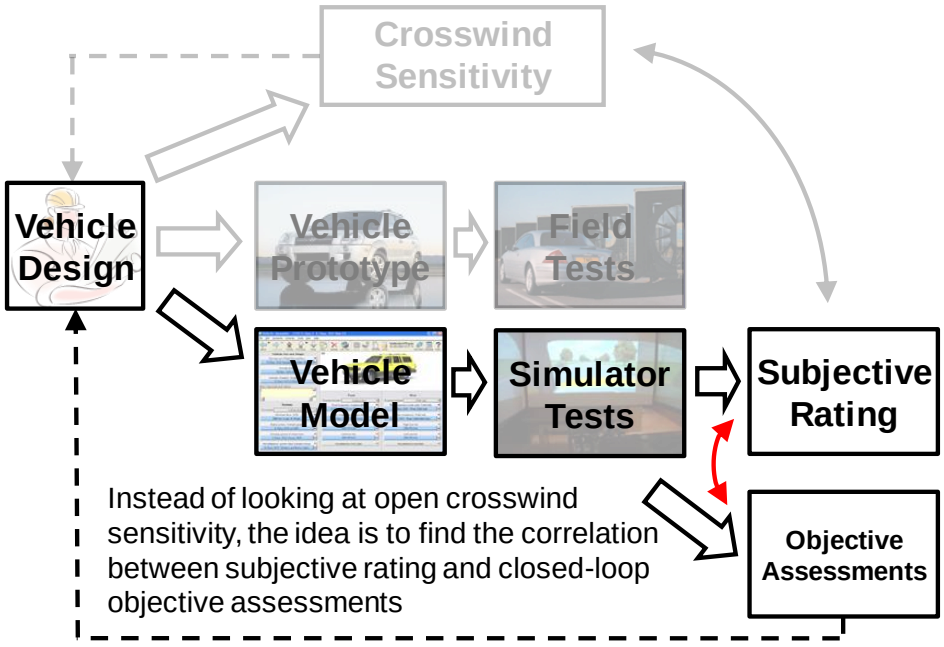

Fig. 3.29 Closed-loop objective assessment through simulator test

The closed-loop objective assessment is defined as RMS of closed-loop yaw rate responses from crosswind impulses 2-9. A ten entries vector of the objective assessment of each participant can be calculated from the simulator test data. Twenty-four sets of the objective assessment are obtained and correlations between each objective assessment and subjective rating are calculated. The result is shown in Fig. 3.30. The improvement can be found by using the closed-loop objective assessment to predict the individual driver subjective rating. The correlations between the subjective rating and the closed-loop objective assessment are higher than correlations obtained from the open-loop sensitivity. Even though the driver 4 and 6 still have the lowest correlation, they are all larger than 0.4, a significant improvement from the open-loop sensitivity prediction.

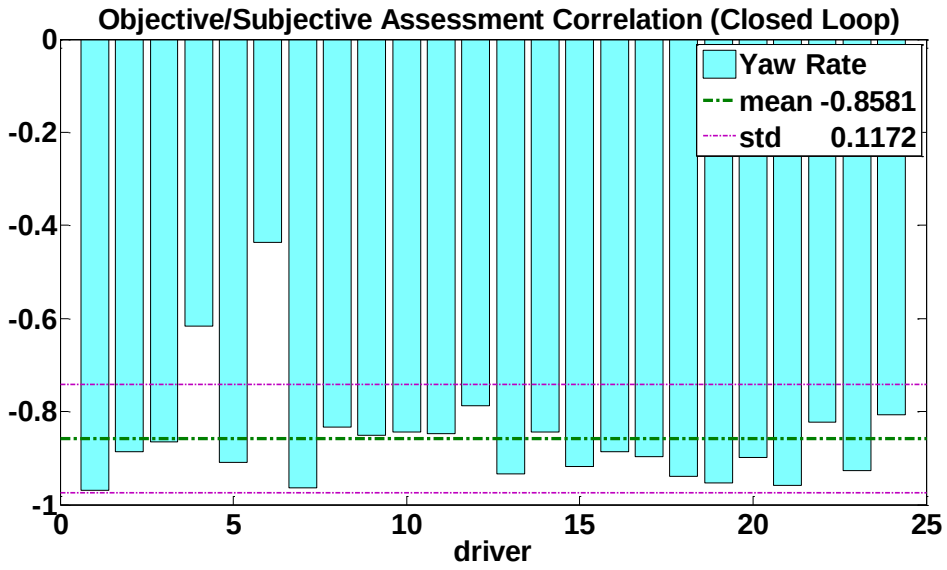

Fig. 3.30 Correlation between closed-loop crosswind sensitivity and individual subjective rating

The closed-loop objective assessment shows better correlation for predicting the subjective rating. However, road tests or simulator tests with drivers are still needed to obtain the closed-loop objective assessment. In the following, we will use the driver model and simulations to replace test participants and simulator tests, so that we do not need to conduct tests for every vehicle designs. The feedback MacAdam's model is used to predict closed-loop behavior of different vehicle configurations. Twenty four sets of parameters are fitted based on baseline vehicle test results and those twenty-four driver model parameters are used to predict the subjective rating of other vehicle configurations. The ability of the feedback MacAdam's model to predict driver's behavior under different vehicle configuration is unknown. In developing the feedback MacAdam's driver model, two hypotheses are made. First, drivers would adapt themselves to different vehicle characteristics and perform a lateral driving if there is no disturbance. Preview time and time delay should be similar under the same driving task if the vehicle model is properly adapted. Second, when unknown disturbance happened, drivers would have a feedback response that is independent of vehicle configurations. The second order system in the model should be the same regardless vehicle configurations. Therefore, the feedback MacAdam's model should be able to predict driver's behavior under different vehicle configurations if a proper internal vehicle model is implemented in the

MacAdam's model. Simulations are done to verify the performance of predicting other vehicle configurations (Fig. 3.31). The model parameters is obtained from baseline vehicle tests and applied to predict other configuration test results.

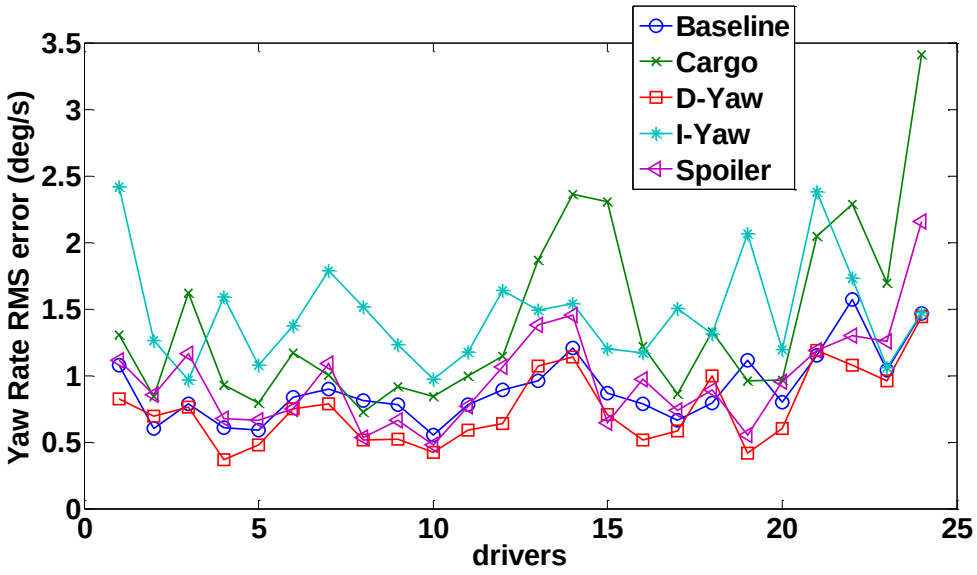

Fig. 3.31 Feedback MacAdam's model prediction of different vehicle configurations

Yaw-rate prediction results for all configurations are similar. The prediction performance of the feedback MacAdam's model has no significant difference under different vehicle configurations. This shows that the feedback MacAdam's model can predict driver behavior of different vehicle configurations with sufficient consistency. Therefore, the feedback MacAdam's model is used to replace test participants and simulate twenty four sets of closed-loop vehicle responses. The model predicted closed-loop yaw-rate responses are compared with the subjective rating (Fig. 3.32). The objective assessment based on model predicted yaw-rates has lower correlation with the objective assessment of the test data, but it is still better than the correlation with the open-loop crosswind sensitivity.

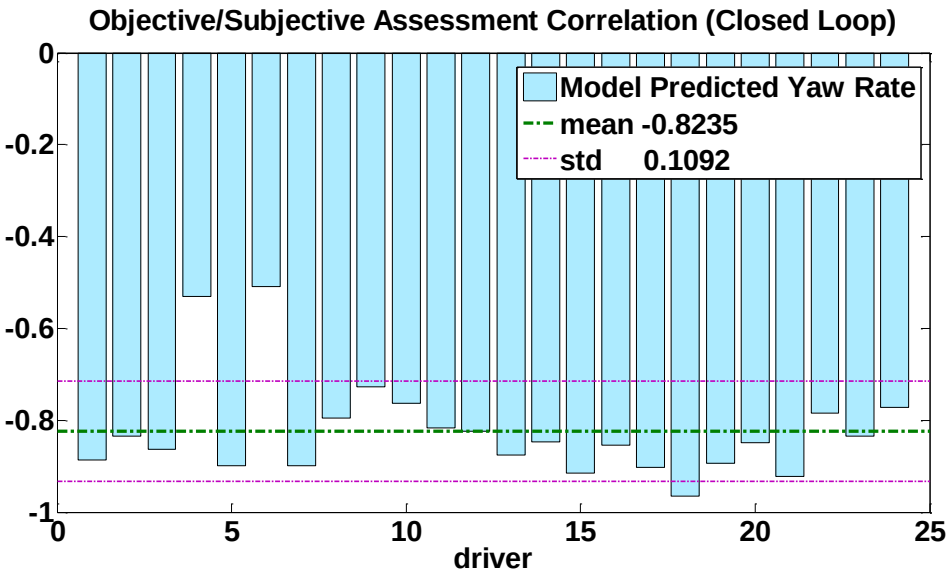

Fig. 3.32 Correlation between model predicted closed-loop yaw-rate and individual subjective rating

Open-loop crosswind sensitivities (yaw-rate) can be used to predict a population's subjective rating, but it cannot guarantee for the individual preference. Closed-loop objective assessment (yaw-rate) has better correlation with the individual driver subjective rating. But real human participant is needed. The feedback MacAdam's model is used to predict closed-loop vehicle responses and the objective assessment. The result shows superior correlation with the individual subjective rating than the open-loop sensitivity assessment and it does not need road or simulation tests for every vehicle designs. This closed-loop simulation method provides a better prediction of the individual preference and without intensive experiments.

3.5.2 **Variable Gear Ratio Steering System**

The objective of this section is to demonstrate the ability of using the feedback MacAdam's model to evaluate and design active safety systems. Active steering system is chosen as an example because of its raising popularity and its ability to generate yaw moment without brake. Variable gear ratio (VGR) steering system is a simplified active steering system and is used here as a preliminary design. VGR can be divided into two categories: angle variable and speed variable [71]. Angle variable VGR system has larger steering ratio around the neutral position and smaller steering ratio around extreme

positions. It improves low-speed parallel parking performance, but has no significant effect on the high-speed lane-keeping [72]. For speed VGR system, larger ratio is desired at high vehicle forward speed for the stability and smaller ratio is used at low vehicle forward speed to reduce steering effort. In this section, the effectiveness of VGR system will be evaluated by using the feedback MacAdam's model. Closed-loop frequency analysis of VGR system will be obtained and its ability to stabilize vehicle will be shown. Meanwhile, the drawback of VGR system will also be discussed. Finally, a new VGR system design will be proposed. The feedback MacAdam's model will be used to help the design process and the performance of this new VGR system will also be discussed.

A simplified VGR system model is shown in Fig. 3.33. VGR system has a smaller gear ratio at low speed and increase the gear ratio at high speed. In our simulation, the vehicle speed is fixed at 160 km/h. Therefore, VGR system should have a fixed and larger gear ratio in the simulation. This is modeled as a simple constant gain K_{GR}. When VGR system has a larger gear ratio design, the K_{GR} is small. K_{GR} will be varied to represent different VGR design and their effectiveness will be discussed in the following.

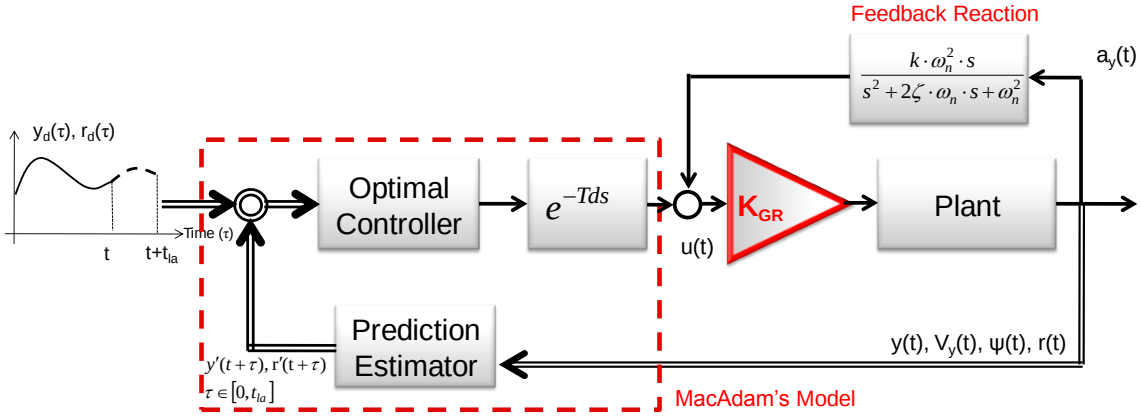

Fig. 3.33 Simplified VGR system modeling

Frequency analysis used in section 3.3 is used to analyze the performance of VGR system. Closed-loop frequency responses of vehicle with VGR system from the natural crosswind input are obtained by using the feedback MacAdam's model. Similar to the discussion in section 3.3, a normalized frequency response that has small magnitude is

desired. Normalized frequency responses of VGR systems with different K_{GR} are shown in Fig. 3.34.

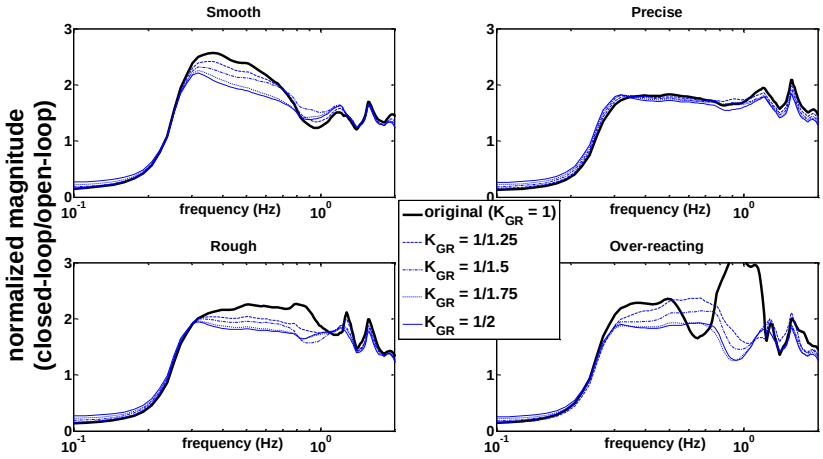

Fig. 3.34 Frequency responses with different VGR system

With increasing the gear ratio (decreasing K_{GR}), the amount of amplification at higher frequency is reduced. A lower peak gain represents better driver/vehicle crosswind stability. However, with larger gear ratio, the amount of attenuation at lower frequency is also reduced (Fig. 3.35). The amount of attenuation at lower frequency represents the driver's ability to control the vehicle for the disturbance rejection. In the ideal case, driver would like to have zero magnitude at low frequency of the normalized frequency response. It means the driver has the full control of the vehicle and rejects the disturbance completely. The frequency analysis in Fig. 3.35 shows that drivers' ability to reject the disturbance at low frequency is decreased when the gear ratio is increased (K_{GR} decreased). In other words, the low frequency maneuverability is sacrificed for obtaining the high frequency stability in this particular VGR design.

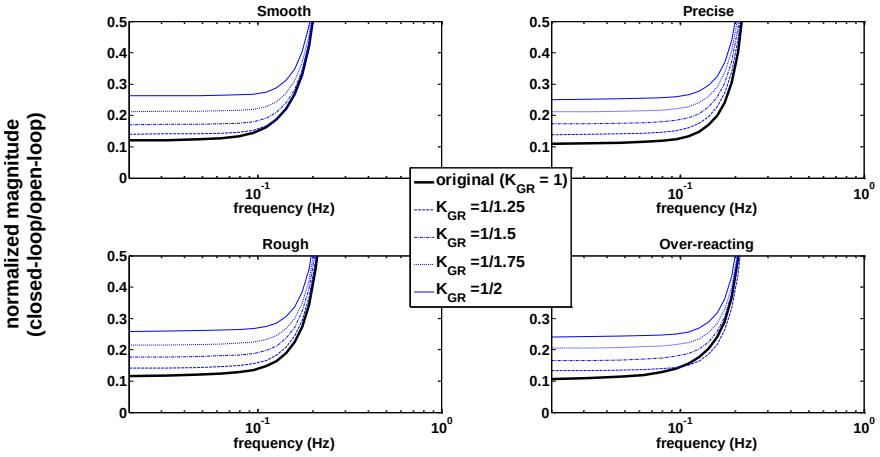

Fig. 3.35 The attenuation at lower frequency responses with different VGR system

In VGR design, both high frequency stability and low frequency maneuverability are preferred. However, trade-offs exist between the low peak gain and the low DC gain by simply increasing the gear ratio. A new VGR system is proposed to minimize this trade-off. A VGR system should have a fixed gear ratio when the steering input is at low frequency so that drivers can have full control of the vehicle. At the higher frequency steering input, the VGR system should increase the gear ratio for better stability (Fig. 3.36).

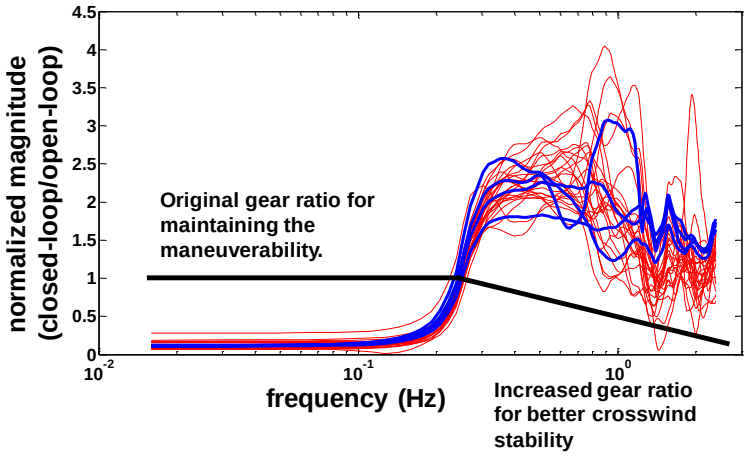

Fig. 3.36 VGR system design concept in frequency domain

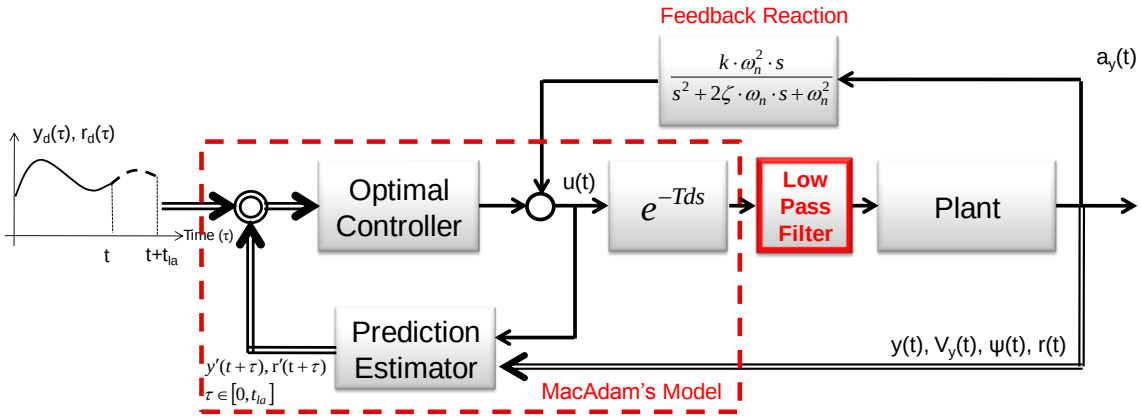

Fig. 3.37 Dynamic VGR system modeling

The design concept is realized as a dynamic VGR system (Fig. 3.37). We suggest that the gear ratio is unchanged when the steering input frequency is low and the gear ratio is increased when steering input frequency is high. A first order low pass filter can be used to realize this design. Cut-off frequency would be the design parameter and can be determined through driver model simulations (Fig. 3.38).

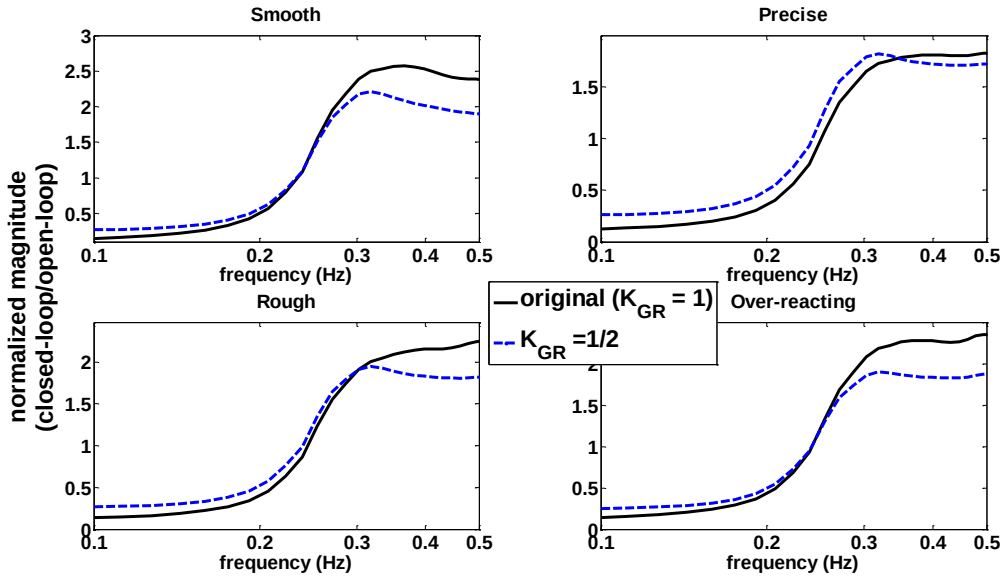

Fig. 3.38 Cut-off frequency identification of dynamic VGR system

Behavior of VGR with different gear ratio is simulated. Its performance changes around 0.2-0.4 Hz. Above this frequency, increasing the gear ratio would help to stabilize the vehicle and below this frequency, the VGR system contaminates the maneuverability. Therefore, a dynamic VGR system that has a cut-off frequency around

0.2-0.4 Hz is desired to improve the stability and to reserve the maneuverability at the same time.

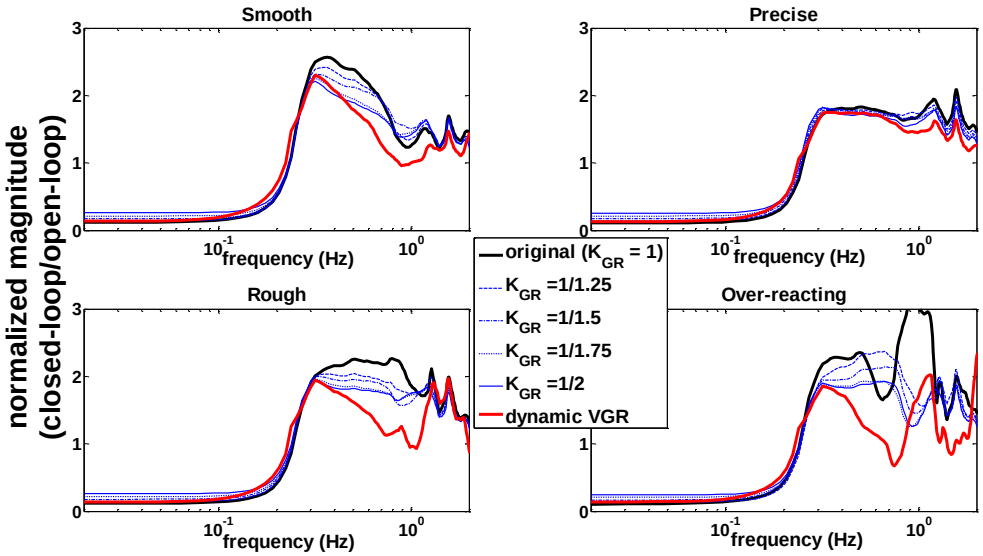

Fig. 3.39 Dynamic VGR system performance compared with speed VGR

The proposed dynamic VGR significantly reduces the high frequency response and maintains the desired low frequency maneuverability (Fig. 3.39). The dynamic VGR design shows superior performance over speed VGR design under natural crosswind input. However, the performance of dynamic VGR cannot be guaranteed under other crosswind input maneuvers. The reason is that the first order low pass filter design in this dynamic VGR system will introduce large phase lag. The phase lag can introduce additional instability. A more advanced filter design can potentially resolve this problem.

3.5.3 **Summary**

A closed-loop objective assessment for vehicle crosswind stability is proposed. The method uses the feedback MacAdam's model to simulate closed-loop responses of different vehicle designs. This method is better than the open-loop sensitivity assessment in term of correlation. It also requires fewer experiments and human participants as needed in obtaining subjective ratings. The feedback MacAdam's model is also used to evaluate the performance of variable gear ratio (VGR) system. VGR system ias found to be helpful for improving the crosswind stability (lower magnitude peak). However, it also reduces the low frequency maneuverability (higher DC gain). To minimize the

trade-off of VGR system, a dynamic VGR system is proposed. Dynamic VGR employs a low pass filter and changes gear ratio in function of steering input frequency. The design concept is to improve the stability and to reserve the maneuverability at the same time. The feedback MacAdam's model is used to help the design and the performance of the dynamic VGR system is superior to original VGR in the lane-keeping task. However, performances of the dynamic VGR in other maneuvers are not guaranteed. The main issue of the dynamic VGR might be the phase lag introduced by the low pass filtering.

3.6 Conclusion

The goal of this lateral driving example is to analyze the vehicle stability problem induced by crosswind and driving accident induced by human driver limitations. Both numerical simulations and driving simulator experiments are conducted to collect lateral driving behavior. An analytical vehicle model (UMTRI wind-steer model) is developed for driver vehicle dynamic response analysis and used for analyzing the vehicle crosswind sensitivity. Based on the sensitivity analysis, variation in C.G. position is found to have the highest sensitivity to the crosswind input. Along with the next four highest design parameters, total five vehicle configurations are selected for the driving simulator test. A CarSim model is used for the fixed-base driving simulator test. Two crosswind scenarios and two vehicle forward speeds are used. Twenty four test participants are recruited and successfully complete the simulator test. The simulator test results are presented and four driving styles are identified in the impulse crosswind input test.

A lateral driver model is developed based on simulator test results. This developed driver model is a combination of the MacAdam's driver model and an instantaneous feedback reaction of crosswind disturbances. This feedback MacAdam's model is shown to be able to model the human normal driving behavior under crosswind. Driver limitations that lead to anomalous behaviors under crosswind are also analyzed. Time delay, panic reaction and the inability to understand the vehicle model are all contributing to the vehicle instability. The feedback MacAdam's model can capture those behavior and result driving accident that observed in simulator tests.

Finally, two applications are provided to demonstrate benefits of this lateral driver model. The feedback MacAdam's model is used to predict closed-loop vehicle responses and the objective assessment. The result shows superior correlation with the individual subjective rating than the open-loop sensitivity assessment and it does not need road or simulation tests for every vehicle designs. This closed-loop objective assessment with the feedback MacAdam's model provides a better prediction of the individual preference and without intensive experiments. The feedback MacAdam's model is also used to evaluate the performance of variable gear ratio (VGR) system and accelerates the design process. The trade-off of VGR system is exposed and a preliminary design is proposed to minimize the trade-off.

CHAPTER 4
LONGITUDINAL DRIVING BEHAVIOR STUDY

4.1 Motivation

In this study, our focus is to model anomalous behaviors in longitudinal driving. A model template that normally achieves car-following tasks and can be adjusted to generate anomalous behaviors is needed. Many existing car-following models can fulfill this need. However, the majority of them assume driving as a deterministic process, i.e., the vehicle states can be calculated exactly from dynamic equations [38], [39] or heuristic rules [44], [45]. Precise prediction of vehicle states might be useful in traffic analysis, but has little benefits for CW/CA development. In the actual driving, human would not perform deterministically. The stochastic behavior of driving has been studied in [76]-[79]. They modeled human randomness with a random noise. By adjusting the magnitude and parameters of this noise, models can be tuned to fit the test data. This modeling procedure can reproduce the stochastic behavior of human drivers. However, those tuning processes of noise magnitude are not convincing and do not reflect actual driving behavior well.

Our aim here is to develop a driver model that emphasizes the stochastic nature of drivers. This model should be able to capture human's normal driving behavior as well as some deviations. Moreover, those normal and deviated behaviors should be consistent with what we observed in realistic driving data in a statistical fashion.

4.2 Naturalistic Driving Data Base

The driving database used for the development and evaluation of this driver model is from the Road-Departure Crash-Warning (RDCW) System Field Operational Test project [73]. The RDCW system was designed to analyze the road departure threat and potential

of active safety devices as a remedy. This system was installed on 11 passenger vehicles with data acquisition systems. Seventy-eight test drivers participated and each of them drove a test vehicle for four weeks. Total data set represented 83,000 miles of driving and over 400 engineering variables were captured at 10 Hz sampling rate. A massive set of numerical, video and audio data were collected, including both lateral and longitudinal driving behavior (vehicle speed, acceleration, range, range-rate). Participates of this FOT received no instruction or interference about their longitudinal driving behavior. Hence, longitudinal driving data can be considered naturalistic and can be used for car following study.

The numerical data signals collected onboard the test vehicles during the FOT are stored in the Microsoft SQL format. There are 89 tables containing over 54 billion data points (204 GB in size). The main database tables are listed below. The fields in the tables of RDCW FOT databases used to analyze longitudinal car-following behavior are listed in Table 4.1.

Table 4.1 List of fields in the tables of RDCW FOT databases [73]

Field Name	Unit	Description
Driver	N/A	Driver identification code
Trip	N/A	Trip index
Road type		0 = Freeway/interstate 1 = Ramp 2 = Ramp near merge point 3 = Surface road 4 = Other (enter in notes)
Time	Csec	Time in centi-seconds since the DAS application launch
StartTime	Csec	Time in centi-seconds when the CIPV detected
EndTime	Csec	Time in centi-seconds when the CIPV disappeared
AccelPedal	Unitless	Acceleration pedal position
Brake	N/A	Brake switch active
Engaged	N/A	Cruise control active
Speed	m/sec	Vehicle speed
Range	m	Range of the target in front

Field Name	Unit	Description
Range-rate	m/sec	Range-rate of the target in front
Acceleration	m/sec/sec	Acceleration of target relative to radar

The data needed for longitudinal driving analysis are queried from the SQL server. The query criteria are as follows:

– Road type 1 & 2 (highway and major road)

– The same target vehicle (lead-vehicle) was detected

– The Cruise Control was off throughout the whole engagement

4,887,660 data points (10 Hz) are queried and sorted based on trip duration. The segments that lasted longer than 50 seconds are considered as eligible car-following maneuvers. The results are a total of 3,508 trips from of 78 drivers.

In the RDCW FOT, the Data Acquisition Systems onboard the test vehicle was failed occasionally and the forward radar systems sometimes lost the target vehicle. These conditions will cause failure points or "shot noise" in the recorded data which need to be removed. Median filter is a simple and efficient way for removing shot noise and is widely used in image processing. Here, a one-dimensional median filter [74] is employed to eliminate those "shot noise".

$$\begin{cases} y(k) = \text{median of } x\left(k - \dfrac{n-1}{2} : k + \dfrac{n-1}{2}\right) \text{ if n is odd} \\ y(k) = \text{median of } x\left(k - \dfrac{n}{2}, k - \dfrac{n}{2} + 1, ..., k + \dfrac{n}{2} - 1\right) \text{ if n is even} \end{cases} \tag{4.1}$$

An example of filtered results is show in Fig. 4.1.

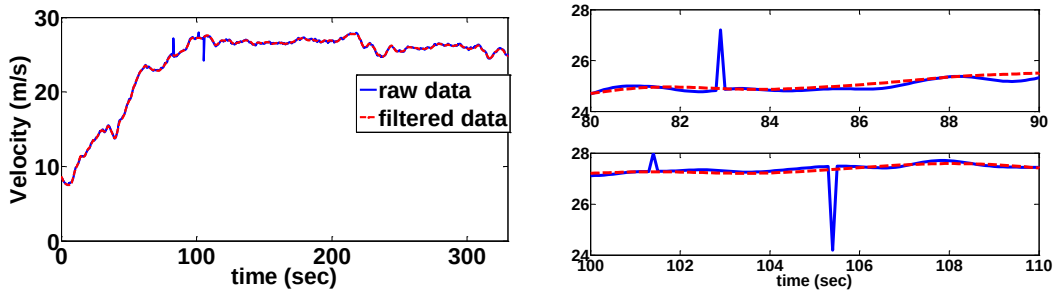

Fig. 4.1 Median filtering example of RDCW data (n = 10)

The shot noises are successfully removed by the median filter. However, the filtered data are still contaminated by high-frequency measurement noise. A simple low-pass filter is used to deal with high frequency noise. A third order Butterworth digital filter is applied and the cutoff frequency is selected to be .5 Hz. Furthermore, to avoid phase distortion after IIR filtering, a zero-phase digital filtering technique is adopted by processing the input signal in the forward and reverse directions [75]. An example of the filtered results is shown in Fig. 4.2.

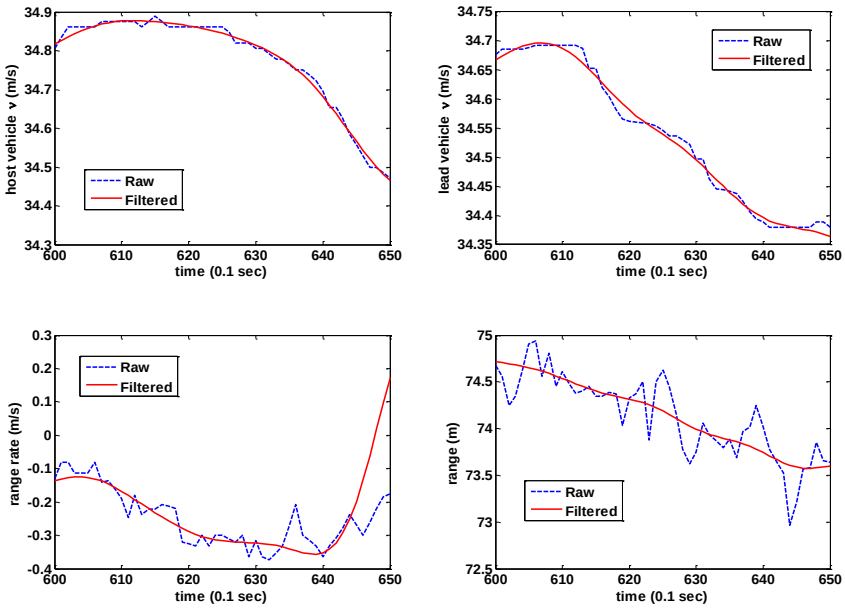

Fig. 4.2 Low-pass filtering example of the RDCW data

A set of two dimensional histograms are presented to illustrate the distribution of the RDCW data (Fig. 4.3). The example plots contain information extracted from ten out of seventy-eight drivers. Data points are plotted in the log scale and the dark color represents area with higher concentration.

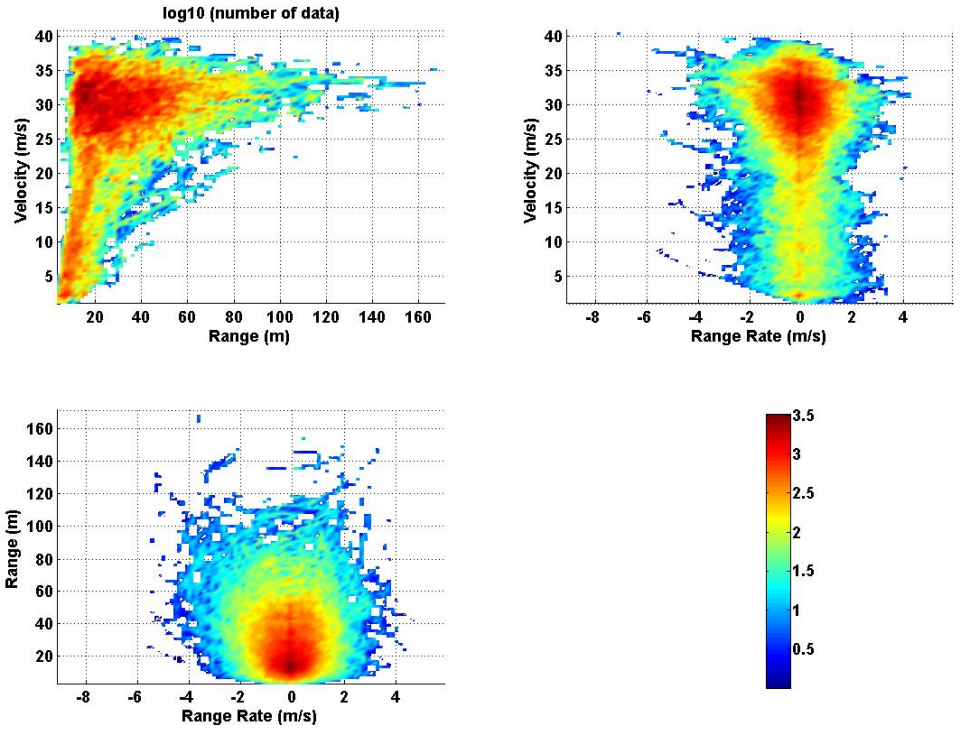

Fig. 4.3 RDCW data distribution

The range and velocity distribution plot shows that drivers increase the vehicle speed with range and maintain the speed after it reaches a desired value (~30m/s). The high concentration of data points around the high velocity and the low range region represents high speed car-following situations and the data distributed symmetrically around zero range-rate implies that drivers are regulating their vehicle with an average range-rate of zero. Several speed profiles are plotted in time domain to provide a better understanding of individual maneuver.

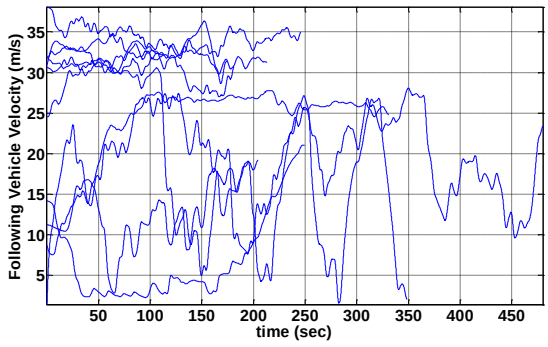

Fig. 4.4 Examples of velocity profiles from the RDCW database

From the RDCW database described above, large number of car-following trips are identified and collected. Simple filtering is applied and to improve data quality. The large quantity of longitudinal human driving data gives us an opportunity to study naturalistic human driving behaviors and a good starting point to develop of humanized longitudinal driver model and CW/CA algorithms.

4.3 Stochastic and Deterministic Behavior

During a car-following task, driver normally regulates the vehicle speed so that the space between the following vehicle and the leading vehicle is comfortable large. In the meantime, the following vehicle tries to travel at a speed close to a desired speed. This assumption is usually modeled by a deterministic process, like many other car-following driver models [31]–[32]. The desired velocity is calculated by certain kinematic or dynamic equations. Thus, the driver's desire is modeled deterministically. It works reasonable well for macroscopic traffic analysis; however, it is definitely not suitable to describe behavior of individual drivers. This is because human cannot perceive, calculate, or control perfectly and human is also unlikely to perform such tasks at a regular pace.

In everyday driving, human driver normally *aims to* regulate the vehicle speed so that the space between the following vehicle and the leading vehicle is large *enough*. The above statement has two assumptions: human driver has intention to achieve a desired vehicle state (speed) and as long as this state was roughly achieved, some deviations would be acceptable. This deviation of control is due to various reasons like driver's imperfections in control, perception, or exogenous disturbances (powertrain dynamics, road gradient, etc). This assumption about deviation of control is discussed in [79] and modeled by a random process. However, the color and magnitude of noises are unknown and a tuning step is needed. In [80], the deviation of braking control of human driver under deceleration is acknowledged and modeled as a truncated Gaussian distribution. In this study, we assumed those deviations exist in both braking and accelerating.

In this section, we assumed that the deviations are related to the space between the two vehicles. When the space (range) is large, there is more room for the driver of

the following vehicle to deviate. Thus, the deviation in control should increase with range. This hypothesis is summarized below and will be verified later in section 4.4. Drivers are assumed to have a target vehicle acceleration which is hypothesized to be a function of range, range-rate, and/or time headway, which can be viewed as a generalized stimulus-response model.

$$a_d(t) = f_{a_d}\left(R(t), \dot{R}(t), T_h\right) \tag{4.2}$$

This desired state will not be achieved exactly and instead will have some deviations, which are a function of range.

$$\sigma(t) \propto f_\sigma(R(t)) \tag{4.3}$$

4.4 Data Analysis and Validation

The RDCW data is used to verify the hypotheses. In equation (4.2), the desired acceleration is assumed to be a function of range, range-rate, and/or time headway. First, we plot the relationship between acceleration of the following vehicle and range-rate. A simple linear relation can be drawn.

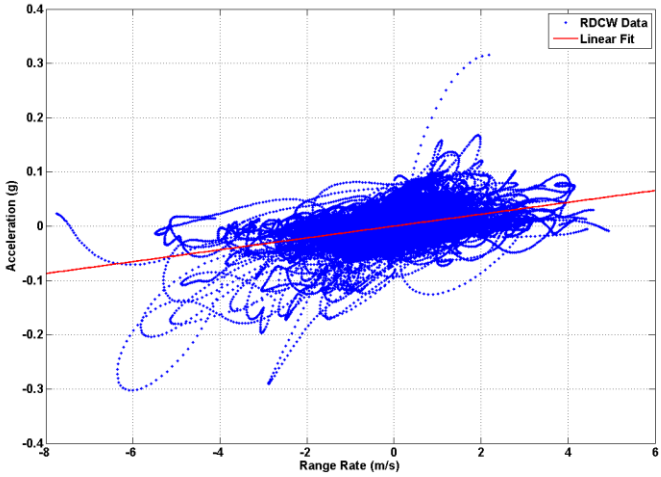

Fig. 4.5 Acceleration vs. range-rate from RDCW data

$$a_d(t) = P \cdot \dot{R}(t) \tag{4.4}$$

This simple relationship is first discussed in Pipe's work [31]. If range is taken into consideration, the relation is not linear anymore. In Fig. 4.6, the acceleration and range-rate are plotted into different range groups. The proportional gain P is decreasing with range, which means the acceleration is more sensitivity to the range-rate if the range is small.

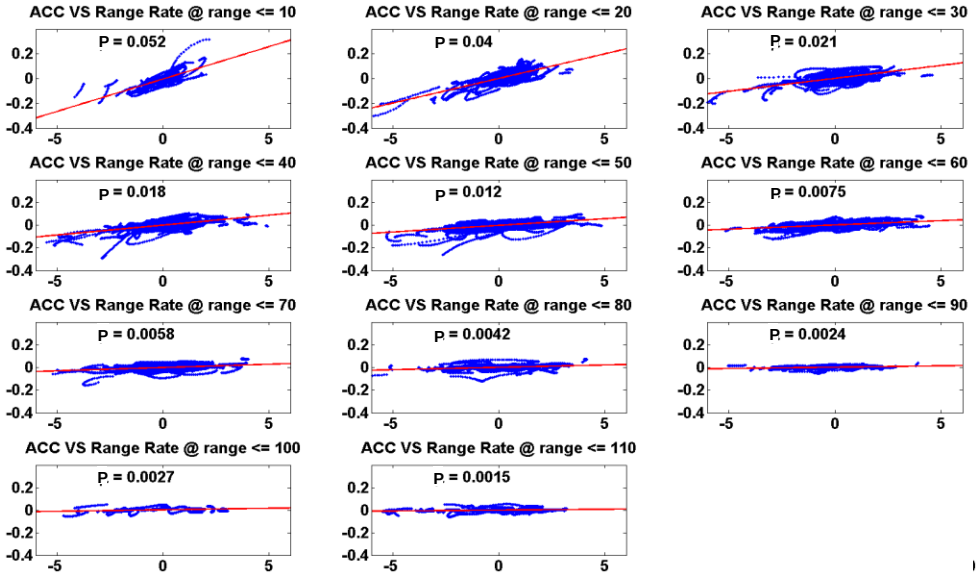

Fig. 4.6 RDCW data acceleration vs. range-rate with various range

$$a_d(t) = P(R(t)) \cdot \dot{R}(t) \tag{4.5}$$

If the constant proportional gain P in equation (4.4) is replaced by a function of range (equation (4.6)), the data fit quality is much improved (Fig. 4.7).

$$P(R(t)) = P_3 \cdot R^3(t) + P_2 \cdot R^2(t) + P_1 \cdot R(t) + P_0 \tag{4.6}$$

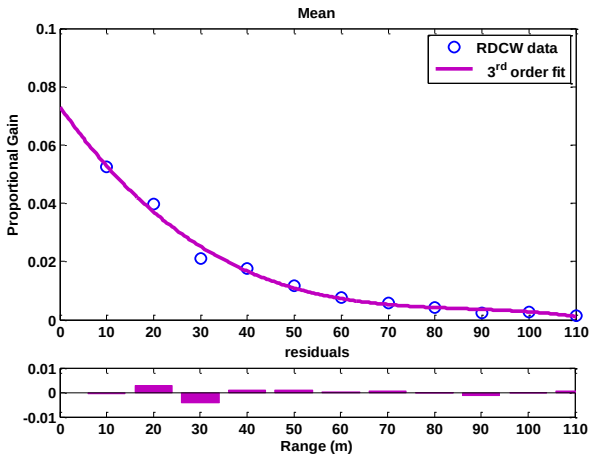

Fig. 4.7 Third order polynomial in function of range for fitting acceleration sensitivity

Fig. 4.6 shows that the accelerations of the following vehicle are largely proportional to the range-rate, but have a scatter around the linear fit. This phenomenon is discussed in section 4.3 and confirmed there. The human driver may have a desired acceleration that is a function of range-rate and range, but the desired acceleration would be achieved in a random distribution. Acceleration distributions along the fitted line are plot in Fig. 4.8 and their standard deviations are calculated (σ). As Fig. 4.9 shows, the standard deviation can be fitted by a second order polynomial.

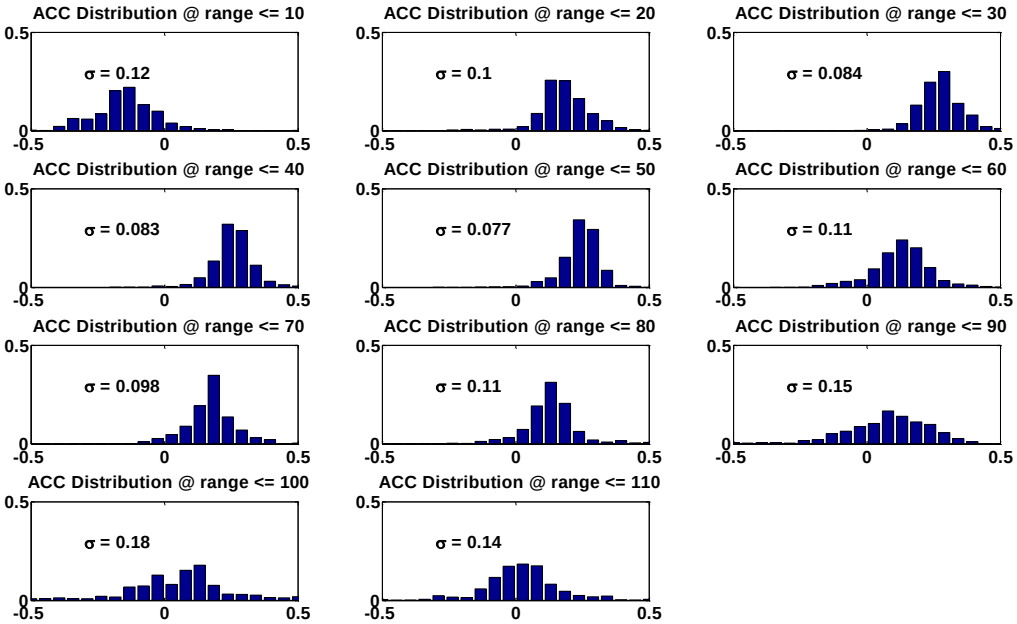

Fig. 4.8 RDCW data acceleration distribution with various range

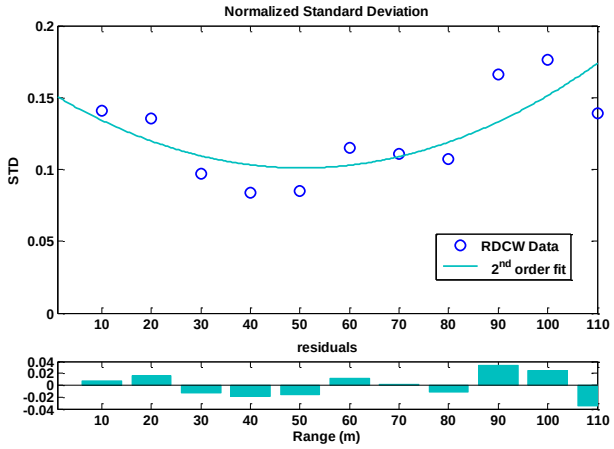

Fig. 4.9 Second order polynomial in function of range for fitting standard deviation of acceleration distribution

$$\sigma\left(R\left(t\right)\right)=\overline{P}_2\cdot R^2(t)+\overline{P}_1\cdot R(t)+\overline{P}_0 \tag{4.7}$$

The parameters $P_i\,(i=0,1,2,3)$ and $\overline{P}_i\,(i=0,1,2)$ are listed in Appendix H.

The driver's actual acceleration is modeled as a stochastic process that has the mean as a function of range ($a_d(R(t))$) and the deviation also as a function of range ($\sigma(R(t))$). A probability density function [81] is used to describe this stochastic process:

$$\left\{ f\left(x\,\middle|\,\mu,\sigma\right)\,\middle|\,\mathrm{P}\left\{X\le a\right\}=\int_0^a f\left(x\right)dx\right\} \tag{4.8}$$

The overall stochastic driver model is summarized below.

$$\begin{aligned}
&a_d\left(t\right)=P\left(R\left(t\right)\right)\cdot\left[\dot{R}\left(t\right)\right]\\
&P\left(R\left(t\right)\right)=P_3\cdot R^3(t)+P_2\cdot R^2(t)+P_1\cdot R(t)+P_0\\
&\sigma\left(R\left(t\right)\right)=\overline{P}_2\cdot R^2(t)+\overline{P}_1\cdot R(t)+\overline{P}_0\\
&a\left(t\right)=f\left(a_d,\sigma\right)
\end{aligned} \tag{4.9}$$

A remaining unknown in the stochastic driver model is the density function *f* in Eq. (4.9). Brunson [80] adopted a truncated Gaussian distribution for decelerating cases. However, the observation in Fig. 4.8 shows that the distribution is not symmetric. In the car-following situation, human drivers have more freedom to decelerate and have more constraints in the acceleration. Therefore, the acceleration distribution shows non-

symmetric shape with a long tail at the deceleration direction. To approximate the non-symmetric distribution, the lognormal distribution (4.10) and the extreme value (4.11) distribution [81] are two possible candidates.

$$f_{\text{logn}}(x \mid \mu,\sigma) = \frac{1}{x \cdot \sigma \cdot \sqrt{2\pi}} \cdot \exp\left(\frac{-(\ln x - \mu)^2}{2\sigma^2} \right) \tag{4.10}$$

$$f_{ev}(x \mid \mu,\sigma) = \sigma^{-1} \cdot \exp\left(\frac{x-\mu}{\sigma} \right) \cdot \exp\left(-\exp\left(\frac{x-\mu}{\sigma} \right) \right) \tag{4.11}$$

Curve fitting shows that the extreme value distribution has better agreement with the RDCW data. Therefore, the extreme value distribution will be used in the following study.

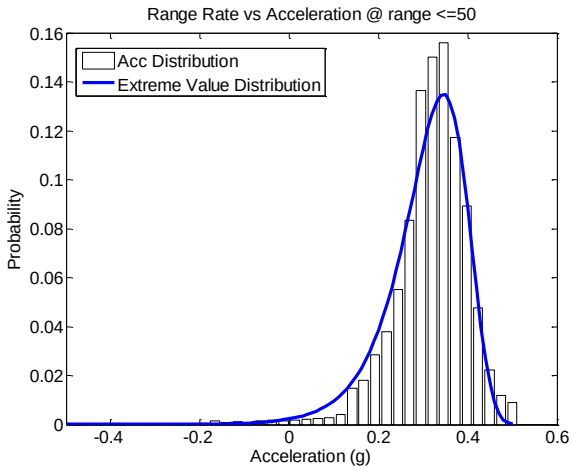

Fig. 4.10 The RDCW acceleration distribution and fitting result of a given range

4.5 Modification for Time Headway and Driver Model Diagram

In Equation (4.5), the driver only responds to non-zero range-rate. Therefore, the model may follow the lead vehicle with a very small range or a very large range. Moreover, the proportional gain in Equation (4.5) is a function of range. If the range is too large (e.g. >70 m), the model will hardly response to any stimulus; the following vehicle will thus fall behind. Both situations are not normal car-following behavior. In reality, human drivers also regulate range or time headway as discussed in [37] and [38]. Human drivers are assumed to have a desired range and regulate the vehicle speed to achieve the desired range. To capture this behavior, an extra term is included in Equation (4.12).

$$a_d(t) = P\big(R(t)\big)\cdot \dot{R}(t) + C\cdot\big(R(t) - T_h \cdot V_F(t)\big) \tag{4.12}$$

where C is a constant gain for range regulation and T_h is the time headway.

The time headway T_h in Equation (4.12) is obtain from the RDCW data. The actual time headway of the human drivers can be calculated by dividing range with range-rate. Its distribution was shown in Fig. 4.11, which contains the data from driver 1 only. The time headway distribution is approximated as a random process with the lognormal distribution. However, this random process generates a random variable every sampling time. In the real driving, human drivers obviously do not adjust their time headway so frequently. By adding a 4-step running average filter, the output becomes smoother and similar to the actual driving data.

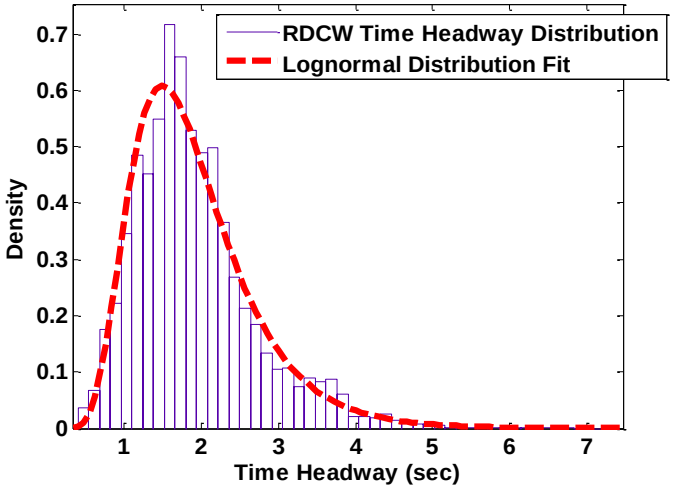

Fig. 4.11 Time headway distribution and fitting results of one example driver

A schematic diagram of the stochastic driver model is shown in Fig. 4.12. The inputs are the desired time headway (T_h) and the lead vehicle velocity (V_L), which is from naturalistic driving data. The average desired acceleration (a_d) and deviation (σ) are calculated from equations (4.12) and (4.7), respectively. The actual acceleration is then generated through a random number generator (MATLAB function "evrnd") and the output V_F can be obtained by the integration. A running average filter is used to model the vehicle longitudinal dynamics so that the acceleration cannot change rapidly. This model simulates the normal driver behavior and random deviations derived from the actual driving data. Three different simulations are shown in Fig. 4.13 to illustrate the

stochastic natural of this model. Those simulations use the same lead vehicle velocity profile (dot in the plot) as the input. For every run, the following vehicle acceleration is a little different due to the probability distribution of the actual acceleration and the resulting following vehicle velocity profiles (colored line) are different. Comparing with the following vehicle velocity (blue line) from the database, the simulated vehicle velocities are distributed around the test data.

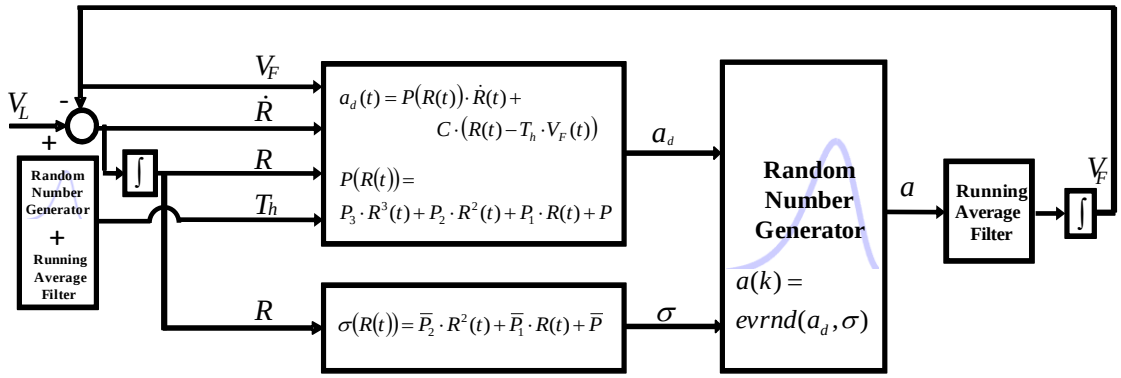

Fig. 4.12 Stochastic driver model diagram

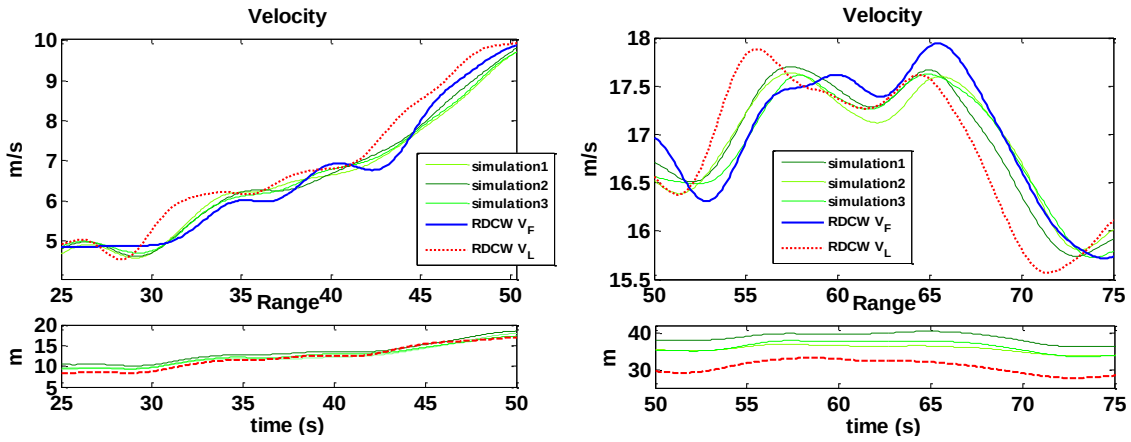

Fig. 4.13 Stochastic driver model simulation example

4.6 Simulation Results and Discussion

The proposed stochastic driver model (SDM) is evaluated by using the RDCW data. The lead vehicle speed is used as the input to the SDM. The SDM response is compared with the following vehicle motion from the RDCW database. The model performance is

evaluated by the model prediction error. If the prediction error is small and randomly scatters around zero, it is considered as a good performance. The SDM performance is also compared with other driver models to benchmark the SDM.

In the RDCW database, driving records of 78 drivers' data are available. Based on the query criteria shown in section 4.2, the car-following driving data is extracted. The results are 20 – 74 maneuvers (20,000 – 600,000 data points) from each driver. These maneuvers are separated into training sets and evaluating sets. The ten longest maneuvers of each driver are used as training sets to obtain the SDM parameters. Then, the eleventh to twentieth maneuvers are used as evaluation sets. Calculated lead vehicle speed is used as input to the SDM (V_L in Fig. 4.12). The model predicted V_F is then compared with the experiment data from the RDCW. Examples of model prediction error distributions are shown in Fig. 4.14.

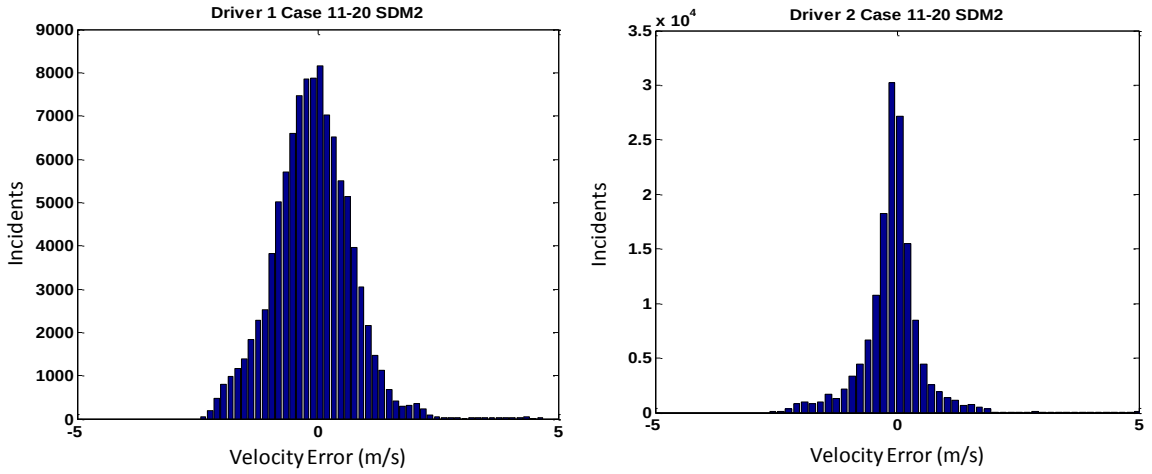

Fig. 4.14 Velocity prediction error distributions of two example evaluation sets

For good model prediction results, the mean of error should be close to zero and the standard deviation should be small and the training/evaluation results should be of similar magnitude. The training and evaluating results for the first ten drivers are shown in Table 4.2. Small means of errors show that the SDM is capable of fitting different driver's normal driving characteristics.

Table 4.2 Training and evaluation results for the first ten drivers

	driver	1	2	3	4	5	6	7	8	9	10	Average
Training	Mean (m/s)	**-.1347**	**-.0447**	**-.1840**	**0.0050**	**-.1154**	**0.0438**	**-.0029**	**-.0574**	**-.0203**	**0.3422**	**0.0950**
	STD	**0.8121**	**0.7060**	**0.6748**	**1.2657**	**0.6662**	**1.0908**	**0.8618**	**0.8191**	**0.7036**	**0.8109**	**0.8411**
Evaluating	Mean (m/s)	**-.0078**	**-.0486**	**-.2878**	**0.0607**	**-.1253**	**0.0403**	**0.0113**	**-.0655**	**-.1100**	**0.3577**	**0.1185**
	STD	**0.7887**	**0.6777**	**0.7562**	**1.2328**	**0.7261**	**1.0847**	**0.7844**	**0.9965**	**0.7023**	**0.7903**	**0.8540**

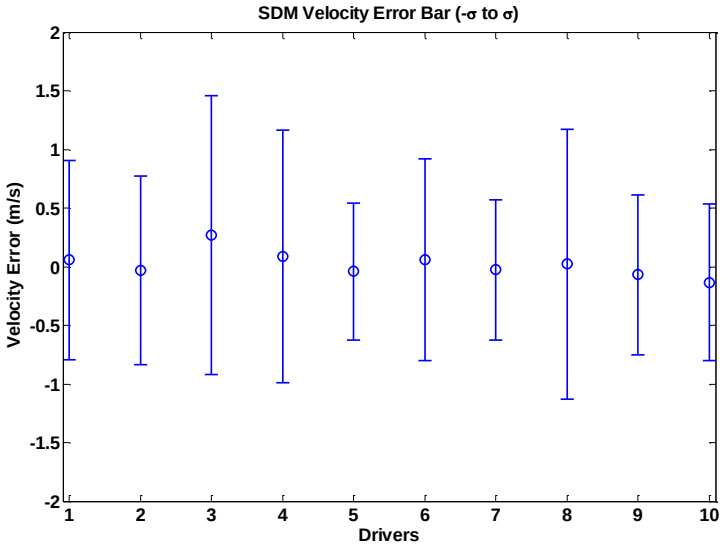

Fig. 4.15 Evaluating results mean and deviation plots

The acceleration, range and range-rate distributions of the SDM are plotted in Fig. 4.16 to compare with the RDCW data qualitatively. Distributions of the SDM show similar characteristics with the RDCW data and same distributions from other deterministic driver models will be discussed to benchmark the SDM in the next section.

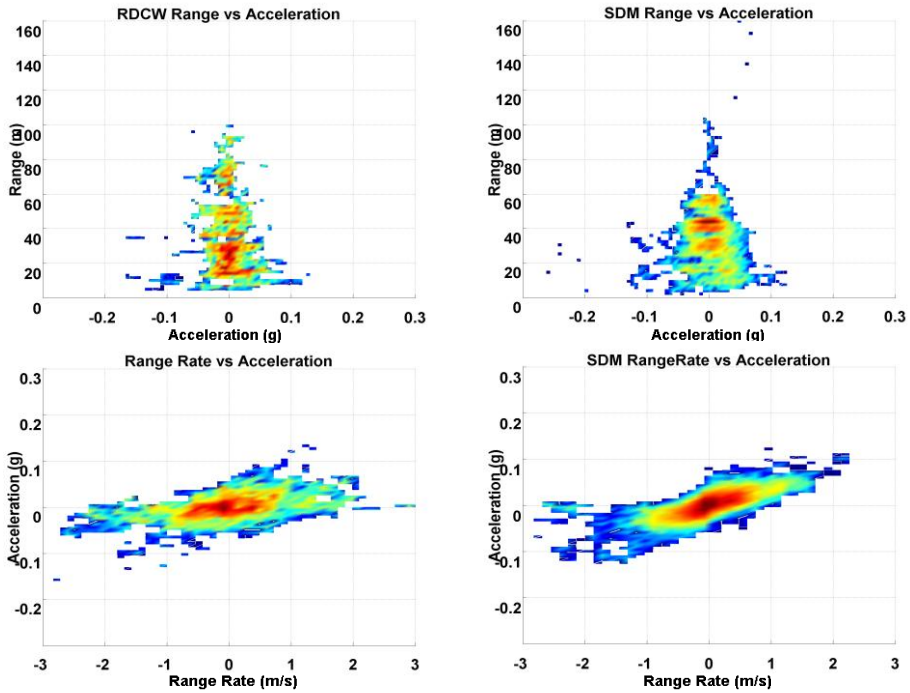

Fig. 4.16 Distribution of RDCW data and SDM simulation.

4.6.1 **Model Comparison**

To benchmark the performance of the stochastic longitudinal driver model, performances of several deterministic longitudinal driver models are also studied. Three models (Table 4.3) are selected because of their simplicity and reasonable accuracy. Note that, Lee [61] reports that the Gipps model [39] has the best performance for fitting human driver in his study. However, the Gipps model generates a desired velocity. When applying parameters to evaluating sets, this desired speed generated from the training sets would not be valid. Therefore, the Gipps model is not selected as a model to compare with.

Table 4.3 Selected deterministic driver models

Model	Model parameters	Equation
Pipes [1] Linear follow-the-leader	K, τ	$a_F(t+\tau) = K \cdot \dot{R}(t)$
Gazis [32] Nonlinear follow-the-leader	C, τ, l, m	$a_F(t+\tau) = \frac{C \cdot V_F(t)^m}{R(t)^l} \cdot \dot{R}(t)$
Tyler [38] Linear optimal control	τ, C_V, C_S, C_C	$a_F(t+\tau) = C_V \cdot \dot{R}(t) + C_S\left[R(t) - C_C \cdot V_F(t)\right]$

The same training sets used for obtaining the SDM parameters are used and a numerical optimization technique is applied to obtain the best parameters for these models. For each driver, there are ten maneuvers in the training sets; hence ten sets of parameters are obtained. The parameter values are averaged and applied to the evaluation sets. The distributions of the velocity error are shown in Fig. 4.17.

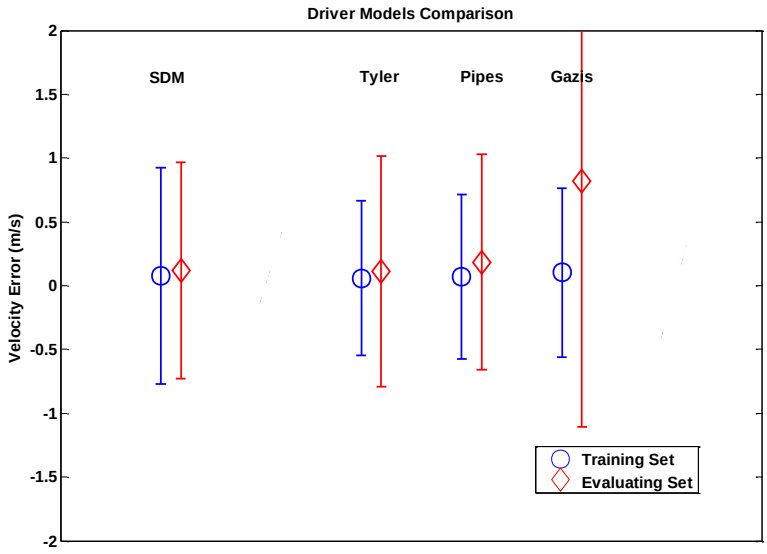

Fig. 4.17 Model comparison results

For the training sets along, the SDM has the worst results in terms of standard deviation of the predicted speed. However, several observations are made:

- SDM did not go through an optimization step for each training maneuver.
- SDM used only one set of parameters for all ten maneuvers, meanwhile all other models used a unique parameter set for each maneuver in the training set.

In the evaluation sets, the SDM is more consistent than all other models. The error of the SDM increases only slightly while the standard deviation remains the same. However, all other models' performances degrade significantly for the evaluation data sets. This indicts that deterministic driver models with optimized parameters are good for fitting human driver behavior but are not robust in predicting drivers' behavior under evaluation maneuvers. The robustness of the SDM is further verified by simulations. In the previous evaluation, the parameters of the training set from one particular driver are applied to the evaluating set of the same driver. However, if we apply the parameters obtained from different drivers, the SDM can still perform relatively well. Table 4.4 shows the evaluation results from different training sets. Drivers 1-5 were evaluated by using the training set parameters from drivers 6-10. And drivers 6-10 are evaluated by using the training set parameters from drivers 1-5.

Table 4.4 Evaluation results from different training sets

driver	1	2	3	4	5	6	7	8	9	10	Average
Mean (m/s)	0.0564	-.1107	-.0981	0.1533	-.0744	0.3109	0.0368	-.1230	-.0300	0.4514	0.1445
STD	0.8821	0.6474	0.7399	1.3782	0.7199	1.2692	0.9725	0.7727	0.6617	0.8758	0.8919

As we can see, the mean and the STD of error increase very slightly. The robustness of the SDM provided a good model template for predicting driver behaviors. An even more significant advantage of SDM is demonstrated by examining the acceleration and range-rate plots (Fig. 4.18).

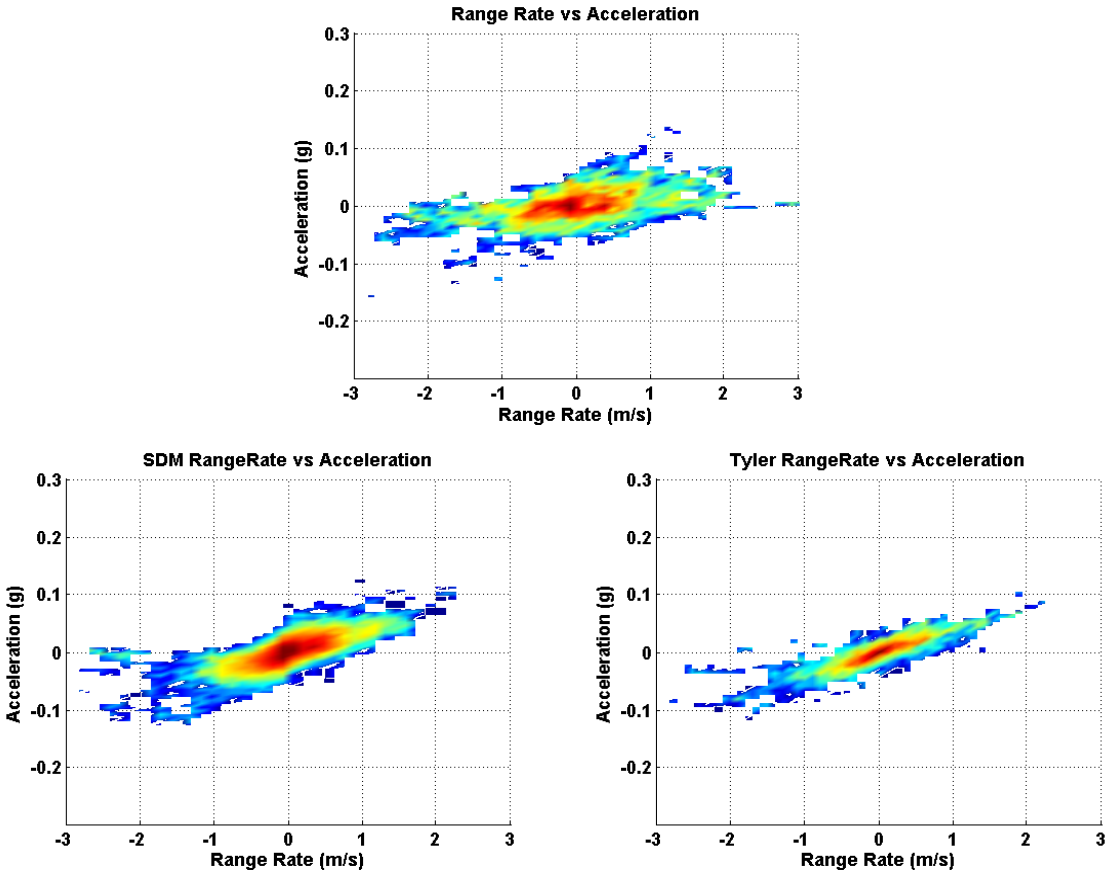

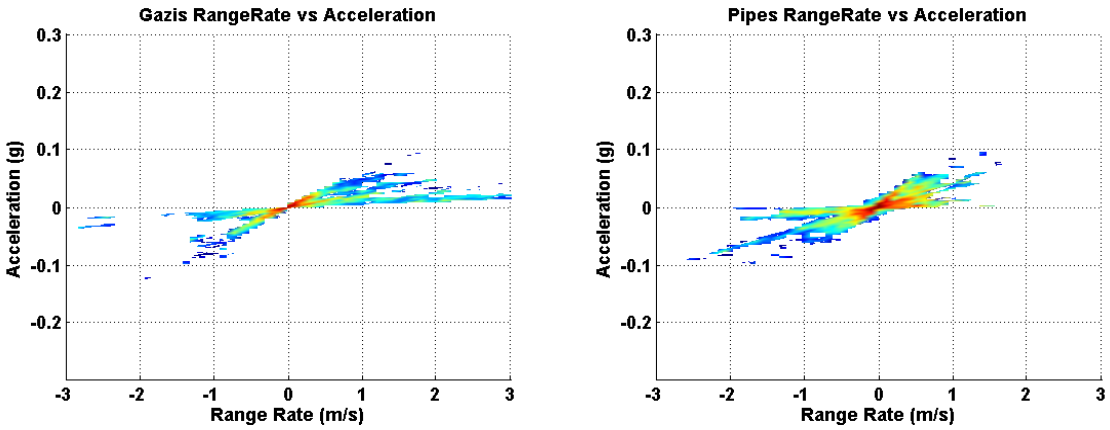

Fig. 4.18 Range and range-rate distribution comparison

It can be seen that besides SDM and Tyler's model, no other model has similar characteristic as observed in the RDCW data. Because of the regulation of time headway, Tyler's model has an elliptic shape distribution like RDCW. However, its distribution still does not spread out enough like SDM.

4.7 Summary

A stochastic longitudinal driver model (SDM) is developed and evaluated against naturalistic driving data. Sufficient flexibility is shown in training this model to fit the data. Meanwhile, superior robustness is demonstrated in predicting the human driving behavior in the evaluation test sets. The SDM can capture human's normal driving behaviors with deviations. Moreover, those normal and deviated behaviors are statistically similar to what we observed in actual driving data.

In the following study, the SDM will serve as driver model template for the development of an errable driver model. Because of its flexibility and robustness, the SDM can be used to model human's normal driving behavior. Combining with error mechanisms derived from human behavior, this model can be made to make mistake, i.e., errable.

CHAPTER 5
LONGITUDINAL ERRABLE DRIVER MODEL

5.1 Motivation

Our goal here is to build a longitudinal driver model useful for the evaluation of CW/CA systems. The purpose of the CW/CA system is to assist a human driver when he or she is not able to avoid or mitigate a crash; in other words, when the driver is either making a mistake or simply is not able to handle the situation. Therefore, for evaluating CW/CA algorithms, models that achieve driving tasks perfectly are not useful. On the contrary, a model that makes mistake similar to human drivers would be more suitable for the development of CW/CA systems.

In this study, three types of error-inducing behavior are analyzed, perceptual limitation, distraction, and time delay. Each of them affects the normal driving and degrades the car-following performance. Individually, their effects might not be significant enough to induce a crash. However, combinations of those behaviors could cause crashes. To validate this hypothesis, the error-inducing behaviors are modeled as stochastic processes based on the frequency of their occurrences. Then, those stochastic processes of error are introduced into the longitudinal driver model (SDM) independently. The goal is to have the model to generate rear-end crashes at a rate that is similar to human drivers.

5.2 Error-Inducing Behavior

5.2.1 Perceptual Limitation

Whether or not, and how accurate the environmental variables can be perceived are critical for performing driving tasks. Human drivers need to perceive environmental variables constantly and accurately. Failure to do so may cause accidents during driving.

Therefore, perceptual limitation is studied as one of the error-inducing behavior in this research.

Human drivers sense and perceive environmental variables such as range, range-rate and vehicle speed to perform the driving task. Among all the feedback mechanisms, vision is the primary source for motor vehicle operations [84], [85]. In a car-following task, abilities to detect changes in distance and velocity are critical. Therefore, vision perception limitations are studied as an error-inducing behavior in this research. The proposed SDM uses range and range-rate as two feedback cues. The range between vehicles is perceived though optical invariants [86]. The perception is then limited by the resolution of human eyes. A typical accepted localization threshold is 6 arc sec (0.5μm on the retina). Other than visual angle, human also utilizes environmental information such as eye-height, relative position, and texture of the ground for reference to obtain a fairly accuracy distance [87]. Therefore, we do not implement the perceptual limitation of distance or range.

How human drivers perceive relative speed has long been a research pursuit. Many researches are done aiming to answer the following question: Can human perceive relative speed directly or is it indirectly inferred through the change in position? This question is sometimes recast in a different form: is perceptual sensitivity of velocity different from sensitivity of position? Nakayama [88] used a random-dot pattern movement to isolate the motion from position cues. Randomly generated dot pattern prevented the position comparison and allow motion detection to be the only mechanism. The result concludes that motion and position perception are two different mechanisms. For low frequency range (< 2 Hz), human has a direct assessment of motion. But for higher frequency (> 2 Hz), using derivative from positions to obtain motion seems to exist. Other than different mechanisms for motion perception, a different perceptual threshold was also reported by McKee [89]. The result confirms that velocity detection is related to the estimation of motion change, in other word, time derivative of position change. A very accurate velocity perception was reported (5%) in McKee's study. Various Just-Noticeable Differences ($\Delta V/V$) of velocity discrimination from 0.05 to 0.2 were found in [90]-[93]. Since velocity detection in the car following task is relatively

easy (comparing to hitting a baseball), a generous velocity threshold (0.1) is selected in this study.

The perceptual limitation is simulated as a quantized range-rate input. The disagreement between perceptual and real signals will be the cause of error. The implementation of this perceptual limitation quantizer is:

$$\dot{R}'(k) = \begin{cases} \dot{R}(k) & \text{if } \dfrac{\dot{R}(k) - \dot{R}'(k-1)}{\dot{R}'(k-1)} \geq 0.1 \\ \dot{R}'(k-1) & \text{otherwise} \end{cases} \tag{5.1}$$

This implementation is done in discrete time 10 (Hz) and $\dot{R}$ represents the actual range-rate and $\dot{R}'$ is perceptual range-rate. An example simulation of the perceptual limitation quantizer is shown in Fig. 5.1. In driving simulation, the perception error will delay or prevent driver model's response if the change of range-rate is not significant enough. This error-inducing behavior is part of in human nature and is assumed to always exist during driving.

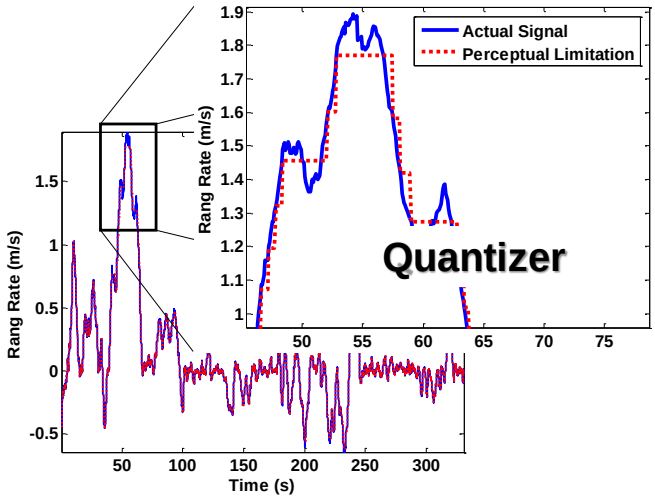

Fig. 5.1 Perceptual limitation quantization simulation

5.2.2 **Time Delay**

Time delay is another source of driving error. Neuromuscular delay and brain processing time are two major sources of time delay. Neuromuscular delay may be a constant for each driver, but the brain processing time is not. Therefore, the total time delay is varying. The truth is that the delay time may very well be related to distraction due to

secondary tasks. However, it is important to include delay as a separate error mechanism in the SDM. A parallel recursive least square (RLS) method is used to estimate the time delay. Thirty ARMA models with different delay steps (0.1 sec) are used to fit the test data simultaneously by the RLS algorithm. For every time instant, the delay step of the most accurate ARMA model is chosen as driver's time delay, and then the time delay sequence can be constructed. The ARMA model (5.2) used here is derived from Tyler's model (Appendix I) because it has similar structure with SDM in the deterministic sense.

$$V_F(k) = a \cdot V_F(k-1) - b \cdot V_F(k-i-1) + c \cdot R(k-i) + d \cdot R(k-i-1) \quad , i = 1 \ldots N \qquad (5.2)$$

The driver time delay was reported to be .5-.9 sec from an instrumented vehicle in a test track [97] responding to a signal change. A longer brake response time was found (1.5-3.5 sec) in a driving simulator [98] for car-following task and in real traffic (3.5-4.5 sec) [99]. The value for N is selected to be thirty (three seconds). The estimated results of the RDCW data are analyzed. One example is shown in Fig. 5.2.

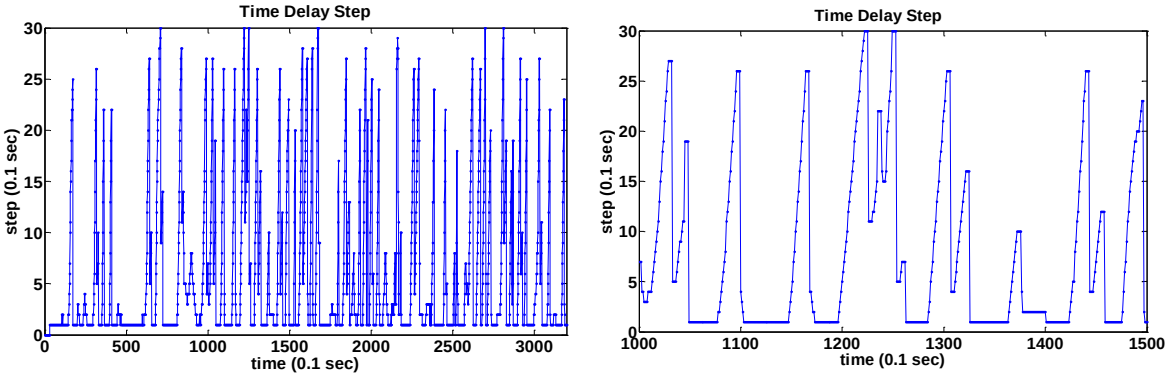

Fig. 5.2 Time delay estimation of RDCW data

This sequence shows a significant character that the delay step increases with time and, then dropped or reset to zero. This can be modeled as a renewal process. To duplicate the characteristic of time delay observed in the previous section, a probability distribution of time delay is first obtained from the time delay sequence. If time delay step is zero, we define it as normal driving and their distribution is shown in Fig. 5.3(a) which can be fitted by an exponential distribution. When time delay step is larger than zero, we define it as delayed driving and their distribution is approximated as uniform (Fig. 5.3(b)).

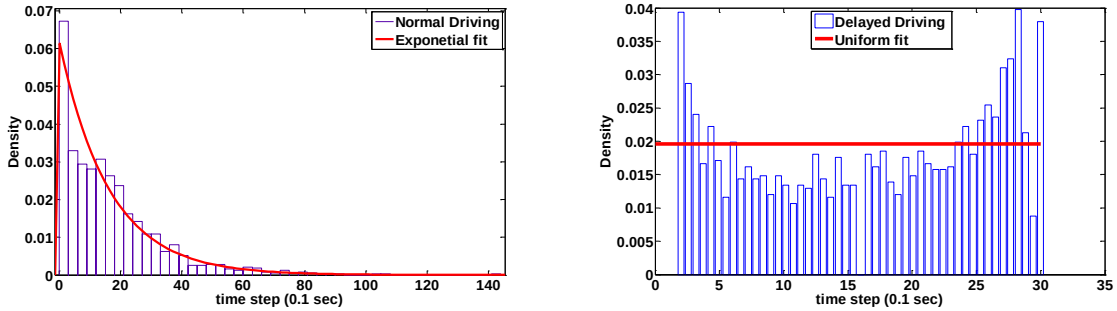

(a) Time delay Distribution (b) Customized PDF fit

Fig. 5.3 Time delay distribution and PDF fitting

Next, the human time delay is modeled by a renewal process which has an inter-arrival time indicated by a probability density function. When a renewal arrives, the time delay step will increase from zero and reset until the next renewal. The resulting time delay sequence is similar to the real sequence obtained by RLS and will be used in simulations (Fig. 5.4).

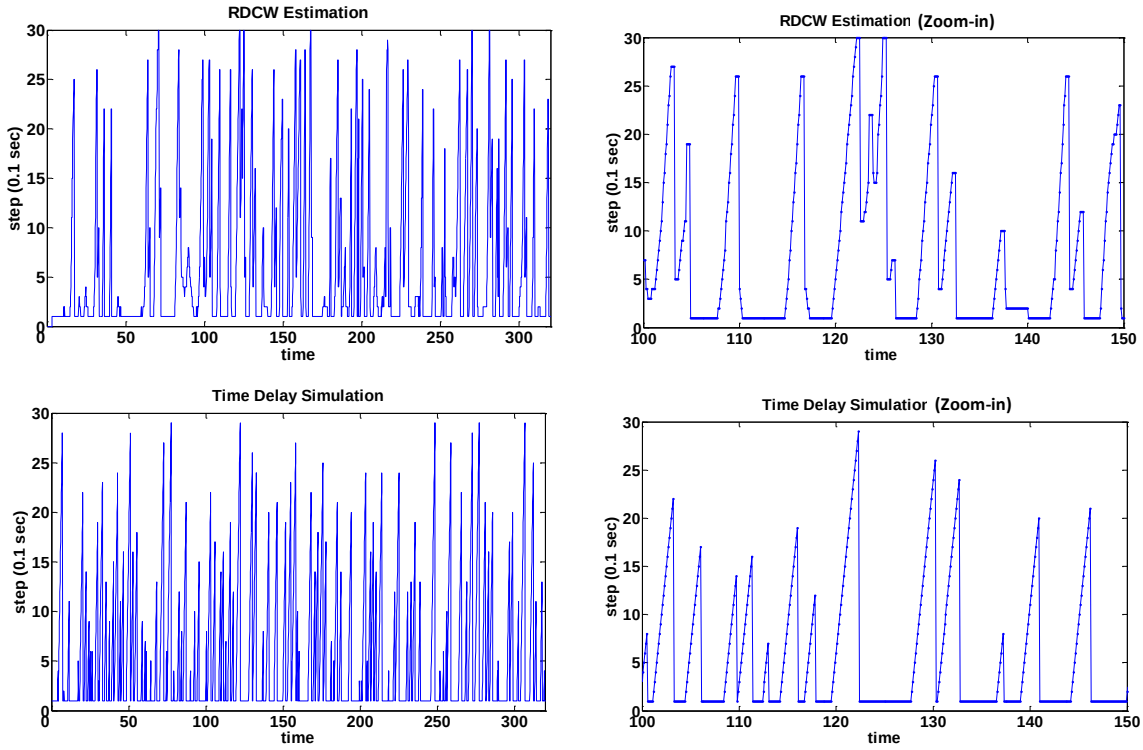

Fig. 5.4 Time delay simulation and comparison with the RDCW estimation

5.2.3 **Distraction**

Driver distraction was reported to be responsible for almost thirty percent of police-reported crashes [1]. Therefore, it is an important error-inducing mechanism that should be included. Driver can be distracted by in-vehicle tasks including cell phone usage, or interaction with other passengers, etc. [6]. The consequences of distraction can be hand-off the steering wheel, eyes off the road, or other adverse vehicle events (wandering in the lane, sudden braking, etc) [1]. To model driver distraction, we need to understand how distraction affects normal driving behavior. During driving, human can be considered as multi-tasking. If there is no distraction, a human driver can control the vehicle with full attention. When a secondary task happens, the human driver will have reduced attention to driving. Some of the secondary tasks may require higher participation and may temporarily disable human driver's ability to attend to driving (Fig. 5.5). Sheridan [94] suggested a switching type of control configuration that can be applied to model the transition between different modes of driving. In this study, we define the multi-task driving as "mind-off-the-road". The human driver is assumed to keep his/her eyes on the road while doing the secondary task. However, the non-driving task increases the mental load and degrades the driving performance. Boer [95] reported an increasing deviation of steering wheel angle for lane-keeping driving. The same increasing deviation of control should exist in car-following driving. Meanwhile, if a human driver fully devotes himself or herself into a secondary task, very often he/she will move the eyes to this task and stop updating the driving information. We define this situation as "eyes-off-the-road".

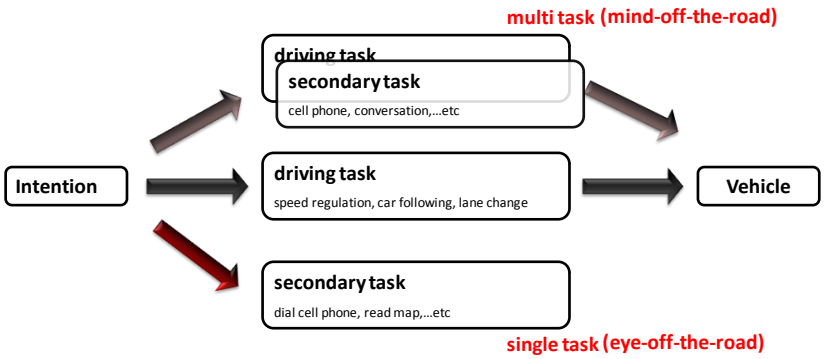

Fig. 5.5 Different driving mode of driver under distraction

One challenge in the errable driver model is to identify the "mind-off-the-road" mechanism and quantify it for modeling. Driving data from 10 drivers was collected from the RDCW database. Based on the actual test data, the SDM can predict the next vehicle states and calculate their deviations. The SDM contains two elements, desired accelerations and possible deviations. Based on the actual test data, the SDM can use desired acceleration to predict next vehicle states and calculate their possible deviations respectively. If the test data lands outside of plus/minus one standard deviation of the prediction, we define it as a deviated behavior (Fig. 5.6). In this study, the deviated behavior is assumed to be a consequence of mind-off-the-road.

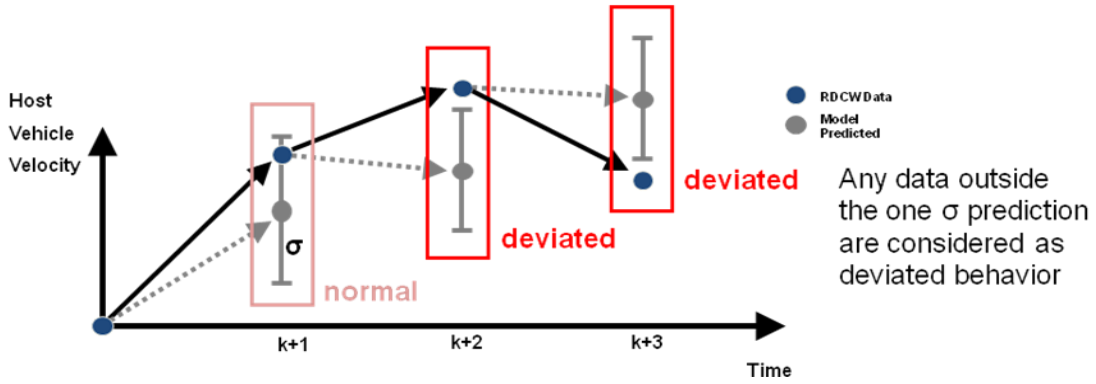

Fig. 5.6 Distraction prediction based on the SDM

This analysis is applied to the RDCW data and the result is shown in Fig. 5.7. The predicted result is shown on the right hand side of Fig. 5.7 with dotted line and can be modeled by an alternative renewal process with two independent identical distributions (IID) (Fig. 5.8).

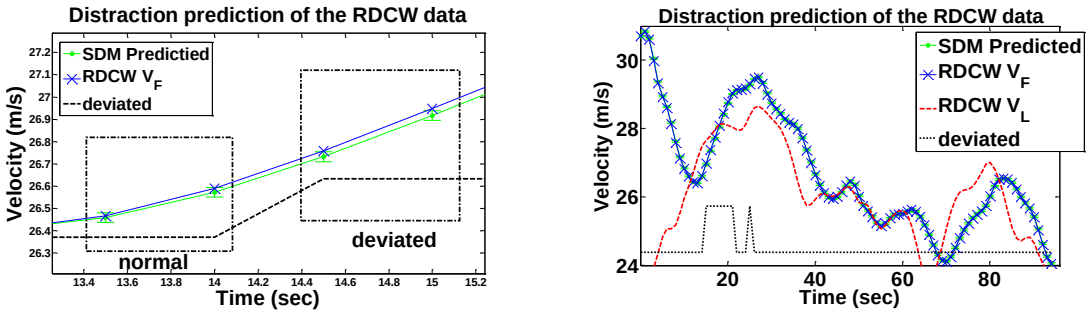

Fig. 5.7 Distraction prediction of the RDCW data

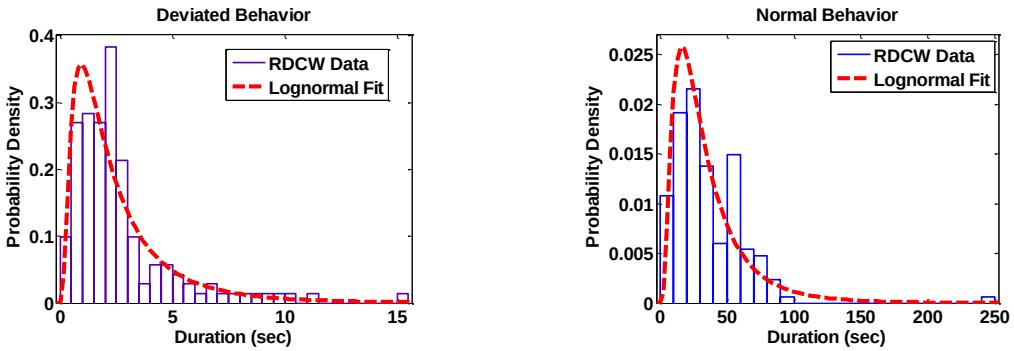

Fig. 5.8 Distribution and fitting of the normal and deviated behavior

Every time the process has a renewal event which indicates the driver is distracted the deviation in the random number generator Equation (4.9) would be increased (to model the increased workload and the degraded control).

Table 5.1 Distributions parameters of mind-of-the-road distraction

Lognormal Distribution	**Mean (sec)**	**STD**
Normal	**26.62**	**0.75156**
Deviated	**1.8465**	**0.89344**

This type of distraction is modeled as alternative renewal processes. Drivers are assumed to start at a normal condition without distraction. After an inter-arrival time, which has mean and standard deviation listed in Table 5.1, drivers will become distracted for a short period of time. This process will be repeated indefinitely in simulations and one simulation example is illustrated in Fig. 5.9.

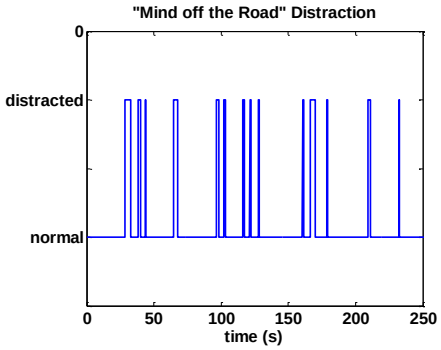

Fig. 5.9 Example of renewal sequence for modeling mind-off-the-road distraction

When eyes are off the road, drivers stop updating the feedback cues and/or the control actions. The perceived range, range-rate, and speed would remain unchanged from the previous step. Drivers are also assumed to freeze their control actions at the previous level. Once the distraction ends, the driver will resume updating the information and perform proper control action. The above statement can be realized by using a switch and a register. The eye-off-the-road behavior are studied in several literatures and frequency of occurrences can be found in [1] and [104]. However, the effect of eye-off-the-road is at least partially included in this errable driver model when the time delay is modeled in section 5.2.2. In Fig. 5.10, the time delay appears to increase linearly with time and they get reset. In other words, the driver model keeps using the same old data without updating, which is equivalent to switch off the information flow. Therefore, another mechanism will not be implemented to avoid double-counting the effect of eye-off-the-road.

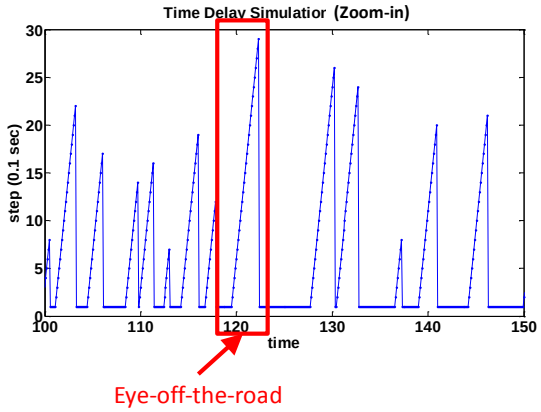

Fig. 5.10 The equivalent effect of eye-off-the-road in modeling time delay

5.2.4 **Simulation Results**

All three error inducing behaviors are implemented on the stochastic driver model. The resulted errable driver model is illustrated in Fig. 5.11.

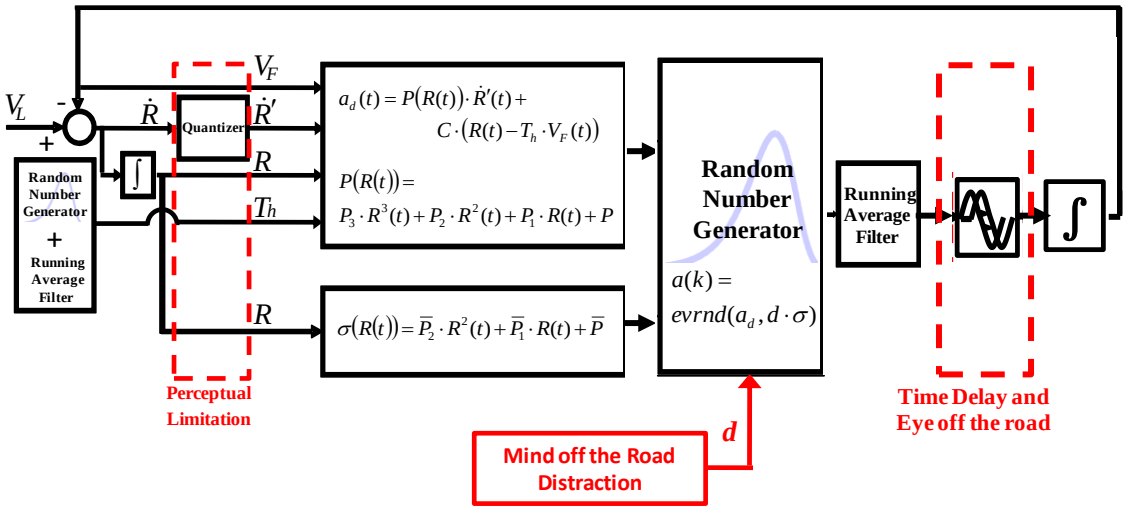

Fig. 5.11 Block diagram of errable driver model

A time-domain simulation example is shown in Fig. 5.12. A minor crash occurs under a lead-vehicle maneuver extracted from the RDCW database. Notice that in this particular case, the simulated driver is much slower than the actual test result, because during the critical moment, the simulated driver happens to have several long delays. If we simulate the same scenarios multiple times, under most cases there will be no crash. The behavior of the simulated driver, we hope, is similar to the actual driver statistically.

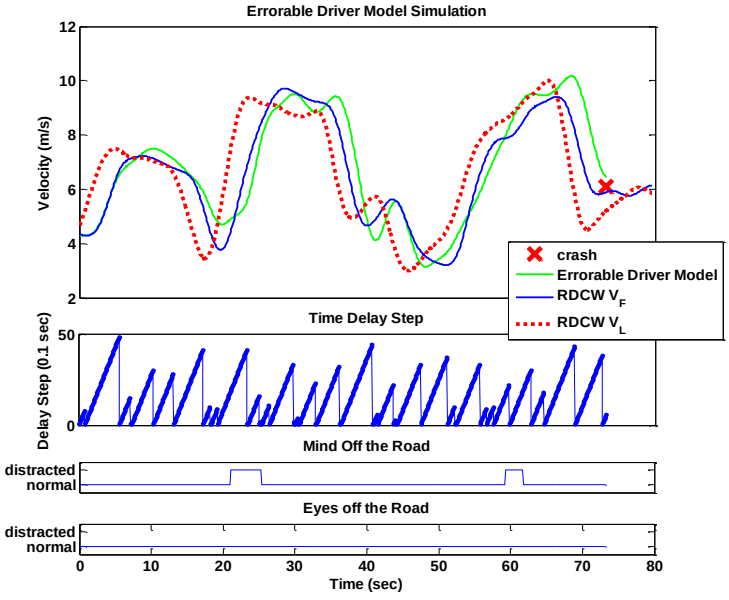

Fig. 5.12 Time domain simulation of the errable driver model

A thorough validation of the proposed model is hard to do because of the statistical nature of human drivers and the proposed model. Despite of great promise, advanced tools such as functional MRI is still far away from practical use to assess real human errors. One measurement known as "confliction" is used for characterizing driver behavior under near the crash situation of car-following [102]. Confliction is defined in ICC FOT as the frequency of being in the "near" region (Fig. 5.13).

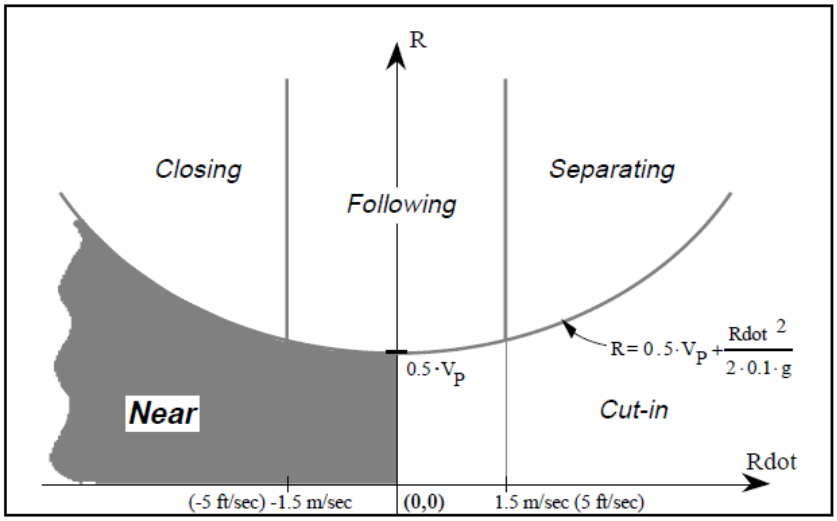

Figure 44. Near region in the range-versus-range-rate space

Fig. 5.13 Near region defined in ICC FOT [102]

The near region is defined by the following equation:

$$\dot{R} < 0 \text{ and } R < 0.5 \cdot V_p + \frac{\dot{R}^2}{2 \cdot 0.1 \cdot g} \tag{5.3}$$

Vp is the lead vehicle velocity. The equation (5.3) can be interpreted as the lead vehicle is within 0.5 sec ahead and decelerated faster than 0.1 g. This represents a near crash situation in the car-following which the proposed errable driver model is meant to simulate. Frequencies of being in the confliction by drivers from RDCW database are first calculated. Then, the errable driver model behavior is generated with the lead vehicle inputs from the same RDCW data set. The example of resulting probability of being in the confliction is compared in Fig. 5.14.

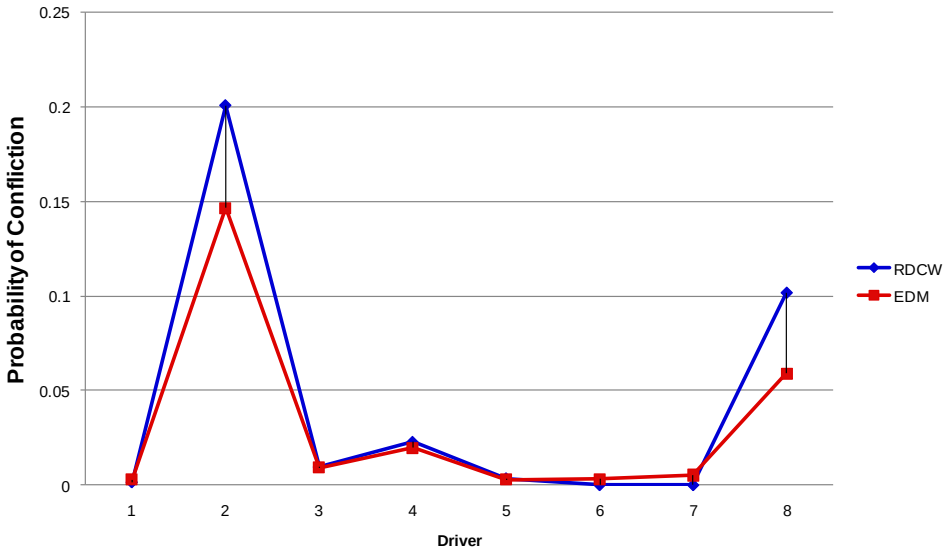

Fig. 5.14 Probability of being in the confliction

The errable driver model has similar probability of being in the confliction with drivers from RDCW database, except for driver 2 and 8. The probabilities of confliction in driver 2 and 8 are underestimated by the errable driver model. The errable driver model does not drive "close" enough like the RDCW driver 2 and 8. This characteristic can also be found by analyzing the driving style of each driver. The driving style is also defined in ICC FOT by the percentage of time being in the different region of normalized range-range rate diagram.

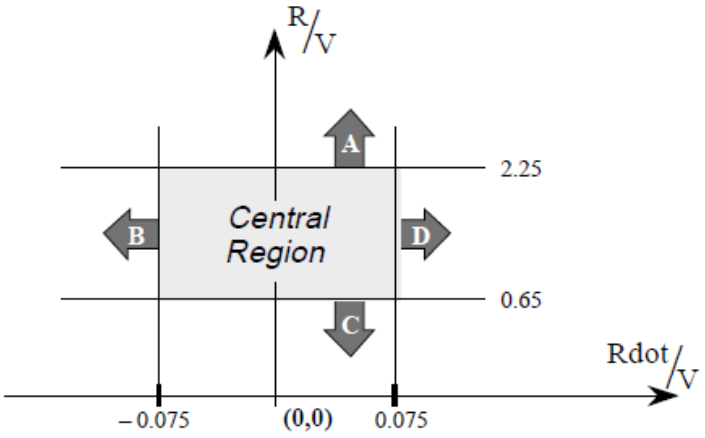

Figure 45. Boundaries used in defining driving styles

Fig. 5.15 The normalized range-range rate diagram for defining driving styles [102]

The four regions A, B, C, and D are defined as:

$$\begin{cases} A = P(R/V > 2.25) \\ B = P(\dot{R}/V < -0.075) \\ C = P(R/V < 0.65) \\ D = P(\dot{R}/V > 0.075) \end{cases} \tag{5.4}$$

where $P(\ldots)$ is the probability of the event enclosed in the parentheses. The measurement A represents the "far" tendency of a driver; B represents the "fast"; C represents "close"; and D represents "slow". The four measurements are used to categorize the driving styles of each driver. The comparison of the RDCW drivers and the errable driver model is showed in Fig. 5.16.

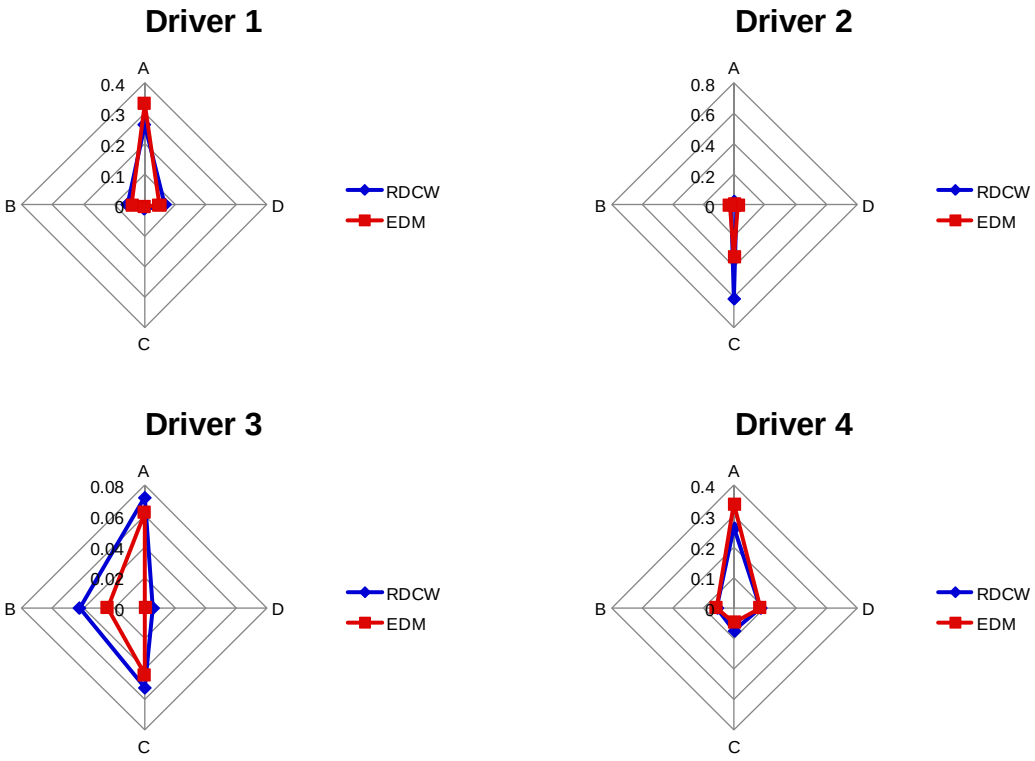

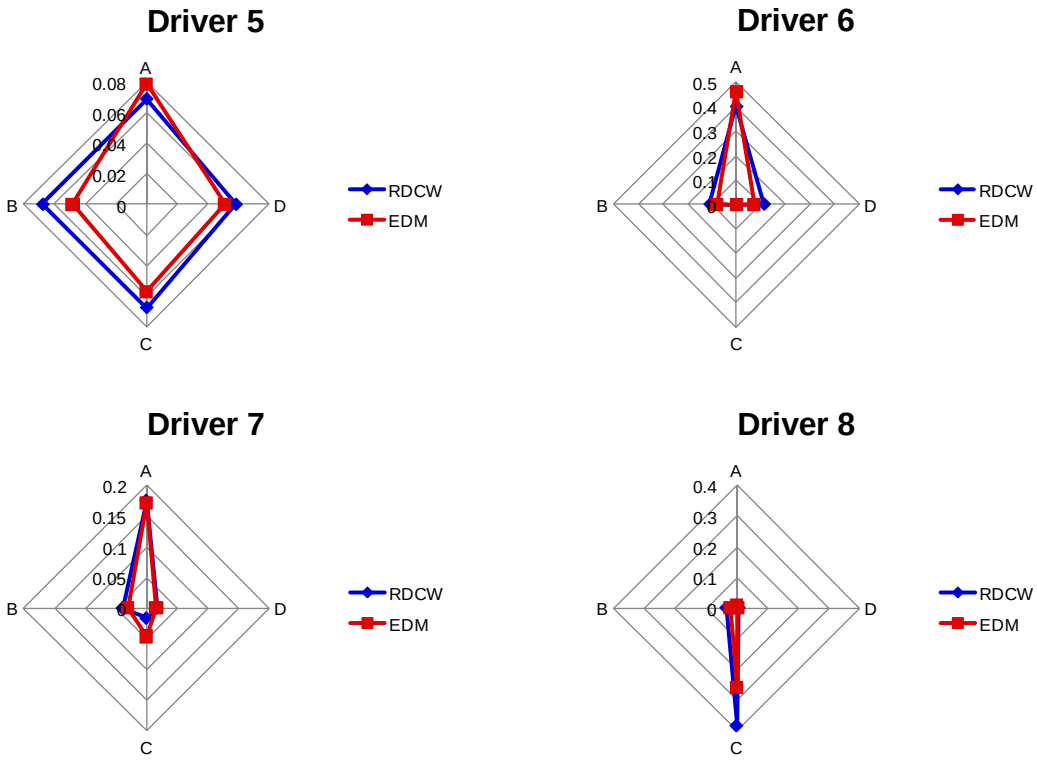

Fig. 5.16 Driving styles defined in ICC FOT comparison

Driver 1, 4, 6, and 7 have tendencies of being far from the lead vehicle and the errable driver model captures their behavior very well. Driver 3 and 5 actually tend to stay in the central region because all four measurements are very small. Driver 2 and 8 in RDCW data have tendencies of being close and the errable driver model is underestimated these tendencies which are consistent with the confliction measurement.

The errable driver model captures RDCW driver behavior of the near crash situation well, but there are some extreme cases (driver 2 and 8) that are underestimated. The ability of modeling the near crash situation is useful for developer of the CW/CA algorithm. A more significant advantage of the errable driver model is the ability to simulate crashes. In the real driving data, no (or very few) crash is available that the performance of CW/CA algorithms can only be estimated. Crashes that generated by the errable driver model can be used to evaluate the performance of CW/CA algorithms thoroughly. Because of the statistical nature of the errable driver model and the lack of real crash data, the validation is hard to make. In this study, the crash rate is used to

represent the statistic of crashes and quantize the performance of the errable driver model in terms of simulate crashes.

Crash per Vehicle Miles Traveled is used to define the crash rate. To evaluate the crash rate of the errable driver model, 340 RDCW driving maneuvers of ten drivers are selected and the lead vehicle speed is used as the input to the errable driver model. Those maneuvers have time-span from fifty to more than three hundred seconds. Each of them is simulated for one thousand times to fully demonstrate the stochastic nature of the model. The simulated crash rate is shown in Table 5.2.

Table 5.2 Errable driver model crash rate

Crash Number	Total Simulation Mileage	Crash/100M VMT
25	**8,846,976**	**282.6**

The simulation results are compared with actual crash data obtained from NHTSA report [1]. In year 2005, the average rate for all type of crash is 206 per 100M VMT. For passenger and light truck, about 30% of the crashes are rear-end crashes. Thus, the actual crash rate for rear-end collision is approximately 60/100M VMT. Our simulation crash rate is too high. One possible explanation is that not all minor crashes are reported. Another possible explanation is the lack of a feedback mechanism in our model under near-crash situations. In the actual near crash driving, a driver may be warned by passengers, brake light, etc. and engage in an emergent maneuver, with much higher deceleration level, which is not captured in our model. In other words, the errable driver model developed in this paper represents a conservative approximation of actual drivers, with all statistical characteristics identified from actual driving data. This conservative characteristic, we believe, is actually useful for evaluating AST, such as Collision Warning/Collision Avoidance systems. CW/CA system is designed for situations when the driver does not properly react to a near crash event, which the proposed model seems to emulate.

5.3 Evaluating CW/CA algorithms

The errable driver model can improve the evaluations of CW/CA algorithms in several ways. In a scenario-based approach, the driving behavior of the target vehicle can be replaced by a humanized errable driver model. The errable driver model could generate more realistic driving behavior than randomly selected scenarios. For a human centered approach, the errable driver model can be used to generate near-crash or crash maneuvers. It should be noted that crashes do not happen frequently. Even for large-scale driving database such as [103] with more than 82,000 miles of driving, all the identified threatening situations did not result in an actual crash. With the errable driver model, actual crashes can be simulated and used for evaluating CW/CA algorithms.

Even though the errable driver model can be used to generate driving behavior under prescribed test matrices. An alternative is proposed to fully utilize the advantage of the errable driver model and not limit it use to prescribed test matrices. The errable driver model is developed based on a stochastic driver model and all error-inducing behaviors are imposed as stochastic processes. Given any initial conditions (vehicle velocity, range-rate, range and lead vehicle acceleration), the probability of future maneuvers can be calculated. Hence, the probability of crash can be predicted without exhaustive simulations. A simple example is done by using only the stochastic driver model without any error mechanisms. To demonstrate this concept, a one step prediction is done. For any given range, range-rate and following vehicle speed, the distribution of the acceleration of the following vehicle can be calculated by the stochastic driver model. With the leading vehicle velocity or even acceleration available, the crash-accelerations that would end up with a crash in a preview time can be calculated from

$$R \le (V_L - V_F)\cdot t + 1/2\cdot(a_L - a_F)\cdot t_{preview}{}^2 \Rightarrow a_{crash} \ge \frac{R - \dot{R}\cdot t_{preview}}{1/2\cdot t_{preview}^2} + a_L \qquad (5.5)$$

After obtaining the crash-accelerations, the probability that driver will actually accelerate at or beyond those crash-accelerations can be calculated by replacing a_d in (4.11) with a_{crash}. A one dimension example is shown in Fig. 5.17. Initial conditions were V_F = 30m/s, range-rate = -4m/s, lead vehicle acceleration = -0.22g and preview time

= 2s. The initial range is varied from zero to twenty meters and their corresponding probability of crash can be calculated.

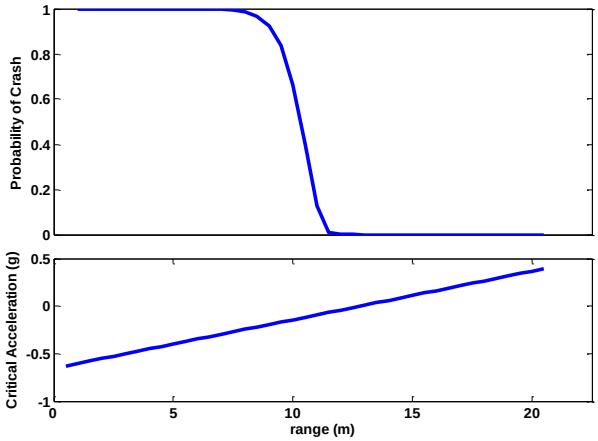

Fig. 5.17 An example of probability of crash (lead vehicle velocity = 30m/s, range-rate = -4m/s, lead vehicle acceleration = -0.22g)

Fig. 5.17 can be interpreted as follows: for the given conditions, whenever the range is smaller than 7.0m, the target vehicle will have a crash within the next two second. And, if the range is large than 12m, the probability of crash within the next two second is zero. This approach can be further extended to multi-dimensions and compared with existing CW/CA algorithms timing. Several algorithms are compared in Fig. 5.18.

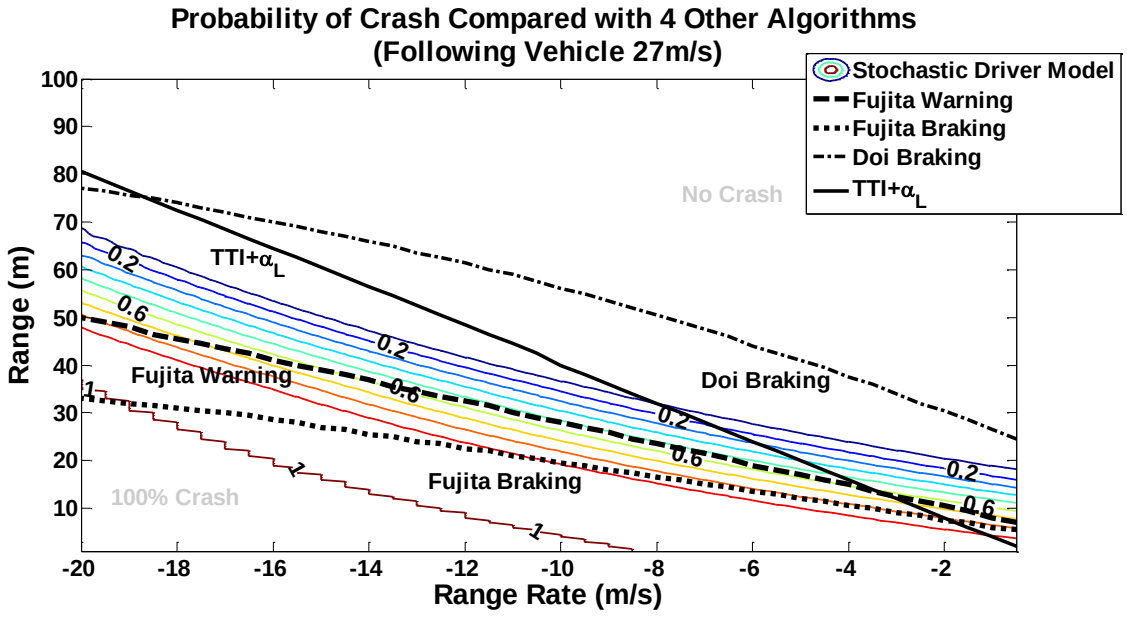

Fig. 5.18 Probability of Crash Predicted by SDM compared with other algorithms

Some preliminary conclusions can be draw from Fig. 5.18. For example, the Doi's algorithm issues warnings earlier than EDM prediction and Fujita's algorithms are generally late. Those conclusions are confirmed with the human-approach evaluation results [103]. However, this preliminary evaluation approach is done without any error-inducing behavior and only one prediction step is used. More detailed and completed evaluation will be done in the future study.

5.3.1 **Developing a humanized CW/CA algorithm**

In the previous section, the errable driver model is used to evaluate the CW/CA algorithms by comparing the warning timing with the probability of crash. This probability of crash can also be used as the warning criteria. The probability of crash can be calculated based on actual vehicle states. If the predicted probability of crash exceeds a threshold, a warning can be issued. The prediction method provided in the previous section estimates the maximum acceleration which would cause a crash and calculates the probability of crash backwards. This method is computation effective but not accurate because it assumes constant acceleration through the whole prediction horizon. A forward multi-step prediction can be used to achieve a higher accuracy. Using current vehicle states as the starting point, the vehicle's possible future states can be predicted with their probability. A simplified example is shown in Fig. 5.19.

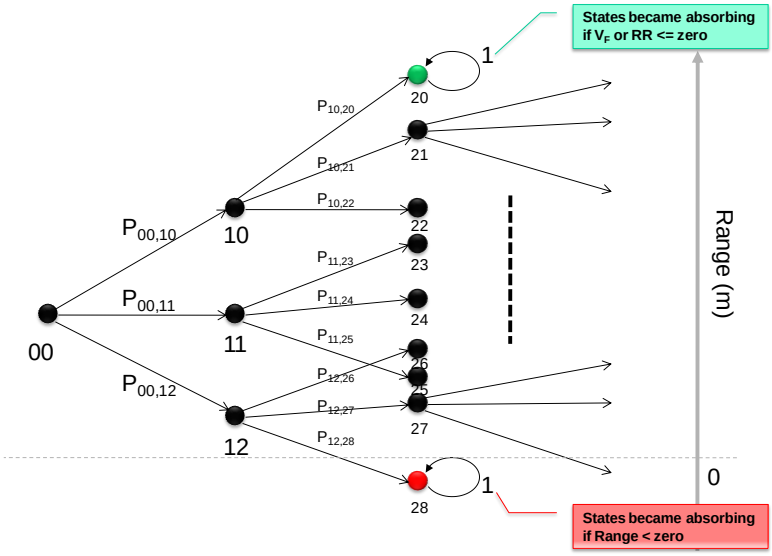

Fig. 5.19 Multi-step prediction for the vehicle future range

The prediction is assumed to start at state 00. The next three possible states 10, 11, and 12 can be calculated with their probability $P_{00,10}$, $P_{00,11}$, and $P_{00,12}$ respectively. The prediction can keep going until the preview time $t_{preview}$ or the states become absorbing. The states will become absorbing if the following vehicle speed V_F and/or range-rate is equal to or smaller than zero, which indicates the vehicle is fully stopped or is slower than the lead vehicle. Meanwhile, the states can also become absorbing if the range is smaller than zero, which represents a crash. The probability of crash can be calculated by summing up probabilities of all the states that result in crashes.

An example is shown in Fig. 5.20. Initial conditions are V_F = 30m/s, range-rate = -4m/s, range = 20m, a_F = -0.6g. The preview time is 2 sec and prediction steps is 4 (0.5 sec each step). For every current state, there are 12 possible future states. Therefore, there would be 12^4 possible final vehicle states at the end of the preview. Each final state can be reached from the given initial state with a possibility. The possibilities are cumulated according to the range of final states, so that the possibility of what the range would be after two seconds can be plotted as Fig. 5.20.

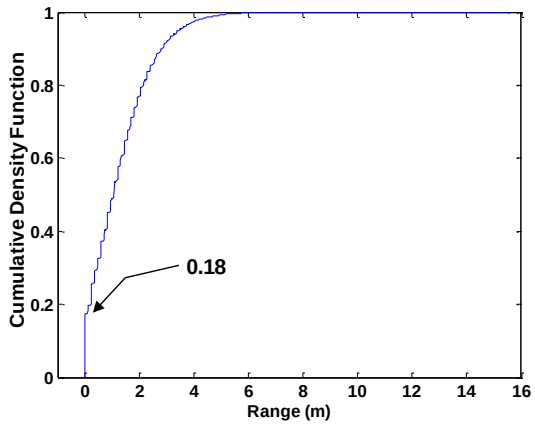

Fig. 5.20 Cumulative probability of vehicle range after two seconds.

The probability of crash (range smaller than zero) in the next two seconds in the future is 18% which may be high enough to issue a warming. Fig. 5.21 shows the probabilities of crash for different initial conditions. With error-inducing behaviors and multi-step prediction, probabilities of crash are slightly different from the prediction made in the previous section. The vehicle has higher probability of crash because of the error-inducing behaviors. However, the probability of crash increases slower because of

the multi-step prediction. The physical interpretation of multi-step prediction means the model has more steps to correct its behavior.

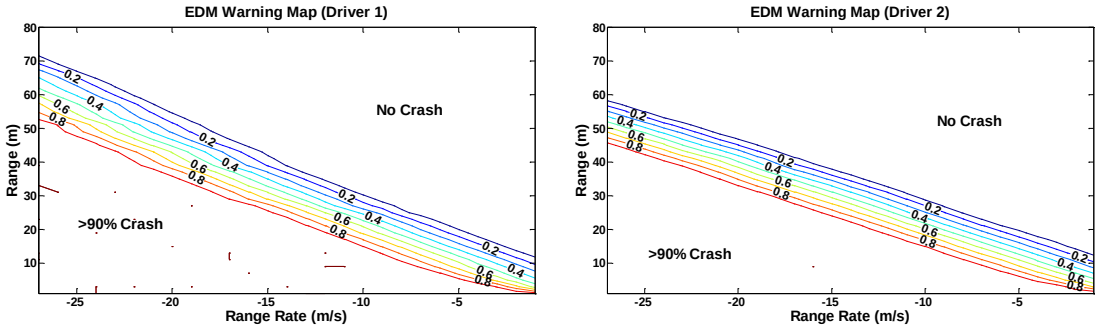

Fig. 5.21 Errable driver model warning map based on the behavior of two different drivers

This probability of crash distribution (Fig. 5.21) can be used to construct a warning map. One benefit of this algorithm is that the probability of crash can be selected to set different levels of warning. Algorithm developers can select appropriate warning levels and they can be driver adjustable. Another strength of using EDM as a CW/CA algorithm is its ability to adapt to different drivers' behaviors. When calibrating the errable driver model, model coefficients ($P_i(i=0,1,2,3)$ and $\overline{P}_i(i=0,1,2)$ in equations (4.6) and (4.7)) are obtained by fitting a set of driving data, which can be customized with individual driving data. Therefore, the errable driver model can be updated in real-time for better customization to the driver. Conventional CW/CA systems tuned under open-loop were frequently found to work unsatisfactorily with human-in-the-loop. If updated in real-time, the obtained CW/CA algorithm has the potential to achieve a much lower level of false positives and false negatives, which are critical for the commercialization of CW/CA algorithms.

5.3.2 **Summary**

A humanized errable car-following driver model is used to evaluate the performance of several CW/CA algorithms. This errable driver model emulates human driver and can generate both nominal (error-free) and devious (with error) behaviors. A large-scale naturalistic driving database is used for developing and validating this errable car-following driver model. Three error-inducing behaviors were implemented in this model,

human perceptual limitation, time delay, and distraction due to non-driving tasks. By combining three error-inducing behaviors, rear-end collisions with the lead vehicle occur, and at a probability similar to what is reported in traffic accident statistics. This ability of emulating rear-ends collision behavior is useful to evaluate the performance of CW/CA algorithms—several of which are shown and the evaluation results are summarized.

Subsequently, a new CW/CA algorithm is suggested based on the errable driver model. The driver model is used to predict the probability of crash, based on which warning or braking action can be issued. This algorithm is tuned with realistic human driving data. The developed CW/CA algorithm has the potential to be tuned in real-time to adapt to individual drivers. Efficient computation and actual performance of this CW/CA algorithm have not been demonstrated can be a future research topic.

5.4 Conclusion

An errable longitudinal driver model was developed. The term "errable" is new, and for which we mean a driver model which achieves the car-following task but can be made to make mistakes similar to real drivers. Those mistakes are induced based on several mechanisms that may be the cause of accidents in actual human driving.

Three types of error-inducing mechanisms are analyzed: perceptual limitation, distraction, and time delay. Each of them affects normal driving and degrades car-following performance. Individually, their effects might not be significant enough to induce a crash. However, combinations of those behaviors could cause crashes. Perceptual limitation is embedded in the errable driver model; distraction and time delay are modeled as stochastic processes. The parameters of those stochastic processes are estimated or adopted from available data in the literature. Then, stochastic processes are introduced into the longitudinal stochastic driver model independently. The resulting crash rate for the errable driver model is lager (282.6/100M VMT) compared with NHTSA data (60/100M VMT). One possible reason could be the lack of feedback mechanisms under near-crash situations. Those feedback mechanisms involve higher level of control which has not yet been included in this model.

The errable car-following driver model is used to evaluate the performance of several CW/CA algorithms. This errable driver model emulates human driver and can generate both nominal (error-free) and devious (with error) behaviors. This ability of emulating rear-ends collision behavior is useful to evaluate the performance of CW/CA algorithms—several of which are shown in this study and the evaluation results are summarized. Subsequently, a new CW/CA algorithm is suggested based on the errable driver model. The driver model is used to predict the probability of crash, based on which warning or braking action can be issued. This algorithm is tuned with realistic human driving data. The developed CW/CA algorithm has the potential to be tuned in real-time to adapt to individual drivers. Efficient computation and actual performance of this CW/CA algorithm has not been demonstrated and are our current research focus.

CHAPTER 6
CONCLUSION AND FUTURE STUDY

6.1 Conclusion

Human anomalous driving behaviors in both lateral and longitudinal driving are analyzed. A new kind of driver models is developed to emulate anomalous driving behaviors. This new type of models is developed based on the concept that a driver model that normally achieves driving tasks could be perturbed to emulate anomalous behaviors like human drivers by considering human's inherent limitations or by incorporating error mechanisms. When driver limitations or error mechanisms are properly designed, these driver models generate accidents or near-accident behaviors that are of interest to engineers who are developing Active Safety Technology (AST). AST is developed for assisting human drivers to avoid or mitigate accidents. They are helpful when drivers are either making a wrong move or are not able to handle the situation. To evaluate the effectiveness of AST, driver models that achieve driving tasks normally and emulate anomalous behaviors at the same time would be more useful. Most existing models focus on describing driver behavior under normal tasks, and few of them include anomalous behaviors. The main contribution of this study is to fulfill the missing link between modeling normal driving tasks and modeling anomalous behaviors and to provide the development of architecture and modeling process for driver models that emulate anomalous behaviors.

The vehicle crosswind stability problem induced by driver limitations is used as an example for the lateral driving. An analytical vehicle model (UMTRI wind-steer model) and a complex commercial software model (CarSim) are used to analyze and simulate the crosswind driving. A fixed-base simulator test is conducted to collect human driving behaviors under crosswind. Finally, a lateral driver model that emulates

both normal and anomalous behaviors is developed. A linear analysis is formulated to provide an insight understanding of driver limitations that induce instability. Two excises are presented for demonstrate the benefit of using the developed lateral driver model to evaluate the stability of vehicle under crosswind and the effectiveness of active safety systems.

The UMTRI wind-steer model is implemented in MATLAB/Simulink and is suitable for driver vehicle dynamic response analysis. The CarSim model is used for the simulator test and potential AST design. Based on the sensitivity analysis with UMTRI wind-steer model, variation in C.G. position is found to have the highest sensitivity to the crosswind input. Along with four other design parameters with high sensitivity, five vehicle configurations are implemented in the fixed-base driving simulator test. Two crosswind scenarios are employed in the simulator: impulse crosswind and natural crosswind. The impulse crosswind is used for the driver model development and the subjective stability assessment. The natural crosswind is used for verification and evaluation of AST design. Twenty four test participants are recruited and successfully complete the simulator test.

Four categories of driving styles under crosswind are identified from the simulator test analysis. Then, a lateral driver model that emulates anomaly behaviors for crosswind maneuver is developed. This driver model is a combination of MacAdam's driver model and an instantaneous feedback reaction for strong crosswind disturbances. It captures the driving behavior better than the original MacAdam's driver model and it also captures the spin-out accidents that also happened in simulator tests. The ability of reproducing yaw-rate responses makes this model suitable for evaluating the vehicle crosswind stability. A new closed-loop crosswind stability evaluation method is proposed. This method evaluates vehicle crosswind stability almost as easy as using the crosswind sensitivity approach. Meanwhile, the developed feedback MacAdam's model is also used for the evaluation and design of active steering systems. Trade-off between stability and maneuverability is identified and a new design is proposed to minimize the trade-off.

A longitudinal errable driver model is developed for understanding anomalous behaviors due to driving errors. This errable driver model normally achieves car-

following tasks and can be made to make mistakes like human. Those mistakes are induced based on the same mechanisms which could cause accidents in actual driving. The accidents or error behaviors emulate real human behaviors, and the error rate matches the real driving error rate statistically. The ability of emulating rear-ends collision behavior is used to evaluate the performance of CW/CA algorithms and develop a new CW/CA algorithm.

A large number of car-following trips are identified and collected from RDCW database. Simple filtering is applied to improve the data quality. Random behavior are observed in the data and modeled by a stochastic driver model. This model is developed and evaluated against the naturalistic driving data. Sufficient flexibility is shown in training this model to fit the data. Meanwhile, superior robustness is demonstrated in predicting the human driving behavior in evaluation test sets. The stochastic driver model captures human's normal driving behaviors with deviations. Moreover, those normal and deviated behaviors are statistically similar to what we observed in the actual driving data.

Three types of error-inducing behaviors are analyzed: perceptual limitation, distraction, and time delay. Each of them affects the normal driving and degrades the car-following performance. Individually, their effects might not be significant enough to induce a crash. However, combinations of those behaviors could cause crashes. To validate this hypothesis, the error-inducing behaviors are modeled as stochastic processes based on the frequency of their occurrences. Then, those stochastic processes of error are introduced into the longitudinal driver model independently. The resulting crash rate for the errable driver model is similar (282.6/100M VMT) compared with NHTSA data (60/100M VMT).

The ability of emulating rear-ends collision behaviors is used to evaluate the performance of CW/CA algorithms—several of which are shown in this study and the evaluation results are summarized. A new CW/CA algorithm is proposed based on the errable driver model. The driver model is used to predict the probability of crash, based on which warning or braking action can be issued. This algorithm is tuned with realistic human driving data. The developed CW/CA algorithm has the potential to be tuned in

real-time to adapt to individual drivers. Efficient computation and actual performance of this CW/CA algorithm have not been demonstrated and are our current research focus.

6.2 Future Study Plan

In the lateral driving behavior study, a fixed-base simulator test is conducted. The visual feedback of vehicle motion provides basic information for performing the lane-keeping task, but is not necessary sufficient for near-accident/accident maneuvers. In the normal driving situation, lane position and vehicle heading information, which can be provided through visual cue, may be enough for driver to control the vehicle. In extreme or anomalous situations, driver may need more information which is lacking from the fixed-base simulator. A motion-base simulator which can provide both visual and motion feedback would be more close to the real driving and, hence, provide a more reliable analysis.

Motion-base simulator test can be conducted using a similar setting of the fixed-base simulator test. However, several refinements should be done. First of all, the learning effect is observed during the simulator test. The recurring impulses crosswind input provides good repetition for identifying and verification of lateral driver model development. But the frequency sweeping type of impulses are predictable and have less surprise for experience drivers. A modification can be done by introducing more randomness into the impulse sequences. An example is shown in Fig. 6.1.

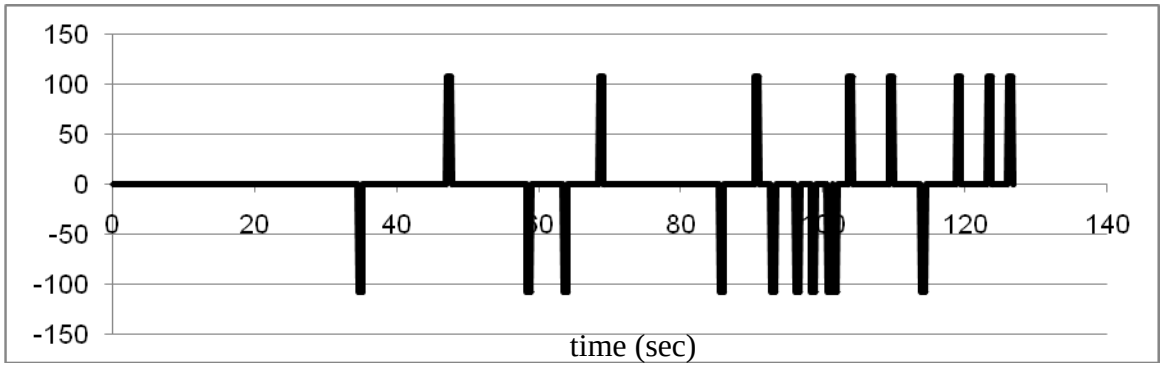

Fig. 6.1 Modified impulse crosswind input to minimize learning effect

This input sequence has identical impulses for repetition but more randomness in occurrence for preventing test drivers from anticipating the disturbance. Another

necessary modification is adding surrounding traffics. In our test scenarios, test drivers can drifted (due to crosswind) to the other lane without immediate dangerous. With surrounding traffic, more realistic recovery maneuver from the lane departure would be needed. Finally, the proposed variable gear ratio strategy can be implemented. The performance of this VGR system can be evaluated and a more insightful understanding of VGR system can be established.

In the longitudinal errable driver model, the distraction and time delay are modeled as renewal processes. The renewal time is only depended on a random distribution and not influenced by the environment, e.g. the lead vehicle motion. Therefore, once the state of the model is set to be distracted, it will not be recovered until the next renewal arrived. However, in actual driving, a driver may recover from his/her distracted driving to attentive driving if the environment is potentially danger, e.g. the lead vehicle is too close. This recovery action can be prompted by passengers, brake light, or CW/CA algorithms. Some of those behaviors require higher level of perception, cognition, and decision modeling. An input-output task-specific model like the errable driver model may not be able to model those behaviors. A more complex, multi-task modeling approach will be needed.

Appendix A Questionnaire Sheets

Date Participant #

PARTICIPANT INFORMATION SHEET

PARTICIPANT INFORMATION

Gender: _____ Age: _____

DRIVING EXPERIENCE

Years driving: _____ Mileage last year (approx.): _____

Average travel per week: _____ Average mileage per travel: _____

VEHICLE INFORMATION

Primary Make: _____ Primary Model: _____ Primary Year: _____

Secondary Make: _____ Secondary Model: _____ Secondary Year: _____

QUESTION

Have you ever experienced crosswind disturbances during your driving? Yes No

If yes, how often?

_____

_____

Have you ever lost control of your vehicle under crosswind? Yes No

If yes, please describe the situation.

_____

_____

Have you ever lost control of your vehicle under other situation? Yes No

If yes, what is the cause for losing control?

_____

_____

Date Participant #

DRIVING SIMULATOR PERFORMANCE ASSESSMENT SHEET

STEERING WHEEL RESPONSE

1 2 3 4 5 6 7 8 9 10

Not realistic Feels real

ACCELERATION PEDAL

1 2 3 4 5 6 7 8 9 10

Not realistic Feels real

BRAKE PEDAL

1 2 3 4 5 6 7 8 9 10

Not realistic Feels real

VEHICLE RESPONSE

1 2 3 4 5 6 7 8 9 10

Not realistic Feels real

VISUAL EFFECT

1 2 3 4 5 6 7 8 9 10

Not realistic Feels real

HOW WOULD YOU RATE THIS DRIVING SIMULATOR EXPERIENCE TO THE REAL DRIVING?

1 2 3 4 5 6 7 8 9 10

Not realistic Feels real

If it's not realistic, what is the main deficiency?

Date Participant #

CROSSWIND STABILITY ASSESSMENT SHEET

CONFIGURATION 1

Vehicle Stability 100km/h

1	2	3	4	5	6	7	8	9	10
Uncontrollable				Has effect but Controllable				No Wind Effect	

Vehicle Stability 160km/h

1	2	3	4	5	6	7	8	9	10
Uncontrollable				Has effect but Controllable				No Wind Effect	

CONFIGURATION 2

Vehicle Stability 100km/h

1	2	3	4	5	6	7	8	9	10
Uncontrollable				Has effect but Controllable				No Wind Effect	

Vehicle Stability 160km/h

1	2	3	4	5	6	7	8	9	10
Uncontrollable				Has effect but Controllable				No Wind Effect	

CONFIGURATION 3

Vehicle Stability 100km/h

1	2	3	4	5	6	7	8	9	10
Uncontrollable				Has effect but Controllable				No Wind Effect	

Date **Participant #**

Vehicle Stability 160km/h

1	2	3	4	5	6	7	8	9	10
Uncontrollable				Has effect but Controllable				No Wind Effect	

CONFIGURATION 4

Vehicle Stability 100km/h

1	2	3	4	5	6	7	8	9	10
Uncontrollable				Has effect but Controllable				No Wind Effect	

Vehicle Stability 160km/h

1	2	3	4	5	6	7	8	9	10
Uncontrollable				Has effect but Controllable				No Wind Effect	

CONFIGURATION 5

Vehicle Stability 100km/h

1	2	3	4	5	6	7	8	9	10
Uncontrollable				Has effect but Controllable				No Wind Effect	

Vehicle Stability 160km/h

1	2	3	4	5	6	7	8	9	10
Uncontrollable				Has effect but Controllable				No Wind Effect	

Appendix B Driver Background Information

Participant	1	2	3	4	5	6
Gender	male	male	male	female	male	male
Age	36	32	25	26	18	28
Years Driving	10	3	6	1	2	1
Primary Model	mini-van	sedan	compact	sedan	sedan	compact
Crosswind Experience	once/week	rare	frequently	no	once	occasionally
Lost control by crosswind	no	no	no	no	no	no
Lost control of any kind	no	yes	no	no	no	yes
Participant	**7**	**8**	**9**	**10**	**11**	**12**
Gender	male	male	male	male	male	male
Age	33	22	28	20	19	31
Years Driving	9	8	5	5	3	13
Primary Model	small SUV	sedan	compact	sedan	compact	small SUV
Crosswind Experience	twice	rare	3~5	frequently	no	rarely
Lost control by crosswind	no	no	no	no	no	no
Lost control of any kind	no	yes	yes	yes	no	no
Participant	**13**	**14**	**15**	**16**	**17**	**18**
Gender	female	male	male	male	male	female
Age	29	31	21	20	22	31
Years Driving	6	8	6	4	6	10
Primary Model	small SUV	compact	hatch back	hatch back	compact	compact
Crosswind Experience	rarely	2-3/yr	occasionally	rarely	rarely	twice/yr
Lost control by crosswind	no	no	no	no	no	no
Lost control of any kind	no	yes	yes	no	no	no
Participant	**19**	**20**	**21**	**22**	**23**	**24**
Gender	male	male	female	male	male	male
Age	18	27	29	18	24	27
Years Driving	2	9	3	2	5	9
Primary Model	mid-SUV	wagon	compact	sedan	van	
Crosswind Experience	1-2/week	often	1/week	twice	seldom	no
Lost control by crosswind	no	no	no	no	no	no
Lost control of any kind	yes	no	no	yes	no	no

Appendix C Driver Spin out Cases

Participant		1	2	3	4	5	6
Baseline	160	spin out	spin out	-	spin out	-	spin out
Cargo	160	spin out	spin out	-	spin out	-	spin out
Decreased yaw	160	-	-	-	-	-	-
Increased yaw	160	spin out	spin out	spin out	spin out	spin out	spin out
Spoiler	160	-	-	-	-	-	-
Participant		**7**	**8**	**9**	**10**	**11**	**12**
Baseline	160	spin out	-	spin out	spin out	-	spin out
Cargo	160	spin out	-	spin out	spin out	-	spin out
Decreased yaw	160	-	-	-	-	-	-
Increased yaw	160	spin out	spin out	spin out	spin out	spin out	spin out
Spoiler	160	spin out	-	-	-	-	-
Participant		**13**	**14**	**15**	**16**	**17**	**18**
Baseline	160	spin out	spin out	-	-	-	spin out
Cargo	160	-	spin out	-	-	-	spin out
Decreased yaw	160	-	-	-	-	-	-
Increased yaw	160	-	spin out	-	-	spin out	spin out
Spoiler	160	-	-	-	-	-	-
Baseline Repeated	160	-	-	-	-	-	-

Participant		19	20	21	22	23	24
Baseline	160	spin out	spin out	spin out	spin out	spin out	spin out
Cargo	160	-	-	spin out	spin out	spin out	-
Decreased yaw	160	-	-	-	-	-	-
Increased yaw	160	spin out	spin out	spin out	spin out	spin out	spin out
Spoiler	160	-	-	-	-	-	-
Baseline Repeated	160	-	-	-	-	spin out	-

Appendix D Driver Subjective Rating

Participant		1	2	3	4	5	6
baseline	100	8	7	7	4	9	5
	160	2	2	5	2	6	4
cargo	100	8	8	7	5	9	6
	160	3	3	5	3	7	5
d-yaw	100	8	9	7	5	9	7
	160	4	7	5	5	8	8
i-yaw	100	7	9	7	6	8	7
	160	2	4	3	5	4	6
spoiler	100	8	9	8	7	8	8
	160	3	8	5	5	8	9
Participant		**7**	**8**	**9**	**10**	**11**	**12**
baseline	100	6	6	8	7	7	7
	160	1	3	1	3	2	2
cargo	100	6	6	8	7	8	8
	160	1	2	2	3	3	2
spoiler	100	6	7	9	8	8	8
	160	1	3	5	5	3	2
i-yaw	100	6	7	9	8	9	7
	160	1	1	2	3	2	1
d-yaw	100	6	8	9	8	9	8
	160	5	5	5	5	4	3
Participant		**13**	**14**	**15**	**16**	**17**	**18**
baseline	100	4	6	8	6	6	9
	160	1	1	4	3	4	2
d-yaw	100	6	8	8	8	7	9
	160	4	6	6	7	5	6
cargo	100	5	4	7	7	5	7
	160	2	2	5	3	3	1
spoiler	100	5	7	7	5	7	8
	160	4	3	5	4	4	6
i-yaw	100	6	4	7	6	6	7
	160	2	3	4	3	3	1
baseline	Repeated	3	4	4	4	3	5

Participant		19	20	21	22	23	24
baseline	100	6	7	6	6	7	6
	160	1	2	2	3	3	1
iyaw	100	6	8	7	7	8	6
	160	2	3	1	3	3	1
dyaw	100	7	9	7	9	9	6
	160	4	5	4	5	5	3
cargo	100	6	8	8	8	8	5
	160	3	4	1	4	3	1
spoiler	100	6	8	8	9	9	5
	160	4	5	5	9	4	2
baseline	Repeated	2	3	4	4	3	3

Appendix E Driver Model Parameters

Smooth	4	9	14	16	18	20	23		
Tp	1.7	1.7	1.7	1.8	1.7	1.8	1.8		
YR	150	150	150	150	150	150	150		
Td	0.7	0.5	0.6	0.5	0.6	0.4	0.6		
K (e-4)	2.35	1.23	6	0.89	2	0.4	0.99		
damp	0.18	0.18	0.785	0.15	0.28	0.07	0.11		
stiffness	4.12	6.7	4.47	6.7	6.32	5	5.48		
Precise	**3**	**11**	**15**	**17**					
Tp	1.9	1.9	1.8	1.9					
YR	200	200	200	200					
Td	0.4	0.3	0.4	0.3					
K (e-4)	0.5	0.34	0.05	0.25					
damp	0.27	0.39	0.47	0.42					
stiffness	5.48	3.87	6.32	5.92					
Rough	**1**	**2**	**6**	**7**	**8**	**13**	**5**	**19**	**22**
Tp	1.7	1.7	1.7	1.7	1.8	1.7	1.9	1.9	1.7
YR	50	50	50	50	50	50	50	50	50
Td	0.5	0.6	0.4	0.4	0.4	0.4	0.4	0.3	0.4
K (e-4)	3	5.45	5.33	1.16	1.6	2	3.75	5	2.5
damp	0.4	0.533	0.63	0.27	0.3	0.4	0.79	1.185	0.55
stiffness	6.32	4.69	3.87	5.48	5	6.32	6.32	6.32	6.32
Over-reacting	**10**	**12**	**21**	**24**					
Tp	1.4	1.4	1.5	1.4					
YR	50	50	50	50					
Td	0.4	0.4	0.4	0.4					
K (e-4)	5	3.33	4.8	4.8					
damp	0.78	0.60	0.7	0.8					
stiffness	5.48	5.48	5	5					

Appendix F Linearization of MacAdam's Driver Model

For a linear 2DOF vehicle model

$$\begin{aligned} \dot{x} &= Ax + Bu \\ y &= C_y x \\ r &= C_r x \end{aligned} \tag{F.6.1}$$

where A is vehicle system matrix, B is input matrix, y is lateral displacement, r is yaw-rate, and C_y and C_r are output matrix respectively.

The cost function proposed in MacAdam's model has the following form

$$u_{opt}(t) = \min_{u}\left\{ \int_{t}^{t+T_p} \left\{ \left[y_d(\eta) - y(\eta) \right]^2 + w_r \cdot \left[r_d(\eta) - r(\eta) \right]^2 \right\} d\eta \right\} \tag{F.6.2}$$

The output of the linear systems can be decomposed into zero input response and zero state response

$$y(t+\tau) = C_y \cdot e^{A\tau} \cdot x(t) + C_y \cdot \left(\int_0^{\tau} e^{A\eta} d\eta \right) \cdot B \cdot u(t) \equiv F_y(\tau) \cdot x(t) + g_y(\tau) \cdot u(t) \tag{F.6.3}$$

$$r(t+\tau) = C_r \cdot e^{A\tau} \cdot x(t) + C_r \cdot \left(\int_0^{\tau} e^{A\eta} d\eta \right) \cdot B \cdot u(t) \equiv F_r(\tau) \cdot x(t) + g_r(\tau) \cdot u(t) \tag{F.6.4}$$

The optimal solution for equation (F.2) can be obtained by substituting equation (F.3) and (F.4) into (F.2) and setting the partial derivation of the cost function J with respect to u to be zero

$$u_{opt}(t) = \frac{\int_{t}^{t+T_p} \left\{ \left[y_d(\eta) - F_y(\eta - t) \cdot x(t) \right] \cdot g_y(\eta) + w_r \cdot \left[r_d(\eta) - F_r(\eta - t) \cdot x(t) \right] \cdot g_r(\eta) \right\} d\eta}{\int_{t}^{t+T_p} \left[g_y(\eta)^2 + w_r \cdot g_r(\eta)^2 \right] d\eta} \tag{F.6.5}$$

For computational purpose, we can discretize the solution

$$u_{opt} \approx \frac{\sum_{i=1}^{N} \left\{ \left[y_d(i) - F_y(i) x_0 \right] \cdot g_y(i) + w_r \cdot \left[r_d(i) - F_r(i) x_0 \right] \cdot g_r(i) \right\}}{\sum_{i=1}^{N} \left[g_y(i)^2 + w_r \cdot g_r(i)^2 \right]} \tag{F.6.6}$$

In crosswind steering scenario, if we assume that driver is driving straight, y_d and r_d will equal to zero.

$$u_{opt} \approx \frac{\sum_{i=1}^{N} \left\{ \left[y_d(i) - F_y(i) x_0 \right] \cdot g_y(i) + w_r \cdot \left[r_d(i) - F_r(i) x_0 \right] \cdot g_r(i) \right\}}{\sum_{i=1}^{N} \left[g_y(i)^2 + g_r(i)^2 \right]}$$

$$= \frac{\sum_{i=1}^{N} \left\{ \left[0 - F_y(i) x_0 \right] \cdot g_y(i) + w_r \cdot \left[0 - F_r(i) x_0 \right] \cdot g_r(i) \right\}}{\sum_{i=1}^{N} \left[g_y(i)^2 + w_r \cdot g_r(i)^2 \right]} = \frac{\sum_{i=1}^{N} \left\{ \left[F_y(i) \right] \cdot g_y(i) + w_r \cdot \left[F_r(i) \right] \cdot g_r(i) \right\}}{\sum_{i=1}^{N} \left[g_y(i)^2 + w_r \cdot g_r(i)^2 \right]} \cdot x_0$$

$$\equiv K_{MacAdam} \cdot x_0 \tag{F.6.7}$$

Here, F and g depend on vehicle model (F.1) and are constants. Optimal steering angle u_{opt} is only depending on x_0.

Appendix G Nomenclature

Symbol	Name
$a_d(t)$	Driver desired acceleration
$a_F(t)$, $V_F(t)$, $X_F(t)$	Following vehicle acceleration, velocity & position
$a_L(t)$, $V_L(t)$, $X_L(t)$	Lead vehicle acceleration, velocity & position
C,K	Gain, sensitivity
C_v, C_s, C_c	Constants for linear optimal control model
E	Saturation function threshold
K	Sample (discrete time)
m, l	Exponent parameters for nonlinear follow-the-leader model
N	Length of interaction
P	Desired acceleration gain of range-rate
P_0 ,P_1 ,P_2 ,P_3	Desired acceleration gain coefficient
$\bar{P}_0, \bar{P}_1, \bar{P}_2$	Deviation gain coefficient
$R, \dot{R}$	Range, Range-rate
R'	Perceptual range-rate
R_{min}	Minimum range
T	Time
$t_{preview}$	Preview time
T_h	Time headway
T	Time delay
V_{Fd}	Desired velocity of the following vehicle
Σ	Deviation

Appendix H Parameters Values

Table H.1 SDM parameters

	P_0	P_1	P_2	P_3	$\overline{P}_0$	$\overline{P}_1$	$\overline{P}_2$	mean	STD
Driver 1	0	0	-.0023	.0732	0	-.002	0.1526	0.5658	0.4042
Driver 2	-0	0.0001	-.0069	.1478	0	-.0001	0.0702	-0.4224	0.4844
Driver 3	-0	0	-.0011	0.0391	0	-.0047	0.2499	0.2291	0.4022
Driver 4	-0	0	-.0029	0.0751	-0	0.0042	0.0678	0.3653	0.6559
Driver 5	-0	0	-.003	0.0786	0	-.0011	0.1093	0.1717	0.4677
Driver 6	-0	0	-.0026	0.0773	0	-.0034	0.2005	0.6727	0.5756
Driver 7	-0	0.0001	-.0047	0.1366	-0	0.0015	0.0912	0.2521	0.4075
Driver 8	-0	0	-.0007	0.0235	0	-.0022	0.1869	-0.2841	0.423
Driver 9	-0	0.0001	-.0042	0.0452	0.0001	-.0045	0.2558	0.142	0.3191
Driver 10	0	-0	0.0021	-.012	0.2727	0.206	0.2926	0.4596	0.4833

Appendix I Derivation of ARMA model

Tyler's model has the following form:

$$\dot{V}_F(t+\tau) = C_v(V_L - V_F) + C_s\left[(x_L - x_F) - C_c \cdot V_F\right] \tag{I.1}$$

V_L, x_L, and x_F can be replaced by R and $\dot{R}$

where $R(t) = x_L - x_F$ and $\dot{R}(t) = V_L - V_F$, and equation (I.1) becomes

$$\dot{V}_F(t+\tau) = C_v \cdot \dot{R}(t) + C_s\left[R(t) - C_c \cdot V_F(t)\right] \tag{I.2}$$

Discretization is done with sampling time T

$$\frac{V_F(k+1+\tau) - V_F(k+\tau)}{T} = C_v \frac{R(k+1) - R(k)}{T} + C_s\left[R(k) - C_c \cdot V_F(k)\right] \tag{I.3}$$

(I.3) is re-organized as follows:

$$\begin{aligned} V_F(k+1+\tau) &= V_F(k+\tau) + C_v \cdot R(k+1) - C_v \cdot R(k) + T \cdot C_s \cdot R(k) - T \cdot C_s \cdot C_c \cdot V_F(k) \\ &= V_F(k+\tau) - (T \cdot C_s \cdot C_c)V_F(k) + C_v \cdot R(k+1) + (T \cdot C_s - C_v)R(k) \end{aligned}$$

$$\Rightarrow V_F(k+1+\tau) = a \cdot V_F(k+\tau) - b \cdot V_F(k) + c \cdot R(k+1) + d \cdot R(k)$$

where a, b, c, d are the coefficients for ARMA model.

Finally, the time step is shifted and the ARMA model can be obtained.

$$V_F(k) = a \cdot V_F(k-1) - b \cdot V_F(k-\tau-1) + c \cdot R(k-\tau) + d \cdot R(k-\tau-1) \tag{I.4}$$

Bibliography

[1] J. Stutts, "Distraction in Everyday Driving", AAA Foundation for Traffic Safety Press Conference, Washington, D.C. August 6, 2003.

[2] S.G. Klauer, et al, "The Impact of Driver Inattention on Near-Crash/Crash Risk", NHTSA, DOT HS 810 594, 2006.

[3] D.H. Weir, D.T. McRuer, "Dynamics of driver vehicle steering control", in Automatica, Vol. 6, Iss. 1 pp. 87-98, 1970.

[4] C. Pattem, A. Kircher, er al, "Using mobile telephones: cognitive workload and attention resource allocation", in Accident Analysis & Prevention, Vol. 36 Iss. 3 pp. 341-350, 2004.

[5] L. Tijerina, "Issues in the Evaluation of Driver Distraction Associated with In-Vehicle Information and Telecommunications Systems", in Transportation Research Inc, 2000.

[6] J. Stutts, "The Role of Driver Distraction in Traffic Crashes", AAA Foundation for Traffic Safety, 2001.

[7] J. Zhou, "Active Safety Measures for Vehicles Involved in Light Vehicle-to-Vehicle Impacts", Ph. D dissertation, Mechanical Engineering, University of Michigan, 2009.

[8] National Highway Traffic Safety Admission (NHTSA), "Traffic Safety Facts 2005: A Compilation of Motor Vehicle Crash Data from Fatality Analysis Reporting System and the General Estimates System." National Center for Statistics and Analysis, US Department of Transportation, Washington, DC, 2005.

[9] D.T. McRuer, H.R. Jex, "A Review of Quasi-Linear Pilot Models", in IEEE trans. on Human Factors in Electronics, Vol. HFE-8, Iss: 3, pp. 231-249, 1967.

[10] R.A. Hess, A. Modjtahedzadeh, "A control Theoretic Model of Driver Steering Behavior", in Control System Magazine, IEEE, Vol. 10, Iss: 5, pp. 3-8, 1990.

[11] S. Horiuchi, N. Yuhara, "An analytical approach to the prediction of handling qualities of vehicles with advanced steering control system using multi-input driver model", in Journal of dyamic systems, measurement, and control, Vol. 122, Iss: 3 pp. 490-497, 2000.

[12] H. Wallentowitz, J.Holtschulze, "Vehicle and Driver in Natural Sidewind – Possibilities for Active Intervention", in Ingenieurs de l'Automobile, 2002.

[13] T.B. Sheridan, "Three Models of Preview Control" in IEEE trans. on Human Factors in Electronics, Vol. HFE-7, No. 2, pp. 92-102, 1966.

[14] D.D. Salvucci, R. Gray, "A two-point visual control model of steering", in Perception, Vol. 33, Iss: 10, pp. 1233, 2004.

[15] C.K. Yip, D.A. Crolla, "Modeling of Aerodynamic Effects on Passenger Car Handling Using Fixed and Closed-loop Steering Control Methods", in AVEC' 92.

[16] Y. Maruyama, F. Yamazaki, “Driving Simulator Experiment on the Moving Stability of an Automobile Under Strong Crosswind”, in J. of wind engineering and industrial aerodynamics, vol. 94, Iss: 4, 2006.
[17] R.S. Sharp, D. Casanova and P. Symonds, “A Mathematical Model for Driver Steering Control, with Design, Tuning and Performance Results” in Vehicle system dynamics, Vol. 33, Iss: 5, pp. 289, 2000.
[18] C.C. MacAdam, “Application of an Optimal Preview Control for Simulation of Closed-loop Automobile Driving”, in IEEE Transactions on systems, man, and cybernetics, Vol. SMC- II, No. 6, pp. 393-399, 1981.
[19] C.C. MacAdam, “Development of a Driver Model for Near/At-Limit Vehicle Handling”, Technical Report for GM Corporation, The University of Michigan Transportation Research Institute, Nov. 2001.
[20] A.Y. Ungoren, H. Peng, “An Adaptive Lateral Preview Driver Model”, in Vehicle System Dynamics Vol. 43, Iss: 4, pp. 245-259, 2005.
[21] L.-K. Chen, A.G. Ulsoy, “Identification of a Driver Steering Model, and Model Uncertainty, From Driving Simulator Data”, in Journal of Dynamic Systems, Measurement, and Control, Vol. 123 pp. 623-629, 2001.
[22] Uffelmann, “Influence of Aerodynamics and Suspension on the Cross-Wind Behaviour of Passenger Cars-Theoretical Investigation under Consideration of the Driver's Response”, in Vehicle system dynamics Vol. 15, pp.568, 1986.
[23] H.P. Willumeit, K. Muller, at el, “Method to Correlate Vehicular Behaviour and Driver’s Judgment Under Side Wind Disturbances”, in Vehicle System Dynamics , vol. 17 pp. 508, 1988.
[24] C.C. MacAdam, M.W. Sayers. et al, “Crosswind Sensitivity of Passenger Cars and the Influence of Chassis and Aerodynamic Properties on Driver Preferences”, in Vehicle System Dynamics, Vol. 19, pp. 201-236, 1990.
[25] K. Maeda, H. Sakai, “Analysis of Aerodynamic Effects on the Vehicle Stability in High Speed Running”, in International Symposium on Advanced Vehicle Control, 1996.
[26] A. Wagner, J. Wiedemann, “Crosswind Behavior in the Driver’s Perspective”, SAE 2002-01-0086.
[27] H. Harada, T. Iwasaki, “Stability Criteria and Objective Evaluation of a Driver-Vehicle System for Driving in Lane Change and Against Crosswind”, in Vehicle system dynamics, Vol. 23, pp.197, 1994.
[28] O. Hanke, T. Berstram, M. Hiller, “Analysis and Control of Vehicle Dynamics Under Crosswind Conditions”, in IEEE/ASME International Conference on Advanced Intelligent Mechatronics Proceedings, Italy, 2001.
[29] W.A.H. Orady, D.A. Crolla, “Passenger Car Stability Under Random Wind Excitation”, in Vehicle dynamics and simulation, 2001.
[30] Y. Maruyama, F. Yamazaki, “Driving simulator experiment on the moving stability of an automobile under strong crosswind”, in Journal of Wind Engineering and Industrial Aerodynamics Vol. 94, pp. 191-205, 2006.
[31] L.A. Pipes, “An Operational Analysis of Traffic Dynamics”, in J. Applied Physics, vol. 24, pp. 271-281, 1953.
[32] D. C. Gazis, R. Herman, R.W. Rothery, “Nonlinear Follow-The-Leader Models of Traffic Flow”, in Operations Research, vol. 9, no. 4, Jul. - Aug., 1961, pp. 545-567.

[33] R. Herman, R.B. Potts, “Single Lane Traffic Theory and Experiment.”, in Proceeding s of the Symposium om Theory of Traffic Flow, Research Labs, GM, New York: Elsevier, 1959.
[34] J. Treiterer, J.J. A. Myers, ”The Hysteresis Phenomenon in Traffic Flow”, in Proceedings of the Sixth International Symposium on Transportation Theory, Sydney, pp. 13-38, 1974.
[35] H. Ozaki, “Reaction and Anticipation in the Car Following Behavior”, in Proceedings of the 13th International Symposium on Traffic and Transportation Theory, pp. 349-366.
[36] G.F. Newell, “Nonlinear Effects in the Dynamics of Car Following”, in Operations Research, Vol. 9, no. 2, pp. 209-229, 1961.
[37] W. Helly, “Simulation of Bottlenecks in Single Lane Traffic Flow”, in Proceedings of the Symposium on Theory of Traffic Flow., Research Labs, GM, New York: Elsevier, 1959.
[38] J Tyler Jr., “The Characteristic of Model-Following Systems as Synthesized by Optimal Control”, in Automatic Control, IEEE Transactions on, Vol. 9, Iss: 4, pp. 485-498, 1964.
[39] P.G. Gipps, “Behavioral Car-Following Model for Computer Simulation”, in Transport. Res., Vol. 15B, no. 2, pp. 105-111, 1981.
[40] M. Bando, et al.,” Phenomenological Study of Dynamical Model of Traffic Flow”, in J. Phys. I France, Vol. 5, pp. 1389-1399, 1995.
[41] R.M. Michaels, “Perceptual factors in car following”, in Proceeding of the Second International Symposium on the Theory of Road Traffic Flow, pp. 44-59, 1963.
[42] D.N. Lee, “A theory of visual control of braking based on information about time-to-collision”, in Perception, Vol. 5, no 4, pp. 437-45, 19769.
[43] E.H. Yilmaz, W.H. Warren, “Visual Control of Braking: A test of the tau-dot Hypothesis”, in Journal of experimental psychology, 1995.
[44] U. Reiter, “Empirical Studies as Basis for Traffic Flow Models”, in Proceedings of the Second International Symposium on Highway Capacity, Vol. 2, pp. 493-502, 1993.
[45] M. Brackstone, B. Sultan, M. McDonald, “Motorway Driver Behavior: Studies on Car Following”, in Transportation Research, pp 329-344, 2002.
[46] Army Aviation Board Fort Rucker al, “Proposed Military Characteristics for Collision Warning Device”, 1957.
[47] Rand Corp Santa Monica CA , “AN AIRBORNE COLLISION-WARNING DEVICE”, 1957.
[48] J.J. Gibson, L.E. Crooks, “A Theoretical Field-Analysis of Automobile-Driving”, in The American Journal of Psychology, Vol. 51, No. 3, pp. 453-471, 1938.
[49] H. Kawashima, “Integrated system of navigation and communication in Japan.”, in IFAC/IFIP/IFORS Symposium, 1989.
[50] J.K. Pollard, “Evaluation of the Vehicle Radar Safety Systems' Rashid Radar Safety Brake Collision Warning System”. Washington, DC, February, 1988, DOT TSC HS 802, PM 88 2.
[51] Z. Parsehhian, “Field Evaluation of A Nissan Laser Collision Avoidance System”. NHTSA Report, Washington, DC, January, 1989, DOT HS 808 375.

[52] W.A. Jr. Leasure, “The Importance of Crash Problem Analysis in Defining NHTSA's IVHS Program”. in Proceedings of the IVHS America 1992 Annual Meeting, pp 727-732, 1992.
[53] R.R. Knipling, D.L. Hendricks, etc, “A Front-End Analysis of Rear-End Crashes”. in Proceedings of the IVHS America 1992 Annual Meeting, pp 733-745, 1992.
[54] R.R. Knipling, M. Mironer, etc, “Assessment of IVHS Countermeasures for Collision Avoidance: Rear-End Crashes”. NHTSA Report, Washington, DC, May, 1993, DOT HS 807 995.
[55] A.L. Burgett, et al. “A Collision Warning Algorithm for Rear-End Collisions”. in 16th International Technical Conference on Enhanced Safety of Vehicles Abstracts, 98-S2-P-3 1, Washington, DC, May, 1998.
[56] R. Kiefer, et al. “Development and Validation of Functional Definitions and Evaluation Procedures for Collision Warning/Avoidance System”, NHTSA Technical Report, 1999.
[57] A. Doi, T. Butsuen, et al. “Development of a rear end collision avoidance system with automatic brake control”, in JSAE Review Vol. 15, pp. 335-340, 1994.
[58] S.J. Brunson, E.M. Kyle, et al. “Alert Algorithm Development Program NHTSA Rear End Collision Alert Algorithm”, NHTSA Technical Report, 2002.
[59] Y. Zhang, E.K. Antonsson, “A New Assessment Measure for Collision Avoidance Systems”, in Proceedings of the IEEE ITCS 2006.
[60] J.J. Gibson, “The Ecological Approach to Visual Perception”, Boston: Houghton Mifflin, 1987.
[61] K. Lee, H. Peng, “Evaluation of automotive forward collision warning and collision avoidance algorithm”, in Vehicle System Dynamics, Vol. 43 no. 10, pp. 735-751, 2005.
[62] S. Hirst, R. Graham, ” The Format and Perception of Collision Warnings”, in Ergonomics and Safety of Intelligent Driver Interfaces, 1997.
[63] R. Miler, Q. Huang, “An Adaptive Peer-to-Peer Collision Warning System”, in Vehicular Technology Conference, 2002., Vol. 1, pp. 317-321, 2002.
[64] Automotive Collision Avoidance System Field Operational Test Report, DOT HS 809 900, NHTSA, August 2005.
[65] J.L. Campbell, C.M. Richard, “Crash Warning System Interfaces: Human Factors Insights and Lessons Learned”, DOT HS 810 697, NHTSA, Jan. 2007.
[66] W.G. Najm, J.D. Smith, “Development of Crash Imminent Test Scenarios for Integrated Vehicle Safety Systems”, DOT HS 810 757, NHTSA, Apr. 2007.
[67] L. Yang, J.H. Yang, “Development of a Performance-Based Approach for a Rear-End Collision Warning and Avoidance System for Automobiles”, IEEE, 2003.
[68] MW Sayers, C.C. MacAdam, Y. Guy, “Chrysler/UMTRI wind-steer vehicle simulation-user's manual”, UMTRI Technical Report, UMTRI-90-19-1, May, 1990.
[69] MW Sayers, C.C. MacAdam, Y. Guy, “Chrysler/UMTRI wind-steer vehicle simulation-Reference manual”, UMTRI Technical Report, UMTRI-90-19-2, May, 1990.
[70] L. Segel, “Theoretical Prediction and Experimental Substantiation of the Response of the Automobile to Steering Control.” In Proceedings of the Automobile Division of the Institution of Mechanical Engineers, No. 7, 1956-57.

[71] S.G. Hill, J.S. Metcalfe, "The Use of a Steering Shaping Function to Improve Human Performance in By-Wire Vehicles", Army Research Laboratory, ARL-TR-4387, 2008.
[72] P.L. Olson, "The Effect of Variable-Ratio Steering Gears on Driver Preference and Performance", in Human Factors, Vol. 12, No. 6, pp. 553-558, 1970.
[73] D. LeBlanc, J. Sayer, .et al, "Road Departure Crash Warning System Field Operational Test", UMTRI, 2006.
[74] W.K. Pratt, "Digital Image Processing", John Wiley & Sons, pp.330-333, 1978.
[75] A.V. Oppenheim, R.W. Schafer, "Discrete-Time Signal Processing", Prentice-Hall, pp.311-312, 1989.
[76] K. Nagel, M. Schreckenberg, "A cellular automation model for freeway traffic", in J. Physic I France, Vol. 2, pp. 2221-2229, 1992.
[77] S. Krauss, P. Wagner, C. Grawron, "Continuous limit of the Nagel-Schreckenberg model", in Physical Review E, Vol. 54 no. 4, pp. 3707-3712, 1996.
[78] D. Jost, K. Nagel, "Probabilistic Traffic Flow Breakdown In Stochastic Car Following Models", in Transportation Research Record, Vol. 1852, pp. 152-158, 2003.
[79] P. Wagner, I. Lubashevsky, "Empirical basis for car-following theory development", in Statistical Mechanics, 2006.
[80] S.J. Brunson, E.M. Kyle, N.C. Phamdo, G.R. Preziotti, "NHTSA Rear-End Collision Alert Algorithm Final Report", NHTSA, 2002, DOT HS 809 526.
[81] A.M. Mood, F.A. Graybill, D.C. Boes, "Introduction to the Theory of Statistics", 3rd edition, McGraw-Hill, pp. 540-541, 1974.
[82] H.K. Khalil, "Nonlinear Systems", third Ed., Prentice Hall, pp.551-571, 2000.
[83] M.S. Chang, C.J. Messer, A.J. Santiago, "Timing Traffic Signal Change Intervals Based on Driver Behavior", in Transportation Research Record, Vol. 1027, pp. 20-30, 1985.
[84] R. Dewar, P. Olson, "Human Factors in Traffic Safety", 2nd ed., Lawyers & Judges Publishing Company, Inc.
[85] R. Henderson, A. Burg, "Vision and Audition in Driving, Final Report", NHTSA, 1974, DOT HS 801-265.
[86] J.J. Gibson, "The Ecological Approach to Visual Perception", Boston: Houghton Mifflin, 1979.
[87] D.R. Proffitt, "Distance Perception", in Current Directions in Psychological Science, Vol. 15, no. 3, pp. 131-135, 2006.
[88] K. Nakayama, C.W. Tyler. "Psychophysical isolation of movement sensitivity by removal of familiar position cues", in Vision Research, Vol.21, pp. 427-433, 1981.
[89] S.P. McKee, "A local mechanism for differential velocity detection", in Vision Research, Vol. 21, pp. 491-500, 1980.
[90] R.H. Brown ," Weber Ratio for Visual Discrimination of Velocity", in Science, Vol. 131. no. 3416, pp. 1809 – 1810, 1960.
[91] J.M. Harris, S. N. J. Watamaniuk, "Speed Discrimination of Motion-in-Depth Using Binocular Cues", in Vision Research, Vol. 35, no. 7, pp. 885-896, 1995.
[92] S.N. J. Watamaniuk (2003), "Perceptual and Oculomotor Evidence of Limitations on Processing Acceleration Motion", in Journal of vision, Vol. 3, Iss: 11, pp. 698 - 709, 2003.

[93] T. Haarmeier, P. Their, “Detection of Speed Changes during Pursuit Eye Movement”, in Exp. Brain Res, Vol. 170, pp. 345-357, 2006.
[94] T.B. Sheridan, “Driver Distraction From a Control Theory Perspective”, in Human Factor, Vol. 46, no. 4, pp. 587-599, 2004.
[95] E.R. Boer, ”Behavioral Entropy as a Measure of Driving Performance”, in Proceeding to Driver Assessment, pp225-229, 2001.
[96] S. Ross, “Stochastic Processes”, Wiley Series in Probability and Mathematical Statistics, 2rd edition.
[97] M. Lesch, L. Simmons, P.A. Hancock, “The Distraction Effects of Phone Use during a Crucial Driving Maneuver”, in Accident Analysis and Prevention, 2003.
[98] H. Alm, L. Nilsson, “The Effects of a Mobile Telephone Task on Driver Behavior in a Car-Following Situation”, in Accident Analysis and Prevention, 1995.
[99] D. Lamble, et al, “Cognitive Load and Detection Thresholds in Car-Following Situations: Safety Implication for Using Mobile Telephone While Driving”, in Accident Analysis and Prevention, 1999.
[100] A. Pick, D. Cole, “Neuromuscular Dynamics and the Vehicle Steering Task”, in Vehicle System Dynamics, Vol. 41, pp. 182, 2004.
[101] Y. Fujita, Y. Akuzawa, M. Sato, “Radar Brake System” in Annual meeting of IT’S America, proceedings of, March 1995, pp. 95-101.
[102] P. Fancher, R. Ervin, et al, “Intelligent Cruise Control Field Operational Test”, University of Michigan Transportation Institute, DOT HS 808 849, 1998.
[103] K. Lee, “Longitudinal Driver Model and Collision Warning and Avoidance Algorithm Based on Driver Databases”, Ph. D thesis, 2004, University of Michigan.
[104] O. Tsimhoni, H. Fuller, M. Reed, “Modeling In-Vehicle Display Position and Driver Performance”, in Annual Meeting Industry Affiliation for Human Factors in Transportation Safety.